THE DEVELOPMENT OF A TSUNAMI-FLOODING MODEL WITH VERSATILE MOVING-BOUNDARY FORMULATION

A THESIS SUBMITTED TO THE GRADUATE DIVISION OF THE UNIVERSITY OF HAWAII IN PARTIAL FULFILLMENT OF THE REQUIREMENTS FOR THE DEGREE OF

MASTER OF SCIENCE

IN GEOLOGY AND GEOPHYSICS

DECEMBER 1982

By

Carter Hamilton Lewis, III

Thesis Committee:

Wm. Mansfield Adams, Chairman
John C. Rose
Doak C. Cox

We certify that we have read this dissertation and that in our opinion it is satisfactory in scope and quality as a thesis for the degree of Master of Science in Geology and Geophysics.

Thesis Committee

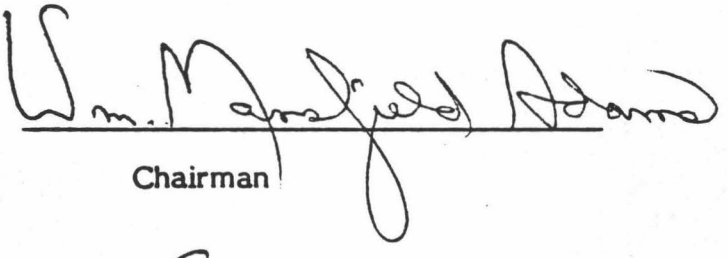

Chairman

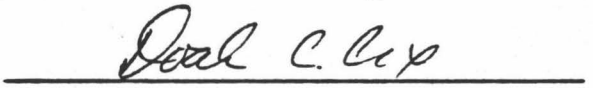

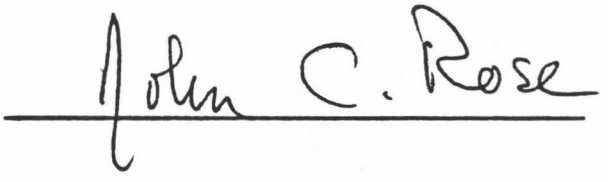

ACKNOWLEDGEMENTS

This work was made possible by funding from the National Science Foundation, NSF award #PFR80-0829. In addition, the resources of the National Oceanic and Atmospheric Administration (NOAA) were made available for this work under the auspices of the Intergovernmental Personnel Act.

Don Hanson, Director of the NOAA's Atlantic Oceanographic and Meteorological Laboratories (AOML), generously made his staff and computer resources available for our benefit. Particularly helpful there were discussions with Dr. Carlisle Thacker.

The direction taken by this work is primarily due to the vision and guidance of Dr. Wm. Mansfield Adams. Also, the successful completion of this thesis is, in large part, attributable to Dr. Adams' skills as a first-rate advisor.

Dr. Doak Cox provided many helpful suggestions for the fine-tuning of this thesis; the clarity has improved by at least an order of magnitude as a result.

In addition to stimulating my thinking with numerous thought-provoking questions, Dr. John Rose has been a source of spiritual guidance for this work.

A very real contribution to the completion of this work was made by Dr. Fred Duennebier, who urged me to keep up the forward momentum of my efforts, and made it possible by providing liberal amounts of leave from work when time was scarce.

Among the many contributions made by Joyce Metzger was the typing of the complete thesis and all the equations. She went beyond the call of duty, however, in correcting my mis-spellings, cross-checking my references with my bibliography, then issuing me a complete report of all the resulting deficiencies, and providing transportation that saved me much valuable time. She applied that extra effort characteristic of A+ work.

Sylvia Marcin drafted all the attractive figures; the crude reproduction of photographs was my handiwork.

Abundant logistical support was provided by Dena Narramore, who made her private study available for my undisturbed use when distractions were abundant everywhere else, and who helped to organize my efforts to finish the writing of this thesis.

An early partial draft of this thesis was typed by Olivia Athens, who also provided logistical support, and cracked a whip whenever progress on this work faltered.

Finally, support in uncountable varieties has been provided every step of the long path from my birth to this point by my parents, Dr. Carter and Peg Lewis, Jr.

I would like to thank those mentioned above, and many others not mentioned, who have helped in some way to make this work possible. Responsibility for all statements made in this thesis, however, rests solely with me.

ABSTRACT

An explicit, split-step, midpoint-leapfrog, finite-difference analog to the nonlinear, shallow-water, Navier-Stokes equations is developed for application to the modeling of tsunami-flooding. A homogeneous, incompressible, inviscid fluid subject only to the forces of gravity and bottom-friction is assumed. Vertical advection of momentum is permitted.

A theoretical stability-analysis is performed, yielding constraints on the permissible space- and time-steps necessary to insure a stable solution. It is concluded that the finite-difference scheme is a consistent approximation to the governing differential equations when the stability requirement is observed.

An evaluation of the most common numerical moving-boundary treatments shows each to be restricted by assumptions made regarding special conditions existing in the neighborhood of the moving boundary. As a result, a heuristic flooding scheme is developed which allows the prognostic equations to be applied without prejudice uniformly across the entire computational grid.

Careful comparison of experimental results with a known, analytical solution is essential to produce a verified model. Model performance is appraised by recording all results as a motion picture, then viewing the results to detect computational anomalies and to assess spatial and temporal coherency. Various formulations of the nonlinear advection term are tested for stability in this fashion, and effects produced by filtering are examined.

TABLE OF CONTENTS

TABLE OF CONTENTS

PAGE

LIST OF FIGURES

LIST OF TABLES

LIST OF SYMBOLS

A	An arbitrary function, A=A(x,z,t)
a	Abbreviation for $\Psi/2\sin^2\theta$
b	Abbreviation for $4\cdot\Psi/\sin^2\theta + \sin^2(2\theta)$
C_o	Nondimensional barrier overflow coefficient
C_s	Nondimensional submerged-barrier overflow coefficient
c	1. Phase speed of propagation of primary disturbance
	2. Abbreviation for $\Delta t/\Delta x$
D	Total fluid-depth
$\bar{D}$	Representative fluid-depth
$\bar{D}_i$	Depth at interface between grid cell i and cell i +1
D_b	Depth over submerged barrier
$D_{j-\frac{1}{2}}^{n+\frac{1}{2}}$	Total depth at center of cell j at time step n+½
Det(G)	Determinant of the matrix G
DQDX	Abbreviation for the appropriate finite-difference analog of $\partial Q/\partial x$
dz	The differential of z
e	Base of natural logarithms
F	Bottom-friction term
f	Frictional coefficient
G	Amplification matrix
g	Gravitational acceleration
H	Representative equilibrium fluid-depth
H_b	Equilibrium depth to barrier top
h	Equilibrium fluid-depth
$h_{j-\frac{1}{2}}$	Equilibrium depth at center of cell j
I	Identity matrix

i	1. $\sqrt{-1}$
	2. Subscript denoting spatial grid step
j	Subscript denoting spatial grid step
k	Index of Fourier expansion
L	Characteristic wavelength of primary disturbance
l_o	Characteristic length for dimensionalization of dimensionless variables
m	Abbreviation for $\sqrt{r-b/2}$
n	1. Superscript denoting time step
	2. Characterization of magnitude of initial disturbance for planar Ball-Thacker model
$O(\Delta x)$	Terms of the first order in Δx
P	1. Fluid pressure
	2. Abbreviation for $2\mu\beta^2/\gamma$
p	Abbreviation for $1/(8(1+\epsilon))$
Q	Volume transport (flux)
$\tilde{Q}$	Volume transport for frictionless case
Q_n	Component of volume transport normal to boundary
Q^n	Time-dependent coefficient in Fourier expansion of volume transport
Q_j^n	Flux across interface between cells j and j+1 at time step n
$Q_{j+1}^{n+1'}$	Approximation of Q_{j+1}^{n+1}
r	Abbreviation for $\frac{1}{2}\sqrt{(16c^2g\bar{D}+\sin^2 2\theta)^2+\sin^2 2\theta \cdot 64c^4g^2(\bar{D}-2cAU)^2}$
T	Characteristic period of primary disturbance
t	Time
t*	Dimensionless time
U	1. Ursell parameter
	2. Representative flux
u	Horizontal component of fluid particle-velocity

w	1. Vertical component of fluid particle-velocity
	2. Angular frequency of fluid oscillation
x	Horizontal spatial dimension
x^*	Dimensionless horizontal distance
z	Vertical spatial dimension
α	1. Abbreviation for $2(\Delta t/\Delta x)\sin\theta$
	2. Beach slope
β	Abbreviation for $c\cdot\sin\theta$
$\sqrt{\ }$	Abbreviation for $2\bar{D}+f\Delta t$
Δx	Spatial grid-step
Δt	Temporal grid-step
$\Delta\eta$	Driving surface-gradient
δ	Abbreviation for $(2\bar{D}-f\Delta t)/\sqrt{\ }$
ϵ	Carrier-Greenspan wave-breaking parameter
$\epsilon(\eta)$	Truncation error in finite-difference expression for η
η	Disturbance height above equilibrium level
η_o	Characteristic disturbance height
$\eta(x,t)$	True tsunami disturbance at (x,t)
η^*	Dimensionless disturbance-height
$\eta_{j-\frac{1}{2}}^{n+3/2}$	Disturbance height at center of cell j at time step n+3/2
$\tilde{\eta}_{3/2}^{n+3/2}$	Approximation of $\eta_{3/2}^{n+3/2}$
η^n	Time-dependent coefficient in Fourier expansion of η
η_1,η_2	Disturbance heights on opposite sides of barrier
θ	Abbreviation for $\frac{1}{2}k\Delta x$
λ	Eigenvalue of amplification matrix
$\lvert\lambda\rvert_{(\ell)}$	Eigenvalue of amplification matrix with largest magnitude
μ	Abbreviation for $4g\bar{D}^2$

ρ Fluid density

σ Defining parameter for Carrier-Greenspan wave

ϕ Abbreviation for $\frac{\bar{U}}{D}\cdot\frac{\Delta t}{\Delta x}$.

ξ Total fluid depth

Ψ Abbreviation for $4(\Delta t/\Delta x)^2 g\bar{D}\sin^2\theta$

PREFACE

This work was initiated during the first semester of my enrollment in the Geology and Geophysics program at the University of Hawaii. Although some have suggested that research into the numerical modeling of tsunami flooding would be more appropriately conducted within an oceanography or mathematics program, I believe otherwise. First, a tsunami is clearly a geophysical phenomenon, and contains information about its source (usually an earthquake). Second, a tsunami can produce profound geomorphological alterations that may be preserved in the geologic record, requiring an interpretation. Third, with the advent of plentiful and inexpensive computer resources, numerical modeling is assuming the position of a standard tool for the scientist interested in investigating geophysical phenomena. It is with such interested scientists in mind that I have assembled some lessons learned during my own experimentation in this still incompletely understood area; for, numerical modeling is still partially an art whose rules can often be derived only through empirical efforts. I sincerely hope that the rules I have been taught can in turn be used by others without the need for their painful reinvention.

CHAPTER I

INTRODUCTION

A tsunami is an impulsively generated water wave-train. It may be caused by an earthquake, landslide, volcanic eruption, nuclear explosion or meteor impact in a large body of water. Even in an open ocean, tsunamis can best be characterized as shallow-water waves. Their speed is controlled by the depth as $c = \sqrt{gD}$ (c: wave speed; g: gravitational acceleration; D: water depth). The strong dependence of wave parameters on bathymetry is particularly evident as the wave enters shallow coastal waters (see Figure 1). In order to maintain its period at greatly reduced velocity, the wavelength must be shortened. And, since total energy is conserved, the energy density increases; hence, the wave amplitude grows. In this way an open-ocean tsunami one foot high propagating smoothly with a speed of 500 mph may be transformed by the operation of the bottom topography into a 100 foot high tsunami propagating destructively with a speed of 30 mph.

From a pragmatic standpoint, the deleterious consequences to populated coastal areas resulting from inundation of such waves make a thorough understanding of tsunami behavior desirable. The goals of such an understanding are twofold: (1) To make an accurate location-specific prediction of the time of tsunami arrival. (2) To make an accurate location-specific prediction of the expected severity of the tsunami occurrence. The Pacific Tsunami Warning System has undertaken the responsibilty for detection of generated tsunamis and prediction of their arrival times at appropriate locations, but as yet the expected extent of tsunami inundation is not routinely predicted. This situation has resulted in panicked evacuation to watch a one cm tsunami pass on the one hand, to disregard born of distrust and leading to demise on the other.

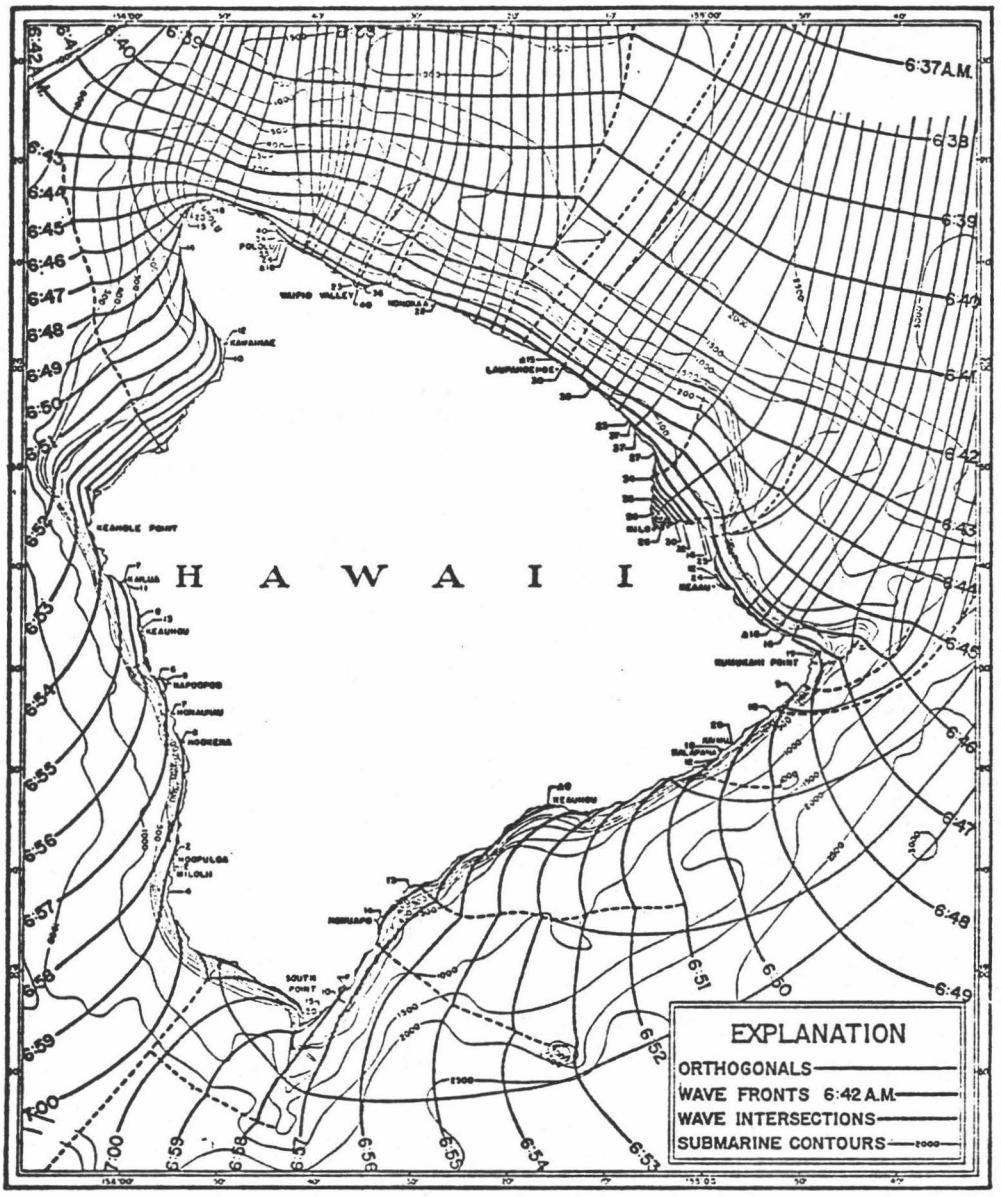

Figure 1. Map of the island of Hawaii, showing the controlling effect of local bathymetry on impinging-tsunami parameters. Shown are run-up heights (in feet above lower low water), water fronts, orthogonals, submarine contours (in fathoms), and computed time of arrival of the first wave (from Shepard, MacDonald and Cox, 1950).

Knowledge of expected tsunami behaviour in a real-earth situation is exceedingly difficult to obtain. Intuition is an unreliable guide: one study found similar tsunami wave spectra at one tide gauge for different tsunamis, and dissimilar spectra at different tide gauges for one tsunami, illustrating the strong influence of local bathymetry (Munk, Snodgrass & Tucker, 1959). Another study found that along the California coast, the bays that had the most protection from the direction of approach of the April 1, 1964 tsunami had the largest rise in water levels (Bascom, 1946). Although differential equations that completely characterize the physics of tsunami behavior exist, (shallow-water form of the Navier-Stokes equations, see later), they are in general not solvable analytically. This mathematical intractability arises from the inherent nonlinearity of the phenomenon, and the complexity of the boundary conditions that must be applied (represented by the bathymetry). Hydraulic scale modeling efforts face numerous difficulties, especially from the fact that the ratio of tsunami height to wavelength may be on the order of 10^{-5}. The resulting model bulkiness, expense and single-location applicability hamper the method's usefulness.

Attempts have been made to obtain a statistical estimate of expected frequencies of occurrence of tsunamis of specified severity and to delineate the areas susceptible to them, based on sparse historical data. Historical run-up data for the Hawaiian Islands reported by Pararas-Carayannis (1969) and Loomis (1975) has been used in conjunction with numerical results obtained by Houston et al (1977) and Bertschneider and Wybro (1976) to define a continuous coastal hazard zone for use by the National Flood Insurance Program. The results were later updated by Cox and Morgan (1977) and Cox (1979), who considered the contribution of locally-generated tsunamis. For reasons to be discussed in this work, the method used by Houston et al. (1977) to obtain run-up values at sites intermediate to those for which historical data exist is certainly subject to improvement. Also,

Bretschneider and Wybro (1976) approximate all coastal areas by constant depth water followed by constant slope beach. As accurate run-up estimates are essential for the establishment of meaningful coastal hazard zones, the need is apparent for a model capable of accurately predicting tsunami effects in the actual coastal area for a specified incident tsunami. These accurate predictions can only be obtained by modeling the flooding process in such a way that the modeled tsunami behavior is consistent with physical reality.

The solution is provided by the method of predicting the "conditional expected tsunami inundation (CETI)" proposed by Adams (1973). Numerical modeling of conditional expected tsunami inundation in coastal areas is the most viable technique for obtaining the complete information required to mitigate the tsunami hazard. The primary shortcoming of numerical modeling of tsunamis has been the unreliability of the results. This is in no way an indication of some intrinsic deficiency in the method, but rather of the inappropriateness of most model formulations: either they have been simplified to the point of trivial inapplicability, or numerous degrees of freedom have been adjusted in the name of "calibration" to the point where the model is applicable only to the region used for calibration (Houston & Butler, 1979). This tendency is due in part to the success that storm surge modeling, the evolutionary precursor of tsunami modeling, enjoyed with its linear approximations of applicable equations and its no-flow boundary condition at the shoreline (Platzman, 1965; Reid & Bodine, 1968).

Several investigators assumed the task of formulating moving boundary conditions that would permit the modeling of tsunami flooding over dry land (e.g., Reid & Bodine, 1968; Runchal, 1975; Sielecki & Wurtele, 1970; Wanstrath, 1978; Xanthropoulos & Koutitas, 1976; Yeh & Chou, 1979). All reported varying amounts of success for the conditions they restricted their attention to. Some implicitly considered only flat or smooth bathymetries and topographies to exist, others

treated dry land as an assemblage of discontinuous barriers. The applicability of the resulting models is shown in this work to be limited by these assumptions.

This work will attempt to develop a numerical model of tsunami flooding valid over the entire spectrum of bathymetry and topography continuity. The approach taken is to apply the numerical analogue of the governing equations uniformly across the computational grid after appropriate depths and values for the driving surface gradient at each grid cell interface have been determined. The moving boundary is permitted to determine its own location in obeyance to the prognostic equations, and is not given special treatment other than the application of an anti-aliasing filter. The result is a versatile model, applicable to smooth as well as discontinuous bathymetries. In addition, several requirements for the successful development of the numerical model are discussed. Particularly important is the need to monitor all results of all calculations after each time iteration.

Chapter II

MATHEMATICAL DEVELOPMENT

If we confine ourselves to non-relativistic mechanics in an incompressible, inviscid, continuous and homogeneous fluid, then the fluid behavior is completely characterized by mathematical statements of the basic physical conservation principles: Newton's laws (Conservation of Momentum) and the equation of mass continuity. We shall assume that the only real forces acting on the fluid are pressure, bottom friction and gravity. Since the horizontal dimensions to be considered are on the order of several kilometers at most, the earth may be considered locally flat, and the Coriolis effect neglected. In addition, we will be concerned only with a two-dimensional vertical slice of the problem (see Figure 2). The equation of motion for an Eulerian frame of reference (fixed to the solid earth) may then be written (see Appendix A for definitions of symbols):

$$(2.1) \quad \frac{\partial u}{\partial t} + u \frac{\partial w}{\partial x} + w \frac{\partial u}{\partial z} + F - \frac{1}{\rho} \frac{\partial P}{\partial x}$$

The equation of continuity may be written:

$$(2.2) \quad \frac{\partial u}{\partial x} + \frac{\partial w}{\partial z} = 0$$

The fluid surface is given by:

$$(2.3) \quad z = \eta(x,t)$$

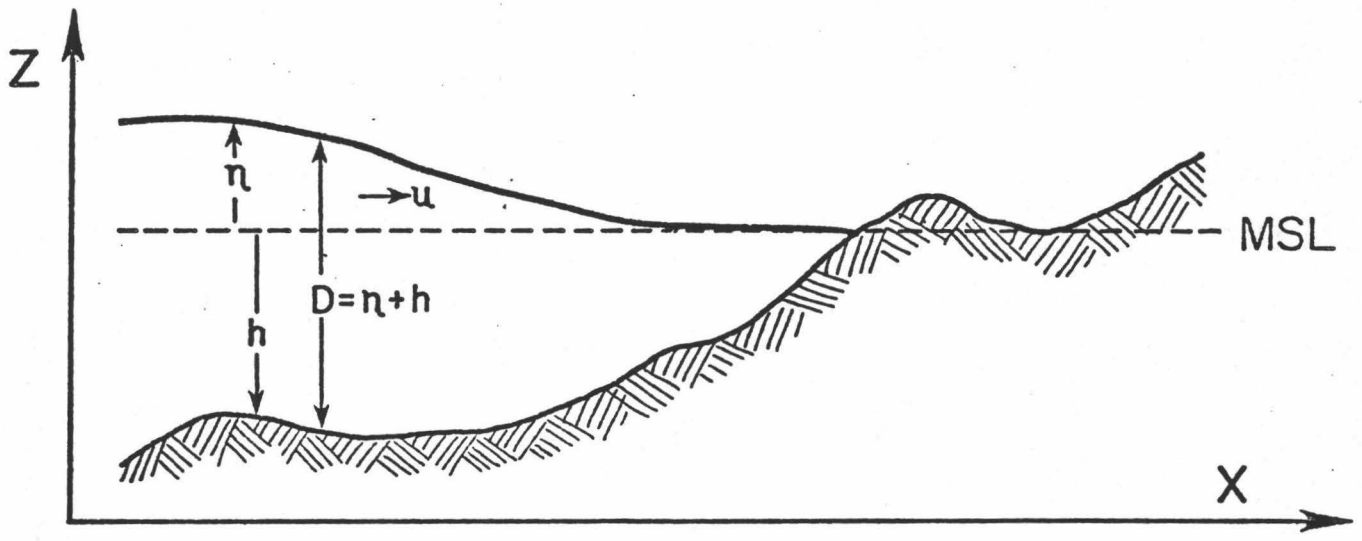

Figure 2. Illustration of fundamental variables considered for tsunami-flooding modelling.

And, the fluid bottom is defined by:

(2.4) $z = -h(x)$

As we are interested in modeling tsunami propagation, the introduction of the shallow-water approximation is appropriate. That is, we will assume that the vertical component of fluid particle acceleration has a negligible effect on the pressure, P, and that P may then be considered to be produced totally by hydrostatic effects:

(2.5) $P(z) = g\rho\ [\eta - z]$

As is readily seen, we now have

(2.6) $\frac{dP}{dx} = \rho g \frac{d\eta}{dx}$

so that dP/dx and hence the fluid particle acceleration, is independent of depth below the surface. But this implies that the fluid particle velocity is independent of depth for all time if it is at any time, since it may be expressed as $u=u_1(x_1t)+u_2(z)$, and if u is independent of z at any time, then $u_2=0$. Taking u to be independent of depth at time t=0, we have:

(2.7) $u = u(x,t)$

and equation 2.1 may now be vertically integrated through the entire fluid column yielding:

$$(2.8)\quad \int_{-h}^{\eta} \frac{\partial u}{\partial t}dz + \int_{-h}^{\eta} u\frac{\partial u}{\partial x}dz + \int_{-h}^{\eta} w\frac{\partial u}{\partial z}dz = \int_{-h}^{\eta} F dz - \int_{-h}^{\eta} g\frac{\partial \eta}{\partial x}dz$$

or

$$(2.9)\quad (\eta+h)\frac{\partial u}{\partial t} + (\eta+h)u\frac{\partial u}{\partial x} = -fu|u| - (\eta+h)g\frac{\partial \eta}{\partial x}$$

where the frictional term F is taken to be quadratic of the form:

$$(2.10)\quad F(x,t) = -f\frac{u|u|}{(\eta+h)}$$

after Leenderste (1967).

As we are rarely interested in the actual instantaneous velocity at a point, but rather with the quantity of fluid passing through a finite area in a finite amount of time (Aleksandrov et. al, 1956), we introduce the volume transport Q:

$$(2.11)\quad Q(x,t) \equiv (\eta(x,t) + h(x))u(x,t)$$

Q is seen to be the volume of water passing through a unit width of our two-dimensional channel (the width is in the missing direction) per unit time. It can be shown that by substitution of 2.11 into 2.9 we obtain the physically meaningful equation:

$$(2.12)\quad \frac{\partial Q}{\partial t} = -\frac{Q}{(\eta+h)}\frac{\partial Q}{\partial x} - f\frac{Q|Q|}{(h+\eta)^2} - g(h+\eta)\frac{\partial \eta}{\partial x}$$

In the Eulerian respresentation of fluid behavior, the rate at which some arbitrary variable A=A(x,z,t) varies with time for a given moving parcel of fluid is called the material derivative, and is given by:

$$(2.13) \qquad \frac{DA(x,z,t)}{Dt} \equiv \frac{\partial A}{\partial t} + u\frac{\partial A}{\partial x} + w\frac{\partial A}{\partial z}$$

Making use of the material derivative, we obtain the boundary condition at the fluid surface:

$$(2.14) \qquad \frac{D(z-\eta(x,t))}{Dt} = -\frac{\partial \eta}{\partial t} - u\frac{\partial \eta}{\partial x} + w = 0 \text{ at } z = \eta$$

or, in terms of the vertical component of velocity:

$$(2.15) \qquad w = \frac{\partial \eta}{\partial t} + u\frac{\partial \eta}{\partial x} \text{ at } z = \eta$$

The boundary condition at the bottom of the fluid is:

$$(2.16) \qquad \frac{D}{Dt}(z+h(x)) = u\frac{\partial h}{\partial x} + w = 0 \text{ at } z = -h$$

or,

$$(2.17) \qquad w = -u\frac{\partial h}{\partial x} \text{ at } z = -h$$

Integrating the continuity equation (2.2) vertically through the water column we obtain:

$$(2.18) \qquad \int_{-h}^{\eta} \frac{\partial u}{\partial x} dz + \int_{-h}^{\eta} \frac{\partial w}{\partial z} dz = \int_{-h}^{\eta} \frac{\partial u}{\partial x} dz + w \Big|_{-h}^{\eta} = 0$$

Substitution of the boundary conditions (2.15) and (2.17) at the limits of integration yields:

$$(2.19)\qquad \frac{\partial \eta}{\partial t} + u\Big|_{z=\eta} \cdot \frac{\partial \eta}{\partial x} + u\Big|_{z=-h} \cdot \frac{\partial h}{\partial x} + \int_{-h}^{\eta} \frac{\partial u}{\partial x} dz = 0$$

With the application of Leibnitz's, rule equation (2.19) is reduced to :

$$(2.20)\qquad \frac{\partial \eta}{\partial t} + \frac{\partial}{\partial x} \int_{-h}^{\eta} u dz = 0$$

Because of the independence of u on the variable z, this is further reduced to:

$$(2.21)\qquad \frac{\partial \eta}{\partial t} = - \frac{\partial Q}{\partial x}$$

Equations (2.12) and (2.21) constitute the nonlinear shallow-water system of equations with allowance for friction. The terms included in the dynamical equation (2.12) represent, from left to right: the inertia term, the nonlinear longitudinal-advection momentum-term, the nonlinear friction term and the gravitational term.

The nonlinear advection term in equation (2.12) is almost always neglected in order to simplify the solution of the shallow water equations (Houston & Butler, 1979; Reid & Bodine, 1968; Platzman, 1953: Reid & Vastano, 1972; Wanstrath, 1978; Yeh & Chou, 1979; etc.). The justification for this linearization is based on the consideration that the ratio of $u\partial u/\partial x$ to $\partial u/\partial t$ is, for order of magnitude considerations, that of u^2/L to u/T, where L and T are the wavelength and period characteristic of the disturbance (Platzman, 1953). This reduces to u/c where c=L/T is the speed of propragation of the primary disturbance. It follows then that the advection term in equation (2.12) may be neglected wherever $u << c$. For long gravity waves, this condition is satisfied almost everywhere away from shore. This has greatly simplified the task of storm-surge modellers, who almost exclusively use linear equations with great success. For tsunami modellers, the

situation is more complicated. Ursell (1953) showed that we must use a nonlinear dispersive model, a linear dispersive model, or a nonlinear non-dispersive model depending on whether the Ursell number, $U=\eta_o L^2/H^3$, is of order unity, small, or large, respectively. Hammack and Segur (1977) generalized this concept and argued that the type of model used should be determined by the initial volume of the disturbance and the water depth rather than merely the amplitude and depth. They were able to show that tsunamis are never described by linear dispersive theory. For tsunamis impinging on harbors with resonance periods greater than 34-50 minutes, a nonlinear dispersive model must be used. In any event, wave behavior becomes highly nonlinear as shoaling begins. We may take as a measure of the wave nonlinearity η/D. Linear behavior is present only for $\eta/D<<1$ (Welander, 1961).

For the purpose of this experiment, it was assumed that the tsunami has been propagated onto the shelf, where our modeling begins. We retain the full nonlinear form of the shallow-water equations as we believe that accurate prediction of near-shore and inland inundation by a tsunami cannot be made without considering nonlinear effects.

Chapter III

FINITE DIFFERENCE ANALOGUE TO CONTINUUM EQUATIONS

The partial differential equations (2.12) and (2.21) describe smooth, unbroken fluid-motion. Their solution yields continuous functions $\eta(x,t)$ and $Q(x,t)$ that give the surface disturbance and volume transport at all points for all time. Yet, the effects of irregular boundaries, nonlinear interactions, variable physical properties, and arbitrary forcing wave combine to make the analytical solution of (2.12) and (2.21) a highly intractable problem. In general, to obtain the solution of a realistic problem requires a numerical approach (Lynch & Gray, 1978). The numerical method consists of discretizing the domain of interest by means of a finite grid overlay, then approximating the descriptive differential equations by algebraic equations. Time is also discretized, and all computations involve only values at the resulting discrete points. The solution takes the form of a numerical value computed separately for each discrete grid- and time-point, rather than a continuous function defined for infinitely many points.

There are virtually as many distinct numerical schemes for obtaining solutions to the governing equations (2.12) and (2.21) as there are investigators of the problem. Several broad classifications of the numerical schemes may be made based on various criteria. First, numerical schemes may be devised to approximate the governing equations in either Lagrangian or Eulerian form. Lagrangian formulations are characterized by a coordinate system that moves with the fluid, while Eulerian calculations employ a fixed grid. Lagrangian schemes have the advantage that they preserve discontinuities, but the coordinate mesh may become badly distorted for violent flows. Second, schemes may be classified as to whether they solve instead for the vorticity and stream function. Within each of the above classifications, schemes may be further categorized as

either finite-element or finite-difference. Within this categorization are the basic techniques such as marker-in-cell, particle-in-cell, CEL, LINC, Crank-Nicolson, leapfrog, split-step, Adams-Bashforth, Lax-Wendroff, Arakawa energy-conserving, real stabilization, artificial stabilization, semi-implicit, recursive and many more. For elucidation of these integrative techniques see Emmons (1970), Fromm (1970), Harlow and Amsden (1960), Kreiss and Oliger (1973), Roache (1972), Leendertse (1967), Strang (1968), Gourlay and Morris (1968), Miyakoda (1962), Forsythe and Wasow (1960), Dorodnicyn (1977), Kawahara, Takeuchi and Yoshida (1978), Kasahara (1965), Lynch and Gray (1978), Gray and Lynch (1977), Fischer (1965), Lilly (1965), Richtmeyer and Morton (1967), or Weare (1976).

Primarily for reasons of symmetry and simplicity, an explicit, time-centered, space-centered, split-step, finite-difference, leapfrog scheme was chosen to model our one-dimensional tsunami inundation problem. Although single-step space- and time-centered schemes applied to linearized versions of (2.12) and (2.21) can be shown to be unconditionally unstable, the same schemes applied to the advection term alone have been shown to exhibit some very desirable stability properties (Roache, 1972). Dorodnicyn (1977) showed that, all other things being equal, central difference experessions tend to reduce the truncation error from $O(\Delta x)$ to $O(\Delta x)^2$. Fischer (1965) found that leapfrog schemes give by far the best approximation to the true solution of the linearized equations, but Phillips (1959) observed that during nonlinear computations the leapfrog approximation may develop a nonlinear instability, which causes energy to cascade from longer to ever-shorter wavelengths. This nonlinear instability was in fact observed during this investigation, and methods were devised to reduce its effect (see Chapter X).

The computational grid used may be considered a linear arrangement of cells. At the center of each cell is a depth and a value for the surface disturbance representative of the cell, with the volume transport given at cell interfaces. The

depths and fluxes for each cell are out of phase in time by one half time step. In space-time the resulting grid may be depicted as a lattice, shown in Figure 3. The subscripts represent the cell location, and the superscripts denote the time step. With centering occurring at the location marked *, the resulting finite-difference analog to equation (2.12) is given by:

$$(3.1)\quad \frac{Q_j^{n+1}-Q_j^n}{\Delta t} = -gD_j^{n+\frac{1}{2}}\left(\frac{\eta_{j+\frac{1}{2}}^{n+\frac{1}{2}}-\eta_{j-\frac{1}{2}}^{n+\frac{1}{2}}}{\Delta x}\right)-\left(\frac{Q_j^n+Q_j^{n+1}}{2D_j^{n+\frac{1}{2}}}\right)\cdot DQDX-\frac{f\left(Q_j^n+Q_j^{n+1}\right)}{2\left(D_j^{n+\frac{1}{2}}\right)^2}\cdot\left|\frac{\left(Q_j^n+Q_j^{n+1}\right)}{2}\right|$$

Where $D_j^{n+\frac{1}{2}} = \left(h_{j-\frac{1}{2}}+\eta_{j-\frac{1}{2}}^{n+\frac{1}{2}}+h_{j+\frac{1}{2}}+\eta_{j+\frac{1}{2}}^{n+\frac{1}{2}}\right)/2$ represents the total fluid depth at the interface between cells j and j + 1 taken at time $t=(n+\frac{1}{2})\Delta t$. DQDX represents the finite-difference analog of $\partial Q/\partial x$, and will not be immediately evaluated. DQDX cannot be centered explicitly without using unknown values, hence, special approximations are required. Several approximations developed in Chapter V were studied, and their effects on model behavior are reported in Chapter X. The presence of the absoulute value in the frictional term (3.1) also complicated the analytical solution for Q_j^{n+1}. The dilemma's solution lies with the fact that the frictional term is relatively insensitive to small changes in Q. This makes it possible to first approximate Q by $\tilde{Q}$, disregarding the frictional term, then to use the result to evaluate the friction term. Q is then evaluated using $\tilde{Q}$ and the frictional term. In this way the couplet of equations is obtained:

$$(3.2)\quad \tilde{Q}_j^{n+1} = \left\{Q_j^n+gD_j^{n+\frac{1}{2}}\frac{\Delta t}{\Delta x}\left(\eta_{j-\frac{1}{2}}^{n+\frac{1}{2}}-\eta_{j+\frac{1}{2}}^{n+\frac{1}{2}}\right)-Q_j^n\frac{\Delta t}{2D_j^{n+\frac{1}{2}}}\cdot DQDX\right\}\Big/\left(1+\frac{\Delta t}{2D_j^{n+\frac{1}{2}}}\cdot DQDX\right)$$

$$(3.3)\quad Q_j^{n+1} = \left\{\tilde{Q}_j^{n+1}-\frac{\Delta t f}{\left(D_j^{n+\frac{1}{2}}\right)^2}\frac{\left(\tilde{Q}_j^{n+1}+Q_j^n\right)}{2}\cdot\left|\frac{\left(\tilde{Q}_j^{n+1}+Q_j^n\right)}{2}\right|\right\}\Big/\left(1+\frac{\Delta t}{2D_j^{n+\frac{1}{2}}}DQDX\right)$$

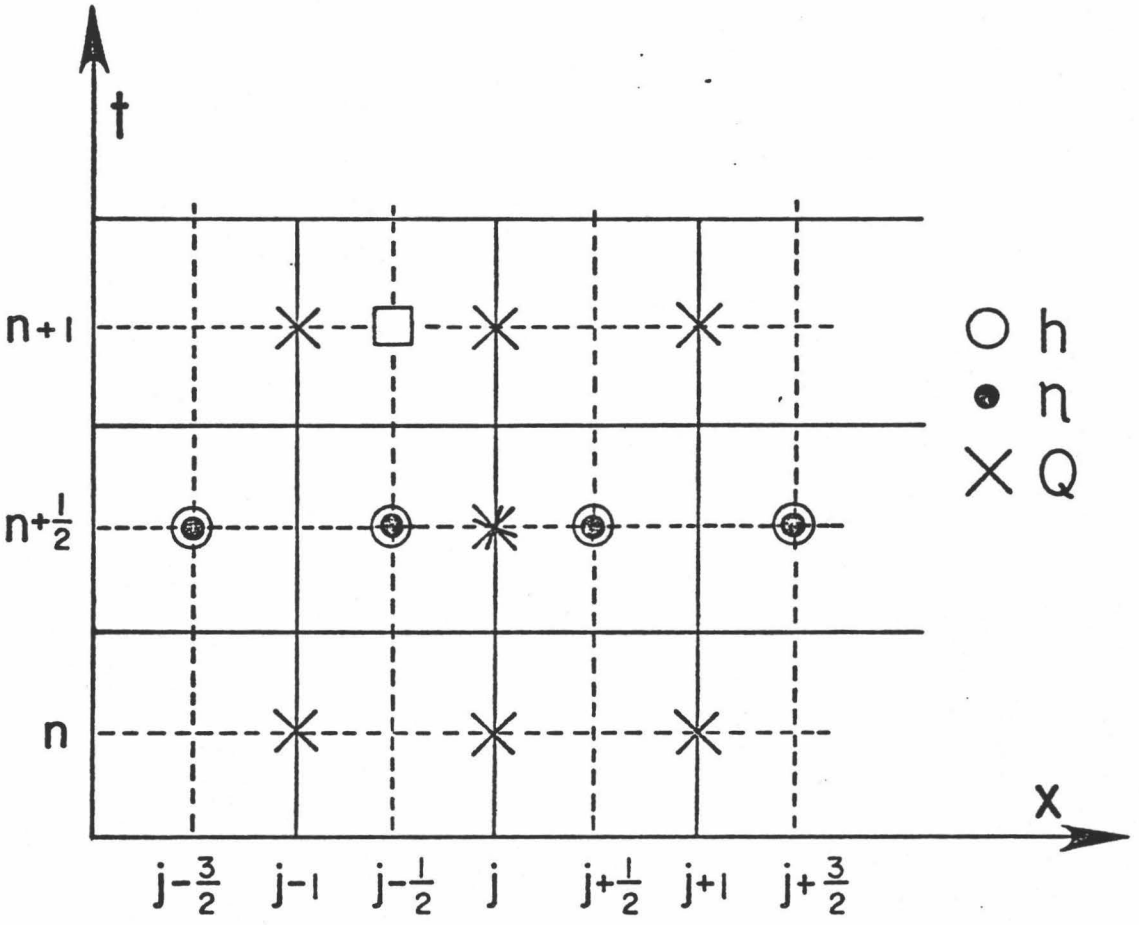

Figure 3. Computational grid system in x--t space.

In all experiments conducted during this investigation, Q was never observed to differ from $\tilde{Q}$ by more than 6%, providing an empirical a posteriori justification for the technique.

After values for the transport have been obtained for time step n+1 using equations (3.2) and (3.3), new values for the disturbance height in each cell are calculated for time step n=3/2. With centering at the location marked '□', the finite-difference approximation to equation (2.21) is:

$$(3.4) \qquad \frac{\eta_{j-\frac{1}{2}}^{n+3/2} - \eta_{j-\frac{1}{2}}^{n+\frac{1}{2}}}{\Delta t} = -\frac{\left(Q_j^{n+1} - Q_{j-1}^{n+1}\right)}{\Delta x}$$

giving as the value for the disturbance in cell j at time t=(n+3/2) t:

$$(3.5) \qquad \eta_{j-\frac{1}{2}}^{n+3/2} = \frac{\Delta t}{\Delta x}\left(Q_{j-1}^{n+1} - Q_j^{n+1}\right) + \eta_{j-\frac{1}{2}}^{n+\frac{1}{2}}$$

Equations (3.2), (3.3) and (3.5) constitute the finite-difference prognostic equations for modelling nonlinear shallow-water wave behavior. They constitute a split-step scheme, as values for the surface disturbance and volume transport are obtained a half time-step apart after each computational cycle: They are each explicit because solution for new values involves only known values from previous time steps after a special approximation to $\partial Q/\partial x$ has been obtained; and, they have the form of the midpoint-leapfrog scheme (Lilly, 1965), in that a value at a new time step is obtained as the sum of the value at an old time step and a change calculated at an intermediate time step, with all computations centered spatially as well as temporally.

CHAPTER IV

BOUNDARY CONDITIONS

The vertically integrated shallow-water equations (2.12) and (2.21) have an advantage over the primitive equations (2.1) and (2.2) in that the boundary conditions at the fluid bottom and surface have been incorporated in their derivation. This leaves, in general, three separate boundary conditions which must be considered during the modeling of a wave impinging upon dry land on a finite computational grid. They are: (1) the oceanside open-boundary, which is the artificial beginning of the computational grid system through which the wave enters; (2) the lateral boundaries, which are roughly perpendicular to the shoreline; and (3) the water-land interfaces. For open coastal areas, all three types of boundaries must be considered.

For the numerical modeling of tsunami flooding, it is assumed that the tsunami has been propagated from the source region, perhaps by the appropriate linear model, and knowledge of its amplitude is available at the oceanside boundary of the flooding computational grid. As the resolution desired in the area of flooding is usually much greater than that required for modeling open-ocean propagation, a fine and a coarse grid may be spliced together at this boundary (Thacker, 1976). Input of the wave into the flooding grid system is accomplished by forcing the oceanside boundary cell with the known tsunami amplitude at that location as a function of time. Thus:

$$(4.1) \qquad \eta_j^{n+3/2} = \eta_o(\tfrac{1}{2}\Delta x,\ (n+3/2)\Delta t)$$

The proper treatment of lateral boundaries is a matter of some controversy. Reid and Bodine (1968) employed a radiative lateral boundary condition, where the

surface disturbance was assumed to be zero off the grid system. A more commonly used specification is that the gradient of the surface disturbance be zero across the lateral boundaries, with the requirement that the lateral boundaries be located perpendicular to the bottom contours. Problems associated with misalignment of these boundaries can be alleviated by their emplacement far from the region of interest.

Many approaches have been formulated to simulate non-reflecting open boundaries of the previous two types, mostly without success (Elvius & Sundstrom, 1973; Orlianski, 1976; Platzman, 1958; Sklarz & Spielvogel, 1979; Wurtele & Sielecki, 1971). The most common complaint was that spurious oscillations would arise at the artificial boundary and propagate inward to contaminate the results. Platzman (1958) observed that the easiest method of dealing with the problem is to simply make all the boundaries totally reflecting and far enough from the region of interest that the reflected waves do not reach the region of interest until the desired results have been obtained. Sklarz and Spielvogel (1979) developed an ingenious method whereby at each time step the boundaries are first treated as fixed (Dirichlet condition) and then free (Neumann condition), with a solution computed for each case. The reflected waves resulting from each case are equal in magnitude but opposite in sign; hence the two solutions obtained at each time step may be averaged to cancel the artificial reflections. They reported a doubling of the useful time history achieved in this manner.

During the course of this work, a novel technique was developed that permits reflected waves travelling normal to open boundaries to be totally transmitted through the boundaries. Making the assumption that at the interface between the first and second cells nearest the oceanside boundary:

$$(4.2) \qquad \left(\frac{1}{gD}\ \frac{\partial Q}{\partial t}\right)_{\substack{t=(n+3/2)\Delta t \\ x=\Delta x}} \doteq \left(\frac{1}{gD}\ \frac{\partial Q}{\partial t}\right)_{\substack{t=(n+1/2)\Delta t \\ x=\Delta x}}$$

and using the relationship (2.12) without the friction and advection of momentum terms gives, after the usual finite-difference formulation described previously:

$$(4.3) \qquad \eta_{1\frac{1}{2}}^{n+3/2} = \frac{\Delta x}{\Delta t} \cdot \frac{Q_1^{n+1} - Q_1^n}{gD_1^{n+\frac{1}{2}}} + \tilde{\eta}_{3/2}^{n+3/2}$$

where $\tilde{\eta}_{3/2}^{n+3/2}$ denotes an approximation to $\eta_{3/2}^{n+3/2}$ obtained by appropriate weighting of surrounding depths at previous time steps:

$$(4.4) \qquad \tilde{\eta}_{3/2}^{n+3/2} = 2\eta_{3/2}^{n+\frac{1}{2}} - \frac{\eta_{1\frac{1}{2}}^{n-\frac{1}{2}} + \eta_{5/2}^{n-\frac{1}{2}}}{2}$$

No assumptions were made regarding the state of the fluid outside the computational grid in this method, the surface disturbance in the first oceanside boundary cell merely assumed a value consistent with the behavior in the next two cells. It should be noted that it would be inappropriate to apply this expected-conformance scheme while the first cell was being forced during the wave-input phase. A similar procedure could be implemented after slight modification at lateral boundaries, but was not needed for this work.

By far the most critical boundary condition for tsunami flooding models is that used for the cells representing the moving water-land interface. Unfortunately, it is also the least well-formulated, as there are numerous difficulties connected with its implementation in any realistic manner (Yeh & Chou, 1979). Many early investigators of storm-surge modeling simply assume a no-flow condition equivalent to an inpenetrable vertical wall at the shoreline (Jelesnianski, 1965; Wanstrath, 1978; Wanstrath et al., 1976; Welander, 1961). Improvements on this method were made by some who permitted overtopping of the shoreline with the use of empirical weir-type formulae (Reid & Bodine, 1968) and predictor-corrector methods whereby water above a certain height was

skimmed off one cell and placed in the adjacent cell (Wantrath, 1978). Although the no-flow boundary condition is the easiest one to apply at the water-land interface, there are numerous problems associated with its use. The work of Yeh and Chou (1979) demonstrated that, as intuitively expected, the no-flow condition was sound only when applied to a shore with a very steep slope inland; otherwise, its use consistently overestimated the surface disturbance to be expected at the original shoreline. Another problem with this type of treatment is that coasts with varying curvature are usually represented by a boundary of many short walls meeting perpendicularly, forming a many-cornered totally reflecting boundary. This generally produces highly undersirable computational artifacts exactly in the region of greatest interest (Sielecki & Wurtele, 1970). Also, attempts to predict the extent of inland inundation by extrapolation of the disturbance surface across the imaginary shoreline-barrier violates basic physical principles. First, the extrapolation obviously involves a mass deficit; hence, continuity of matter is violated; and second, specifying a zero velocity across the boundary prevents the real deficit in momentum that the system would experience due to the not-insignificant frictional losses in the very shallow water at the shoreline. This results in total reflection from the shoreline, whereas in reality the reflection would be imperfect (Lynch & Gray, 1978).

The only realistic water-land interface boundary condition is that of allowing the instantaneous shoreline to determine its own position in obeyance to the shallow-water prognostic equations. Several pioneering attempts have been made in this direction, notably those of Sielecki and Wurtele (1970), Lynch and Gray (1978), and Yeh and Chou (1979). Lynch and Gray (1978) developed a finite-element model that tested several approximations to the condition of zero depth at a moving boundary. They concluded that frictional losses incurred at moving boundaries produce a dramatic effect throughout the computational domain not

observed with the no-flux boundary condition. Sielecki and Wurtele (1970) developed a method to extrapolate water into the first dry inland-cell, and then to include it in the normal calculations. Yeh and Chou (1979) simply included a dry cell in the calculations if a neighboring cell contained water at a level above the height of the dry cell. The method of Sielecki and Wurtele had the advantage of reducing the kink at the leading edge of the advancing fluid which tends to produce numerical noise. Both methods were philosophically sound and successful for the cases tested; however, the results of this work indicate that both methods are valid only when the bathymetry is very smooth. When there is a significant change in depth from one cell to the next, both methods fail.

During the course of this work, the previously-mentioned water-land boundary conditions were tested on a "proving ground" of varying bathymetry and topography. As a result of considering the subsequent model performances, a heuristic refinement of the assignment of depths at grid cell interfaces was made, consistent with the stair-step nature of the bathymetry and topography representation. It is believed that the resulting model is valid for any degree of discontinuity between cells.

CHAPTER V

SPECIAL APPROXIMATIONS TO THE ADVECTIVE TERM

It is not possible to derive an explicit difference expression for $\partial Q/\partial x$ centered at the location marked * in Figure 2 , as Q_{i+1}^{n+1} is undetermined. In fact, even if Q_{i+1}^{n+1} were known, the centered expression for $\partial Q/\partial x$ would consist of a time average between time steps n and n+1. For the purpose of this experiment, three methods of approximating $\partial Q/\partial x$ at cell i and time step n+½ were devised:

Method 1. Straightforward time extrapolation.

As illustrated in Figure 4, finite difference expressions for $\partial Q/\partial x$ centered at cell i are evaluated at time steps n-1 and n using the known values Q_{i-1}^{n-1}, Q_{i+1}^{n+1}, Q_{i-1}^{n} and Q_{i+1}^{n}. This gives:

$$(5.1) \qquad \left.\frac{\partial Q}{\partial x}\right|_{\substack{x=i\Delta x \\ t=(n-1)\Delta t}} = \frac{Q_{i+1}^{n-1} - Q_{i-1}^{n-1}}{2\Delta x}$$

and

$$(5.2) \qquad \left.\frac{\partial Q}{\partial x}\right|_{\substack{x=i\Delta x \\ t=n\Delta t}} = \frac{Q_{i+1}^{n} - Q_{i-1}^{n}}{2\Delta x}$$

The results are then linearly extrapolated to the time step n+½, giving:

$$(5.3) \qquad DQDX_1 = \left[3Q_{i+1}^{n} - 3Q_{i-1}^{n} - Q_{i+1}^{n-1} + Q_{i-1}^{n-1} \right] /4\Delta x$$

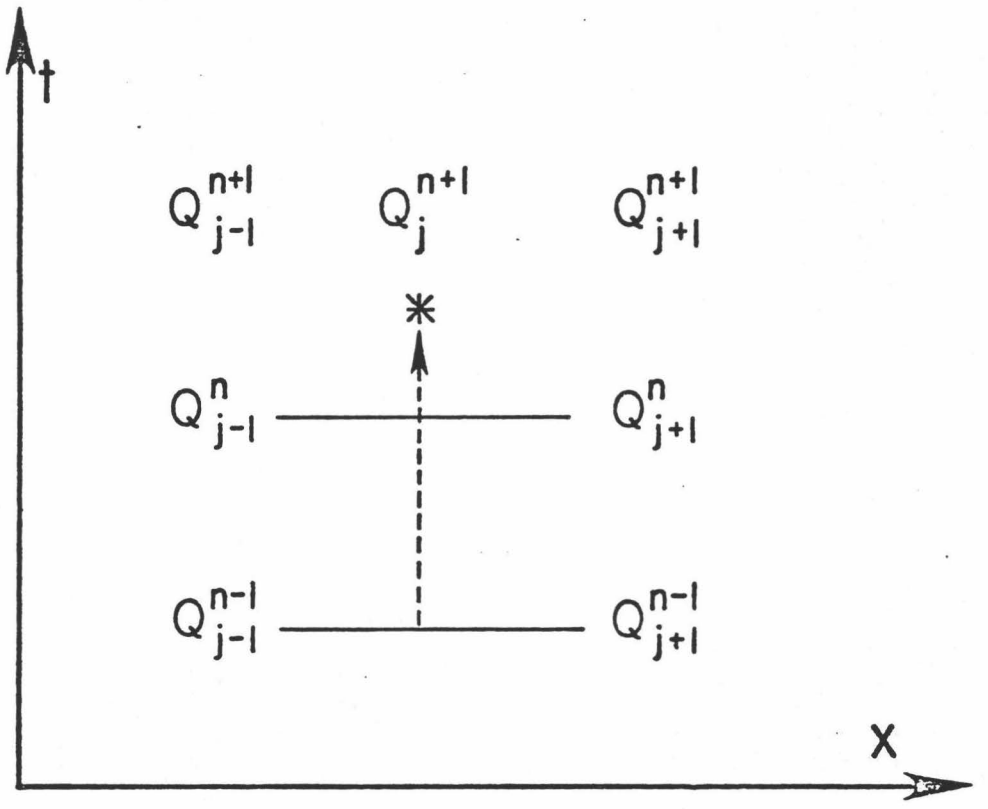

Figure 4. Straightforward time extrapolation scheme for approximating $\partial Q/\partial x$. Solid lines connect values used in calculation; dotted lines shows sense of extrapolation.

Method 2. Diagonal extrapolation.

In this method, an approximation for Q_{i+1}^{n+1} is first obtained, followed by time averaging of $\left(\frac{\partial Q}{\partial x}\right)_{\substack{x=i\Delta x \\ t=(n+1)\Delta t}}$ and $\left(\frac{\partial Q}{\partial x}\right)_{\substack{x=i\Delta x \\ t=n\Delta t}}$ to obtain DQDX. Q_{i+1}^{n+1} is approximated as the average of two extrapolations: One is taken through space-time, beginning with Q_{i-1}^{n-1} and proceeding through Q_i^n to give Q_{i+1}^{n+1}; The other is a simple extrapolation of Q through time at cell i+1 as shown in Figure 5. The resulting approximation of Q_{i+1}^{n+1} is:

$$(5.4) \qquad Q_{i+1}^{n+1\prime} = Q_i^n - \frac{Q_{i-1}^{n-1}}{2} + Q_{i+1}^n - \frac{Q_{i+1}^{n-1}}{2}$$

giving

$$(5.5) \qquad DQDX_2 = \frac{1}{4\Delta x}\left(Q_{i+1}^{n+1\prime} - Q_{i-1}^{n+1} + Q_{i+1}^n - Q_{i-1}^n\right)$$

The motivation for developing this method was to incorporate the known value Q_{i-1}^{n+1} and to more closely approximate structurally a space- and time-centered finite-difference formulation of the advective term. The stability of the numerical evaluation of Q_i^{n+1} was enhanced upon application of this scheme, but an undersirably strong "handedness" also became apparent (see Chapter X). Here, handedness is taken to mean the tendency to favor, in some way, one component of a multi-component symmetry.

Method 3. Right-handed time extrapolation.

In this method an approximation for $Q_{i+1}^{n+\frac{1}{2}}$ is obtained by linear extrapolation of Q_{i+1}^{n-1} and Q_{i+1}^n, as illustrated in Figure 6. $Q_{i-1}^{n+\frac{1}{2}}$ is approximated by time averaging of Q_{i-1}^n and Q_{i-1}^{n+1}. As DQDX is ultimately defined as $\frac{Q_{i+1}^{n+\frac{1}{2}} - Q_{i-1}^{n+\frac{1}{2}}}{2\Delta x}$, we

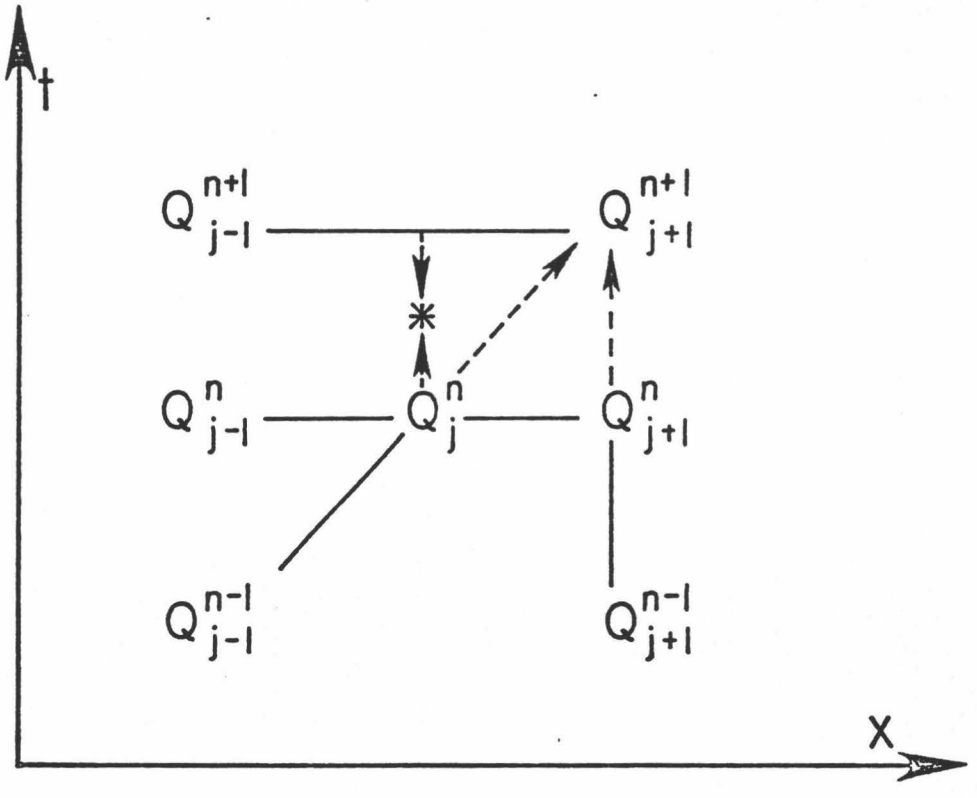

Figure 5. Diagonal extrapolation scheme for approximating $\partial Q/\partial x$.

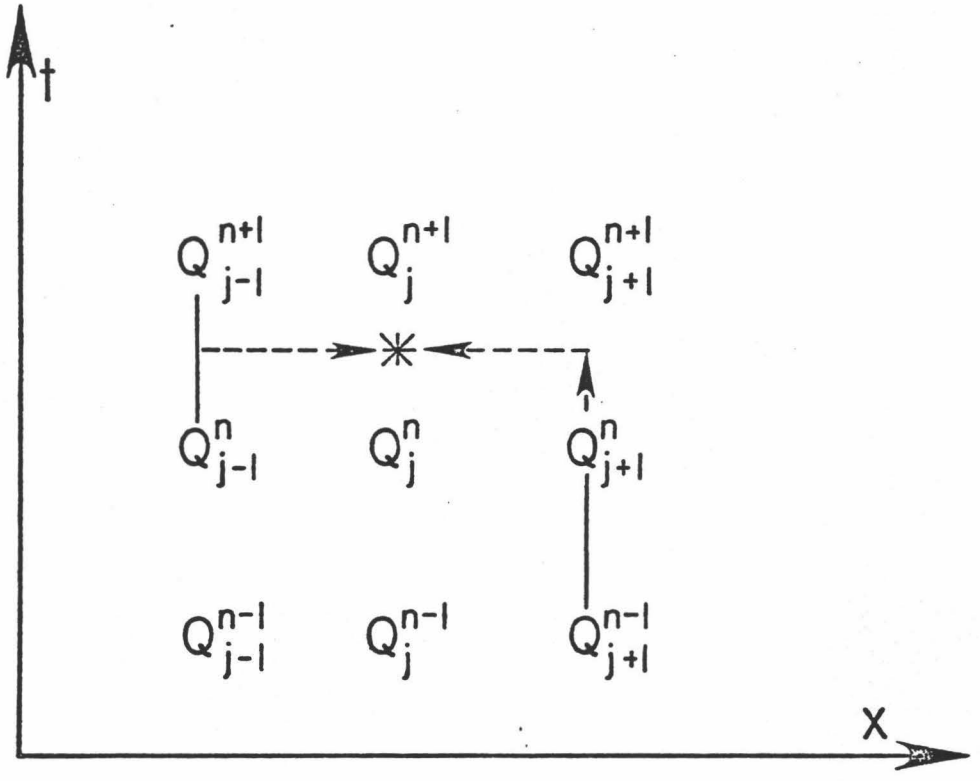

Figure 6. Right-handed time extrapolation scheme for approximating $\partial Q/\partial x$.

obtain in terms of previously computed values:

$$(5.6) \qquad DQDX_3 = \frac{3Q_{i+1}^{n} - Q_{i+1}^{n-1} - Q_{i-1}^{n} - Q_{i-1}^{n+1}}{4\Delta x}$$

The motivation for development of this method was the strong handedness and moderate instabilities encountered with application of the previous two methods. By avoiding excessive weighting of fluxes located inappropriately in space and time, improvement in model behavior was expected. Although some handedness is obviously present in this scheme, it is minimal, and the most promising model behavior was associated with this method.

CHAPTER VI

STABILITY ANALYSIS

The nonliniear shallow-water equataions (2.12) and (2.21) constitute an initial-value problem. If the state of the represented physical system is specified at time $t=t_0$, then a solution exists for all $t \geq t_0$ and is uniquely determined by the governing equations together with the boundary conditions. However, when the partial differential equations are replaced by their finite-difference approximations, some error is generally produced in the resulting solution. If a component of the error grows without bound as the solution is evaluated through time, the finite-difference system is said to be unstable. As the mathematical foundations for investigations of stability of numerical schemes are well-developed only for linear systems, the results of linear theory are used as guidelines for nonlinear problems (Roache, 1972). The most commonly used method of stability analysis was developed by Von Neumann (Charney, Fjortoft, & Von Neumann, 1950), and is apparently the most dependable (Roache, 1972). The method consists of representing the solution to the finite-difference equations by a Fourier series expansion, and considering the amplification or decay with time of each harmonic with time separataely to determine stability. The Von Neumann stability analysis was applied to three linearized approximations of equations (2.12) and (2.21), following closely the treatment of Richtmeyer and Morton (1967).

Stability of basic linearized governing equations

Consider the linearized equation:

$$\frac{\partial Q}{\partial t} = -g\bar{D}\,\frac{\partial \eta}{\partial x} \tag{6.1}$$

This equation, together with (2.21), constitute a linear approximation to the nonlinear shallow-water equations of sufficient simplicity to permit a rigorous stability analysis. Variable depth, vertical advection of momentum and frictional effect are not considered.

Approximating (6.1) and (2.12) by a space- and time-centered split step leapfrog scheme yields, after slight rearrangement:

$$(6.2) \qquad Q_i^{n+1} = Q_i^n - \frac{\Delta t}{\Delta x} g\bar{D} \left(\eta_{i+\frac{1}{2}}^{n+\frac{1}{2}} - \eta_{i-\frac{1}{2}}^{n+\frac{1}{2}} \right)$$

and (3.5).

Assuming we may represent the spatial variation in the volume transport and the surface disturbance by a superposition of trigonometric functions we can write:

$$(6.3) \qquad Q_j^n = \sum_{k=-\infty}^{\infty} Q^n e^{ikj\Delta x}$$

$$(6.4) \qquad \eta_j^n = \sum_{k=-\infty}^{\infty} \eta^n e^{ikj\Delta x}$$

As the system under consideration is linear, and the Fourier series is actually finite due to the finite nature of the computing lattice, it will be sufficient to consider the stability of a single arbitrary mode of the solution. We may write:

$$(6.5) \qquad \begin{aligned} Q_j^n &= Q^n e^{ikj\Delta x} \\ Q_j^{n+1} &= Q^{n+1} e^{ikj\Delta x} \\ Q_{j-1}^{n+1} &= Q^{n+1} e^{ik(j-1)\Delta x} \end{aligned}$$

(6.5) continued

$$\eta_{j+\frac{1}{2}}^{n+\frac{1}{2}} = \eta^{n+\frac{1}{2}} e^{ik(j+\frac{1}{2})\Delta x}$$

$$\eta_{j-\frac{1}{2}}^{n+\frac{1}{2}} = \eta^{n+\frac{1}{2}} e^{ik(j-\frac{1}{2})\Delta x}$$

$$\eta_{j-\frac{1}{2}}^{n+3/2} = \eta^{n+3/2} e^{ik(j-\frac{1}{2})\Delta x}$$

Substitution of equations (6.5) into (6.2) and (3.5) gives, after some manipulation:

$$(6.6) \qquad Q^{n+1} = Q^n - \frac{\Delta t}{\Delta x} g\bar{D} \left(e^{ik\frac{\Delta x}{2}} - e^{-ik\frac{\Delta x}{2}} \right) \eta^{n+\frac{1}{2}}$$

$$(6.7) \qquad \eta^{n+3/2} = \frac{\Delta t}{\Delta x} \left(e^{-ik\frac{\Delta x}{2}} - e^{ik\Delta x/2} \right) Q^{n+1} + \eta^{n+\frac{1}{2}}$$

After applying Euler's identity,

$$(6.8) \qquad e^{i\theta} = \cos\theta + i\sin\theta$$

and substituting (6.6) into (6.7), the predictive equations become:

$$(6.9) \qquad Q^{n+1} = Q^n - 2i\frac{\Delta t}{\Delta x} g\bar{D} \sin(\tfrac{1}{2}k\Delta x)\eta^{n+\frac{1}{2}}$$

$$(6.10) \qquad \eta^{n+3/2} = -2i\frac{\Delta t}{\Delta x}\sin(\tfrac{1}{2}k\Delta x)Q^n + \left(1-4\left(\frac{\Delta t}{\Delta x}\right)^2 g\bar{D} \sin^2(\tfrac{1}{2}k\Delta x)\right)\eta^{n+\frac{1}{2}}$$

Upon making the substitutions

$$(6.11) \qquad c \equiv \frac{\Delta t}{\Delta x}; \qquad \theta \equiv \tfrac{1}{2}k\Delta x; \qquad \alpha \equiv 2c\sin\theta.$$

the matrix equations relating new time functions to old is obtained:

$$(6.12) \qquad \begin{pmatrix} Q^{n+1} \\ \eta^{n+3/2} \end{pmatrix} = G \begin{pmatrix} Q^{n} \\ \eta^{n+1/2} \end{pmatrix}$$

G is known as the amplification matrix, and is given by:

$$(6.13) \qquad G = \begin{pmatrix} 1 & -i\alpha g\bar{D} \\ -i\alpha & 1 - \alpha^2 g\bar{D} \end{pmatrix}$$

The Von Neumann condition for stability may be written:

$$(6.14) \qquad |\lambda|_{(\ell)} \leq 1 + O(\Delta t)$$

where $|\lambda|_{(\ell)}$ represents the largest absolute value of the eigenvalues, of G, and $Q(\Delta t)$ is to be read as "terms of the first order in Δt". The presence of the $O(\Delta t)$ term is to permit "legitimate" exponential growth in the solution (Richtmyer & Morton, 1967). As the Von Neumann necessary condition is also sufficient to insure stability only when G is a normal matrix, i. e., when $G^{*}G-GG^{*}=0$ (Richtmeyer and Morton, 1967), the slightly more restrictive condition will be adopted herein:

$$(6.15) \qquad |\lambda|_{(\ell)} \leq 1$$

The eigenvalues of the amplification matrix may be obtained by solving for the roots of the characteristic equation:

(6.16) $\quad \mathrm{Det}(G-\lambda I) = \lambda^2 + \lambda(\alpha^2 g\bar{D} - 2) + 1 = 0$

This gives:

(6.17) $\quad \lambda = 1 + \frac{\alpha^2 g\bar{D}}{2}\left(-1 \pm \sqrt{1 - 4/\alpha^2 g\bar{D}}\right)$

The eigenvalues given by (6.17) will be real or complex, depending on the sign of the expression under the radical.

Case 1. Real eigenvalues.

If the eigenvalues are real, then $\alpha^2 gD \leq 4$; or, equivalently: $\Delta t \leq \frac{\Delta x}{\sqrt{g\bar{D}}}$ and the largest eigenvalue magnitude is:

(6.18) $\quad |\lambda|_{(\ell)} = \left|1 - \frac{\alpha^2 g\bar{D}}{2}\left(1 + \sqrt{1 - 4/\alpha^2 g\bar{D}}\right)\right|$

To satisfy the stability condition (6.15) it is obviously necessary that:

(6.19) $\quad \frac{\alpha^2 g\bar{D}}{2}\left(1 + \sqrt{1 - 4/\alpha^2 g\bar{D}}\right) \leq 2$

But (6.19) is only satisfied for $\alpha^2 gD \leq 4$, i.e., $\Delta t \leq \frac{\Delta x}{\sqrt{g\bar{D}}}$ hence, the stability requirement is contradictory to the real nature of the associated eigenvalue, except marginally for the single choice of: $\Delta t = \frac{\Delta x}{\sqrt{g\bar{D}}}$.

Case 2. Complex eigenvalues.

If $\alpha^2 g\bar{D} < 4$ then the amplification matrix eigenvalues are complex, and are

given by:

$$(6.20) \qquad \lambda = 1 + \frac{\alpha^2 g\bar{D}}{2}\left(-1 \pm i\sqrt{4/\alpha^2 g\bar{D} - 1}\right)$$

The magnitude of the pair of complex conjugate eigenvalues is unity; hence, for

$$(6.21) \qquad \frac{\Delta t}{\Delta x} \leq \frac{1}{\sqrt{g\bar{D}}}$$

the Von Neumann necessary condition for stability of the system (6.2) and (3.5) is marginally satisfied.

Stability of the linearized governing equations with friction

When a frictional term proportional to the volume transport and inversely proportional to a representative depth is considered, the linearized approximation to (2.12) becomes:

$$(6.22) \qquad \frac{\partial Q}{\partial t} + f\frac{Q}{\bar{D}} + g\bar{D}\frac{\partial \eta}{\partial x} = 0$$

Applying a midpoint leapfrog split-step finite-difference operator to (6.22) gives, after some rearrangement:

$$(6.23) \qquad Q_i^{n+1} = \left\{ Q_i^n \left(\frac{1}{\Delta t} - \frac{f}{2\bar{D}} \right) - \frac{g\bar{D}}{\Delta x}\left(\eta_{i+\frac{1}{2}}^{n+\frac{1}{2}} - \eta_{i-\frac{1}{2}}^{n+\frac{1}{2}}\right) \right\} \Big/ \left(\frac{1}{\Delta t} + \frac{f}{2\bar{D}}\right)$$

Considering, as before, only one component in the Fourier expansion of the soulution, and using (6.5) and (6.8) gives:

$$(6.24) \qquad Q^{n+1} = \left(\frac{2\bar{D} - f\Delta t}{2\bar{D} + f\Delta t}\right) Q^n - i4g\frac{\bar{D}^2 c \sin\theta}{2\bar{D} + f\Delta t}\eta^{n+\frac{1}{2}}$$

Substitution of (6.24) into the unchanged finite difference expression for the surface disturbance (6.7) yields:

$$(6.25)\qquad \eta^{n+\frac{1}{2}} = -2ic\sin\theta\,\frac{2\bar{D}-f\Delta t}{2\bar{D}+f\Delta t}\,Q^{n} + \left(1 - 8g\,\frac{\bar{D}^2c^2\sin^2\theta}{2\bar{D}+f\Delta t}\right)\eta^{n+\frac{1}{2}}$$

If we let:

$$(6.26)\qquad \beta \equiv c\sin\theta;\quad \gamma \equiv 2\bar{D} + f\Delta t;\quad \delta \equiv \frac{2\bar{D} - f\Delta t}{\gamma};\quad \mu \equiv 4g\bar{D}^2$$

then we get, for the resulting amplification matrix defined by (6.12):

$$(6.27)\qquad G = \begin{pmatrix} \delta & -i\mu\beta/\gamma \\ -2i\beta\delta & 1-2\mu\beta^2/\gamma \end{pmatrix}$$

The eigenvalues of the amplification matrix are then:

$$(6.28)\qquad \lambda_1 = \frac{1 + \delta - P+\sqrt{(p-\delta-1)^2 + 4(2P - 1)}}{2}$$

$$(6.29)\qquad \lambda_2 = \frac{1 + \delta - P - \sqrt{(p-\delta-1)^2 + 4(2P-1)}}{2}$$

where the additional substitution has been made:

$$(6.30)\qquad P \equiv 2\mu\beta^2/\gamma$$

It is readily seen that, depending on which eigenvalue has the larger magnitude, there exist two possible criteria necessary to insure the stability of the system (6.23) and (6.7):

(6.31) $|\lambda_1| \geq |\lambda_2| \rightarrow P \leq 1 - \delta$

(6.32) $|\lambda_1| \leq |\lambda_2| \rightarrow P \leq 1 + \frac{\delta}{3}$

Which criterion is the more restrictive will depend on whether δ is less than or greater than zero.

Case 1. $\delta > 0$

$\delta > 0$ implies that (6.31) is the appropriate stability condition. After substituting (6.26) and (6.30) into (6.31), and rearranging, the stability requirement becomes:

(6.33) $4g\bar{D}^2\Delta t^2 \sin^2(\frac{1}{2}k\Delta x) \leq f\Delta t\Delta x^2$

This is certainly satisfied by the more restrictive condition:

(6.34) $4g\bar{D}^2\Delta t^2 \leq f\Delta t\Delta x^2$

giving, as the necessary Von Neuman stability condition:

(6.35) $\frac{\Delta t}{(\Delta x)^2} \leq \frac{f}{4g\bar{D}^2}$

Case 2. δ less than zero

When $\delta<0$ it is true that:

(6.36) $f\Delta t>2\bar{D}$

and the stability requirement (6.32) becomes:

$$(6.37) \qquad 12g\bar{D}^2\sin^2(\tfrac{1}{2}k\Delta x)\Delta t^2 \leq (4\bar{D} + f\Delta t)\Delta x^2$$

Making use of (6.36) and eliminating the sine term yields the more restrictive condition:

$$(6.38) \qquad \frac{\Delta t}{\Delta x} \leq \frac{1}{\sqrt{2g\bar{D}}}$$

This is the well-known Courant-Friedrichs-Lewi criterion for hyperbolic systems (Lax, 1967). It obviously is also the required condition when δ =0. (6.35) is a more stringent constraint on the choice of Δt when:

$$(6.39) \qquad \Delta x \leq \sqrt{8g\bar{D}^3/f}$$

When Δx is greater than the above critical value, then (6.38) is the stricter criterion.

Stability of linearized governing equations with advection.

Consider the linearized equation:

$$(6.40) \qquad \frac{\partial Q}{\partial t} + g\bar{D}\frac{\partial \eta}{\partial x} + \frac{U}{\bar{D}}\frac{\partial Q}{\partial x}$$

The form of (6.40) is similar to that of (2.21), neglecting friction. Here U is taken to be a representative value of the volume transport, rather than the variable transport appearing in (2.21). For a finite-difference approximation of (6.40) to be centered in space and time at $x=j\Delta x$ and $t=(n+\frac{1}{2})\Delta t$, it is necessary to

approximate $\left(\frac{\partial Q}{\partial x}\right)_{x=j\Delta x}$ at $t=(n+\frac{1}{2})\Delta t$. As the volume transport is not known at that time, it will be assumed for this analysis that $\left(\frac{\partial Q}{\partial x}\right)_{\substack{x=j\Delta x \\ t=(n+\frac{1}{2})\Delta t}}$ can be approximated by $A\left(\frac{\partial Q}{\partial x}\right)_{\substack{x=j\Delta x \\ t=n\Delta t}}$. The resulting finite-difference scheme for evaluating the volume transport is given by:

$$(6.41) \qquad Q_j^{n+1} = Q_j^n - g\bar{D}\frac{\Delta t}{\Delta x}\left(\eta_{j+\frac{1}{2}}^{n+\frac{1}{2}} - \eta_{j-\frac{1}{2}}^{n+\frac{1}{2}}\right) - \frac{AU}{2\bar{D}}\frac{\Delta t}{\Delta x}\left(Q_{j+1}^n - Q_{j-1}^n\right)$$

Considering a single arbitrary component of the Fourier series expansion of the solution to (6.41) as before yields:

$$(6.42) \qquad Q^{n+1} = \left(1 - i\frac{AU}{\bar{D}}\frac{\Delta t}{\Delta x}\sin(k\Delta x)\right)Q^n - i2g\bar{D}\frac{\Delta t}{\Delta x}\sin(\tfrac{1}{2}k\Delta x)\eta^{n+\frac{1}{2}}$$

The corresponding expression for the surface disturbance is:

$$(6.43) \qquad \eta^{n+3/2} = -2c\sin(\tfrac{1}{2}k\Delta x)\left(i + \frac{AU}{\bar{D}}\frac{\Delta t}{\Delta x}\sin(k\Delta x)\right)Q^n + \left(1 - 4\left[\frac{\Delta t}{\Delta x}\right]^2 g\bar{D}\sin^2(\tfrac{1}{2}k\Delta x)\right)\eta^{n+\frac{1}{2}}$$

Forming the amplification matrix and solving the charactistic equation gives as eigenvalues:

$$(6.44) \qquad \lambda = \frac{2 - \psi - i\sin 2\theta \pm \sqrt{-4\psi - \sin^2 2\theta + i\psi 2\sin 2\theta(2 \quad - 1)}}{2}$$

where,

$$(6.45) \qquad \psi \equiv 4\left[\frac{\Delta t}{\Delta x}\right]^2 g\bar{D}\sin^2\theta; \qquad \phi \equiv \frac{AU}{\bar{D}}\frac{\Delta t}{\Delta x}$$

Separating the real and imaginary parts of (6.45) by solving for the square root gives as the complex eigenvalues:

$$(6.46) \qquad \lambda = 1 - \frac{\psi}{2\sin^2\theta} \pm \tfrac{1}{2}\sqrt{r - \frac{b}{2}} - i\left[\frac{\sin 2\theta}{2} \pm \tfrac{1}{2}\sqrt{r + \frac{b}{2}}\right]$$

The square of the largest magnitude is then given by:

$$(6.47) \qquad |\lambda|^2_{(\ell)} = (1-a)^2 + \left(1 + \frac{\sin 2\theta}{2} - a\right)m + \frac{2m^2 + b + \sin^2 2\theta}{4} \leq 1$$

where it has been assumed that at least the Courant-Friedrichs-Lewi criterion holds, and the following additional substitutions have been made:

$$(6.48) \quad a \equiv \psi/2\sin^2\theta; \qquad r \equiv \tfrac{1}{2}\sqrt{(16c^2g\bar{D}+\sin^2 2\theta)^2 + \sin^2 2\theta \cdot 64c^4g^2(\bar{D}-2cAU)^2};$$

$$b \equiv 4\psi/\sin^2\theta + \sin^2 2\theta; \qquad m = \sqrt{r - \frac{b}{2}}$$

Explicit solution of (6.47) to obtain an exact condition which must be satisfied by $\frac{\Delta t}{\Delta x}$ to guarantee stability of the finite-difference system is a difficult matter. An examination of the first term of (6.47) will reveal that at least the condition $a \leq 2$, or $\Delta t \leq \frac{\Delta x}{\sqrt{g\bar{D}}}$ must be met. This condition is already satisfied by the earlier assumption that $\Delta t \leq \frac{\Delta x}{\sqrt{2g\bar{D}}}$. A further constraint on the permissible values for $\frac{\Delta t}{\Delta x}$ may be obtained as follows: First, note that in order for (6.47) to be satisfied, the restrictions on m are:

$$(6.49) \qquad \frac{2a-3-\sqrt{-4a^2+20a-5+2\sin^2 2\theta}}{2} \leq m \leq \frac{2a-3+\sqrt{-4a^2+20a-5+2\sin^2 2\theta}}{2}$$

Because m is always real, as can be seen from its definition in (6.48), we must have:

$$(6.50) \qquad -4a^2 + 20a - 5 + 2\sin^2 2\theta \geq 0$$

and this in turn implies:

$$(6.51) \qquad a \leq \frac{5 + \sqrt{20}}{2}$$

or, in terms of fundamental variables:

$$(6.52) \qquad \frac{\Delta t}{\Delta x} \leq \sqrt{\frac{5 + \sqrt{20}}{2}} \cdot \frac{1}{\sqrt{2g\bar{D}}}$$

(6.52) is automatically satisfied by the previous restriction of $\frac{\Delta t}{\Delta x}$ to values given by the Courant-Friedrichs-Lewi criterion.

In conclusion, the most restrictive condition necessary to insure the stability of each of the three linearized finite-difference schemes considered in this chapter is given by:

$$(6.53) \qquad \Delta t \leq \frac{f\Delta x^2}{4g\bar{D}}$$

when (6.39) is satisfied for the frictional case. This stability requirement provides a first approximation to that required for the more general nonlinear case with variable coefficients.

CHAPTER VII

TRUNCATION ERROR AND CONSISTENCY

The truncation error is defined as the difference between a differential equation and its finite-difference formulation, and is a measure of how closely the solution of a finite-difference scheme approximates the genuine solution of the original differential equation. For this analysis the finite-difference formulation for the surface disturbance, (3.5), and the differential equation (2.21) will first be examined; then the linearized volume transport equation with advection, (6.40) and its finite-difference formulation will be examined. Similar results were found to hold for the remaining two linearized equations and their finite-difference appproximations, so they will not be treated here.

If we assume that $\eta(x,t)$ and $Q(x,t)$ are continuous and have continuous partial derivatives over the area of interest, we may represent them by their corresponding Taylor expansion about the point $x=(j-\frac{1}{2})\Delta x$, $t=(n+1)\Delta t$.

This gives:

(7.1)

$$\eta_{j-\frac{1}{2}}^{n+3/2} = \eta_{j-\frac{1}{2}}^{n+1} + \frac{\Delta t}{2}\left(\frac{\partial \eta}{\partial t}\right)_{\substack{n+1\\ j-\frac{1}{2}}} + \frac{\Delta t^2}{4\cdot 2!}\left(\frac{\partial^2 \eta}{\partial t^2}\right)_{\substack{n+1\\ j-\frac{1}{2}}} + \frac{\Delta t^3}{8\cdot 3!}\left(\frac{\partial^3 \eta}{\partial t^3}\right)_{\substack{n+1\\ j-\frac{1}{2}}} + \cdots$$

$$\eta_{j-\frac{1}{2}}^{n+\frac{1}{2}} = \eta_{j-\frac{1}{2}}^{n+1} - \frac{\Delta t}{2}\left(\frac{\partial \eta}{\partial t}\right)_{\substack{n+1\\ j-\frac{1}{2}}} + \frac{\Delta t^2}{4\cdot 2!}\left(\frac{\partial^2 \eta}{\partial t^2}\right)_{\substack{n+1\\ j-\frac{1}{2}}} - \frac{\Delta t^3}{8\cdot 3!}\left(\frac{\partial^3 \eta}{\partial t^3}\right)_{\substack{n+1\\ j-\frac{1}{2}}} + \cdots$$

$$Q_j^{n+1} = Q_{j-\frac{1}{2}}^{n+1} + \frac{\Delta x}{2}\left(\frac{\partial Q}{\partial x}\right)_{\substack{n+1\\ j-\frac{1}{2}}} + \frac{\Delta x^2}{4\cdot 2!}\left(\frac{\partial^2 Q}{\partial x^2}\right)_{\substack{n+1\\ j-\frac{1}{2}}} + \frac{\Delta x^3}{8\cdot 3!}\left(\frac{\partial^3 Q}{\partial x^3}\right)_{\substack{n+1\\ j-\frac{1}{2}}} + \cdots$$

$$Q_{j-1}^{n+1} = Q_{j-\frac{1}{2}}^{n+1} - \frac{\Delta x}{2}\left(\frac{\partial Q}{\partial x}\right)_{\substack{n+1\\ j-\frac{1}{2}}} + \frac{\Delta x^2}{4\cdot 2!}\left(\frac{\partial^2 Q}{\partial x^2}\right)_{\substack{n+1\\ j-\frac{1}{2}}} - \frac{\Delta x^3}{8\cdot 3!}\left(\frac{\partial^3 Q}{\partial x^3}\right)_{\substack{n+1\\ j-\frac{1}{2}}} + \cdots$$

The truncation error in the approximation of the surface disturbance is given by:

$$(7.2) \qquad \varepsilon(\eta)^{n+1}_{j-\frac{1}{2}} = \left(\frac{\eta^{n+3/2}_{j-\frac{1}{2}} - \eta^{n+\frac{1}{2}}_{j-\frac{1}{2}}}{\Delta t} + \frac{Q^{n+1}_{j} - Q^{n+1}_{j-1}}{\Delta x} \right) - \left(\frac{\partial \eta}{\partial t} + \frac{\partial Q}{\partial x} \right)^{n+1}_{j-\frac{1}{2}}$$

Substituting the Taylor series expansions (7.1) into (7.2) gives:

$$(7.3) \qquad \varepsilon(\eta)^{n+1}_{j-\frac{1}{2}} = \frac{\Delta t^2}{24} \left(\frac{\partial^3 \eta}{\partial t^3} \right)^{n+1}_{j-\frac{1}{2}} + \frac{\Delta x^2}{24} \left(\frac{\partial^3 Q}{\partial x^3} \right)^{n+1}_{j-\frac{1}{2}} + \text{HOT}$$

The truncation error may then be expressed as:

$$(7.4) \qquad \varepsilon(\eta) = O\left[(\Delta t)^2\right] + O\left[(\Delta x)^2\right] + \text{HOT}$$

where HOT represents higher order terms.

To evaluate the truncation error in the finite-difference formulation of the linearized volume transport equation (6.40), it will be assumed that the methods used to approximate the advective term at time $t=(n+\frac{1}{2})\Delta t$ are successful and yield the values for $Q^{n+\frac{1}{2}}_{j\pm1}$ that would have been obtained had they actually been computed; alternately, it would be assumed that $Q^{n+\frac{1}{2}}_{j\pm1}$ was actually calculated by evaluating all variables at fractional as well as integral time steps. We then have as the finite-difference formulation of (6.40):

$$(7.5) \qquad \frac{Q^{n+1}_{j} - Q^{n}_{j}}{\Delta t} + \frac{g\bar{D}}{\Delta x} \left[\eta^{n+\frac{1}{2}}_{j+\frac{1}{2}} - \eta^{n+\frac{1}{2}}_{j-\frac{1}{2}} \right] + \frac{U}{2\bar{D}\Delta x} \left[Q^{n+\frac{1}{2}}_{j+1} - Q^{n+\frac{1}{2}}_{j-1} \right]$$

The Taylor series expansions of the surface disturbance and volume transport about the point $x=j\Delta x$ and $t=n\Delta t$ are given by:

(7.6)

$$\eta_{j+\frac{1}{2}}^{n+\frac{1}{2}} = \eta_j^n + \frac{\Delta x}{2}\left(\frac{\partial \eta}{\partial x}\right)_j^n + \frac{\Delta x^2}{4\cdot 2!}\left(\frac{\partial^2 \eta}{\partial x^2}\right)_j^n + \frac{\Delta t}{2}\left(\frac{\partial \eta}{\partial t}\right)_{j+\frac{1}{2}}^n + \frac{\Delta t^2}{4\cdot 2!}\left(\frac{\partial^2 \eta}{\partial t^2}\right)_{j+\frac{1}{2}}^n$$

$$\eta_{j-\frac{1}{2}}^{n+\frac{1}{2}} = \eta_j^n - \frac{\Delta x}{2}\left(\frac{\partial \eta}{\partial x}\right)_j^n + \frac{\Delta x^2}{4\cdot 2!}\left(\frac{\partial^2 \eta}{\partial x^2}\right)_j^n + \frac{\Delta t}{2}\left(\frac{\partial \eta}{\partial x}\right)_{j-\frac{1}{2}}^n + \frac{\Delta t^2}{4\cdot 2!}\left(\frac{\partial^2 \eta}{\partial x^2}\right)_{j-\frac{1}{2}}^n$$

$$Q_j^{n+1} = Q_j^n + \Delta t\left(\frac{\partial Q}{\partial t}\right)_j^n + \frac{\Delta t^2}{2!}\left(\frac{\partial^2 Q}{\partial t^2}\right)_j^n$$

Substituting the expansions given by (7.6) into the finite difference equation (7.5) gives as the truncation error:

(7.7)

$$\varepsilon(Q)_j^n = \Delta t\left\{\tfrac{1}{2}\left[\left(\frac{\partial^2 Q}{\partial t^2}\right)_j^n + \left(\frac{\partial Q}{\partial t}\right)_j^n - \left(\frac{\partial Q}{\partial t}\right)_{j-1}^n\right]\right\} + \Delta x^2\left\{\frac{U}{6\bar{D}}\left(\frac{\partial^3 Q}{\partial x^3}\right)_j^n\right\} +$$

$$\frac{\Delta t}{\Delta x}\left\{\frac{g\bar{D}}{2}\left[\left(\frac{\partial \eta}{\partial t}\right)_{j+\frac{1}{2}}^n - \left(\frac{\partial \eta}{\partial x}\right)_{j-\frac{1}{2}}^n\right]\right\} + \frac{\Delta t^2}{\Delta x}\left\{\frac{g\bar{D}}{8}\left[\left(\frac{\partial^2 \eta}{\partial t^2}\right)_{j+\frac{1}{2}}^n - \left(\frac{\partial^2 \eta}{\partial x^2}\right)_{j-\frac{1}{2}}^n\right]\right\}$$

which in turn may be written as:

$$(7.8) \qquad \varepsilon(Q) = O\left[\Delta t\right] + O\left[(\Delta x)^2\right] + O\left[\frac{\Delta t}{\Delta x}\right] + O\left[\frac{(\Delta t)^2}{\Delta x}\right]$$

A finite-difference equation is said to be a consistent approximation to the associated differential equation if the truncation error goes to zero uniformly as the computing lattice is increasingly refined, i.e. as $\Delta x \to 0$ and $\Delta t \to 0$. For the finite difference equation (3.5) this is obviously the case, as can be seen from (7.4). For the truncation error in the mass transport, finite difference equation to go to zero we must have $\Delta t \to 0$, $\frac{\Delta t}{\Delta x} \to 0$, and $\frac{(\Delta t)^2}{\Delta x} \to 0$ as $(\Delta x)^2 \to 0$. This is indeed the case when the stability criterion given by (6.35), $\Delta t \leq \frac{f(\Delta x)^2}{4g\bar{D}^2}$ is satisfied. It can therefore be concluded that the split-step, midpoint, leapfrog, finite-difference schemes are consistent approximations to the linearized governing equations.

It should be emphasized at this point that the analyses in this chapter and the previous chapter were predicated on the assumption that information on the behavior of the finite-difference formulation of the nonlinear shallow-water equations with variable coefficients could be obtained by examining a linear approximation with constant coefficients. As relatively little has been written on the stability of nonlinear systems of equations, this is the only option available if a theoretical understanding of the expected stability is desired. Harlow (1960) has investigated the stability of two specific nonlinear examples, but was not able to generalize his method. Studies by Richtmyer and Morton show that for nonlinear problems, stability depends not only on the structure of the finite-difference formulation but also on the structure of the solution being obtained (Richtmyer & Morton, 1967, pp. 201-206). Phillips (1959) has given an example of a so-called nonlinear instability that arose even though the stability criterion derived by

analysis of the linearized approximation was met. Lilly (1965) was later able to show that this instability was a result of non-constant coefficients. Kasahara (1965) demonstrated by counterexample that the practice of analyzing the stability of each term in a complicated equation separately, then choosing a stabilty criterion inclusive of all those derived is not a dependable procedure. On the other hand, Roache (1972) worked with a numerical model that, while satisfying the conventional definition of stability, oscillated unstably about an incorrect solution; yet, for practical purposes the solution was close enough to the true one. Finally, few, if any, of the established stability analyses take account of the effect of boundary conditions, which may be of prime importance (Roache, 1972).

In summary, when the usual procedure for analyzing the stability of finite-difference schemes is applied to a nonlinear system with nonconstant coefficients, information is obtained about another model that is not, in fact, the one used. The conclusion supported by this work and that of previous researchers is that stability criteria so derived should be regarded as a crude first approximation only, not believed.

CHAPTER VIII

THE PROGRAMS

The profound differences in the treatment of various boundary and initial condition formulations necessitated the development of several, essentially distinct programs. The general flow of operations in each was similar and is charted in Appendix A. The different water/land boundary conditions treated include: (1) total reflection from the shoreline, (2) Reid and Bodine (1968)-style empirical engineering-type flooding, (3) Sielecki and Wurtele (1970) inland extrapolation, (4) Yeh and Chou (1979) dry cell inclusion, and (5) Lewis and Adams heuristic flooding. The oceanside open boundary conditions include (1) forcing of the input wave height, and (2) expected conformance non-reflecting boundary condition. In addition to inputting a wave by forcing the oceanside boundary cell, cases arose which required specifying the initial disturbance synoptically over the entire grid.

Several special features were included in each program:

(1) A compilation of statistics was obtained for the frequency of occurrence of each of the 14 possible adjacent cell configurations. This provided a means for comparing the performance of different models of the same problem, and also gave information on individual model behavior.

(2) A facility for dumping the values of all variables to the printer existed, making a numerical examination of the grid and the state of the entire model accessible at preselected times.

(3) Powerful interrupt and restart capabilities were built into the programs that permitted program interruption at any time by setting a predetermined switch on the computer's front panel; an interrupt routine would then transfer all critical program variables to mass storage and halt execution. At some

later time, the program is restarted and informed of the situation, resulting in retrieval of stored variables and continuation of execution. This feature proved convenient for making it possible to release a batch-mode, computer operating-system to other users prior to normal completion. The ability to alter model parameters during execution was also provided by this feature.

(4) The most indispensable feature from the standpoint of obtaining complete information on model behavior was the capacity for monitoring all results at each time step in the form of a motion picture. The bathymetry, topography, computed fluid surface and volume transport vectors were simultaneously graphed on a C.R.T. screen after each time iteration; a movie camera was then activated by a photo subroutine (see Appendix D) for the desired number of frames (usually about four), then the entire process was repeated for the next computational cycle. The resulting movie can be easily viewed to assess the spatial and temporal coherency of the model performance, and to detect computational anomalies.

System and Hardware Dependency

Due to the current emphasis on incompatability in the computer industry, the program and subroutines given in the appendices will undoubtedly require modification before their successful use at various locations. They were originally developed on an IBM 370/168 computer using a DOS operating system and Waterloo standard Fortran IV. Significant modification of syntax and parameter bounds was required for subsequent use on a Burroughs Univac 1103. Some additional restructuring enabled execution on a PDP 11/40 with VO3-02B operating system and PDP Fortran. The PDP-compatible versions are given in Appendices B - D. The subroutines are Macros written in PDP 11/40 assembly language. Eight months of further intensive modification has yielded versions that execute, for the most part successfully, on a Harris 800 computer with

Vulcan 9A operating system and Harris standard Fortran 66. Although an attempt has been made to write the bulk of the program in a version of the Fortran language that is the lowest common denominator of all possible versions, there are portions that remain system dependent. They are primarily: (1) file assignments, (2) graphics subroutine calls, (3) photo and interrupt handling, (4) permissible magnitude limits, (5) the use of expressions as loop index limits, and (6) the method of representing literal data.

CHAPTER IX

VERIFICATION OF PROGRAM INTEGRITY

Before drawing any conclusions based on results produced by the numerical model formulated in Chapter III, it is essential to verify the model by comparison of its performance with a known analytical solution. Very few solutions to nonlinear shallow-water problems exist, which has prompted many investigators to calibrate their models until a fit to historical data has been obtained, rather than truly verify the correctness of model performance (Reid & Bodine, 1968; Houston et al., 1977; Houston & Butler, 1979). The distinction between verification and calibration is critically important, though often overlooked: A verified model is one in which the physics of the modeled situation is faithfully simulated; a calibrated model is one in which a multitude of parameters--the depth and frictional coefficient for each grid cell, the input wave, etc.--are adjusted under the pretense of their uncertainty until a match with some historical data such as maximum run-up is obtained. The model dynamics may even be altered in a physically unrealistic way to achieve the historical match (Houston et al,. 1976; Houston & Butler, 1979). The contrasting utility of the two results is obvious: The first is a versatile model which should be readily adaptable to varying conditions, while the second is like a "black box" custom-made to reproduce one set of results, with no guarantee of reliability under other than the original, adjusted conditions. It is this second type of model that is most frequently encountered in the literature, whereas this work is concerned with the development of the first type.

An elementary test of the linear portion of the prognostic equations was made by inputting an offset sinusoid wave into one end of a channel of unit width and constant depth, and observing the expected doubling of amplitude on

reflection from a perfectly reflecting wall at the other end, along with the correct wave-speed as given by $c = \sqrt{gD}$.

A more exacting test was required for the nonlinear version of the model, and so the results of Thacker (1980) were chosen as a verifying standard. Thacker was able to show, following Ball (1962), that if the water in a frictionless paraboloidal canal was displaced from its equilibrium position as shown in cross-section in Figure 7, the resulting behavior of the water is completely characterized by the following:

$$u = -n \cdot w \cdot \sin(wt) \tag{9.1}$$

$$\eta = 2n \frac{D_o}{L} \cos(wt)\left(x - \frac{n}{2L}\cos(wt)\right) \tag{9.2}$$

$$w = \sqrt{\frac{2gD_o}{L^2}} \tag{9.3}$$

$$x_s = n \cdot \cos(wt) \pm L \tag{9.4}$$

where D_0 is the maximum equilibrium depth, w is the angular frequency of fluid oscillation, L is the half-width of the equilibrium fluid surface, n characterizes the amplitude of the initial displacement, and x_s is the location of the instantaneous shoreline. In particular, his solution indicates that if the surface of the initial displacement is planar, it will always remain planar. For the purpose of this test, the following values of parameters were used:

$$D_o = 1\text{m}; \quad L = 2500\text{m}; \quad n = 1250\text{m}; \quad x = 50\text{m}; \quad \Delta t = 2.5\text{s} \tag{9.5}$$

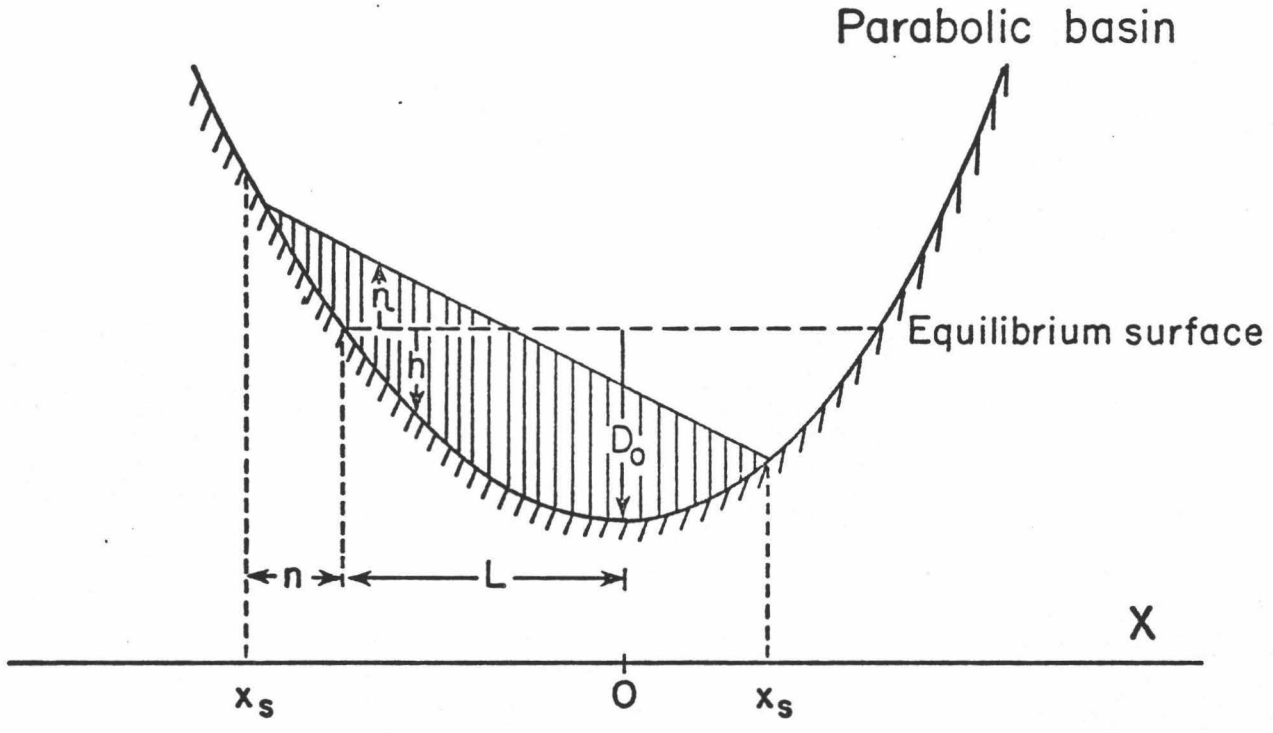

Figure 7. Cross-section of Ball-Thacker model with planar initial water surface.

It is seen that the space- and time- steps used satisfy the stability requirement given by (6.38), which is appropriate for the frictionless case. In addition, the approximation for $\partial Q/\partial x$ obtained by diagonal extrapolation, $DQDX_2$, is used.

The theoretical and experimental values for the position of the instantaneous shoreline are shown in Figure 8. The theory predicts a fluid oscillation period of 3548.07 seconds, in agreement with the experimental results. Figure 9 shows synoptic views of the water profile at selected times. The vertical segments represent volume transport, upward-directed segments representing rightward flow. Although some deviations from perfection are evident, the general qualitative behavior is encouraging. The development of a bore-like leading edge is probably a result of sluggish flooding. The depth at each interface was taken as the average of the depths in the two adjacent cells, with no prior extrapolation of water onto the first dry cell. This can be expected to provide a low estimate of the depth at the shoreline, hence producing sluggish flooding. Although the shoreline lags behind its theoretically predicted position, the volume transport goes to zero almost everywhere when half the period has elapsed, then reverses as expected. This indicates that the fluid body as a whole is behaving properly.

The disturbance height at a specific location can be monitored by the computational equivalent of a hydrograph. The theoretical and experimental values for the disturbance as a function of time at the location x = 1250 are presented in Figure 10. As is readily apparent, the correlation between theoretical and experimental results is unacceptably low. At this point there is a tendency to modify the program in an attempt to reproduce the expected results, a tendency that would prove disasterous in this case. For, assuming that the analytical expression (9.4) for the shoreline position is correct, and making use of the condition that at the instantaneous shoreline $h+\eta=o$, it can be shown that:

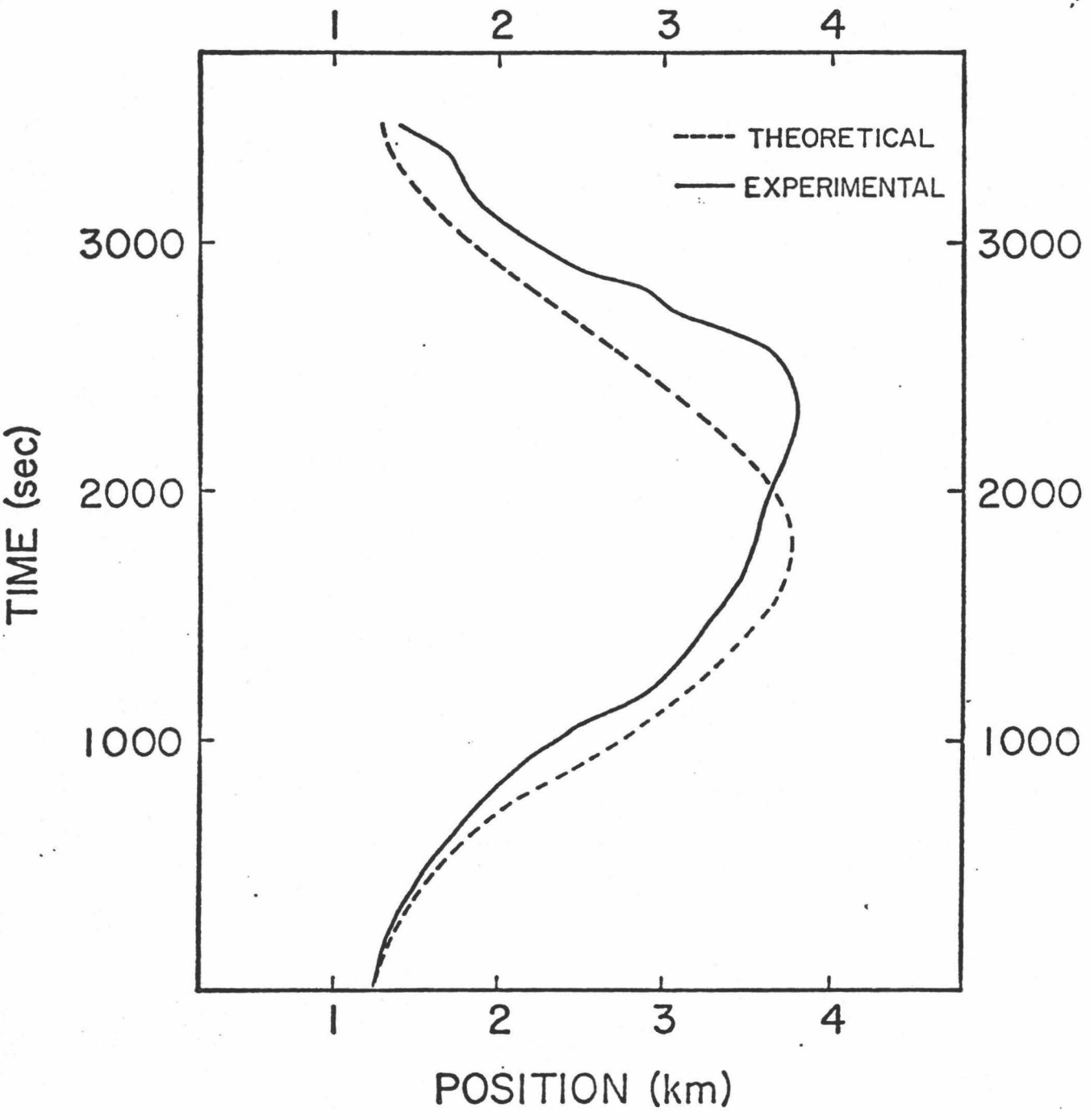

Figure 8. Position of instantaneous shoreline for Ball-Thacker model.

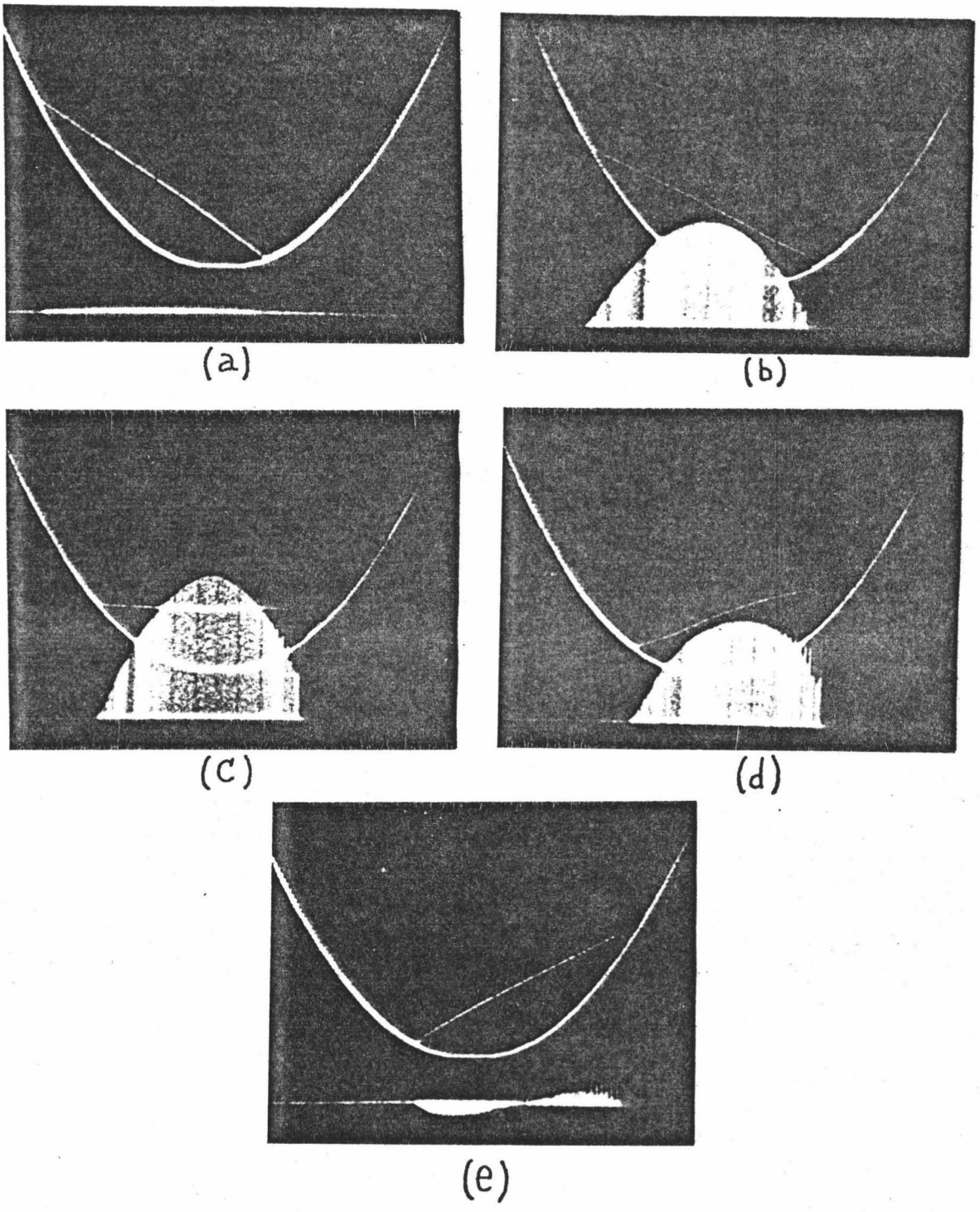

Figure 9. Synoptic water-surface profiles for Ball-Thacker problem at selected times.

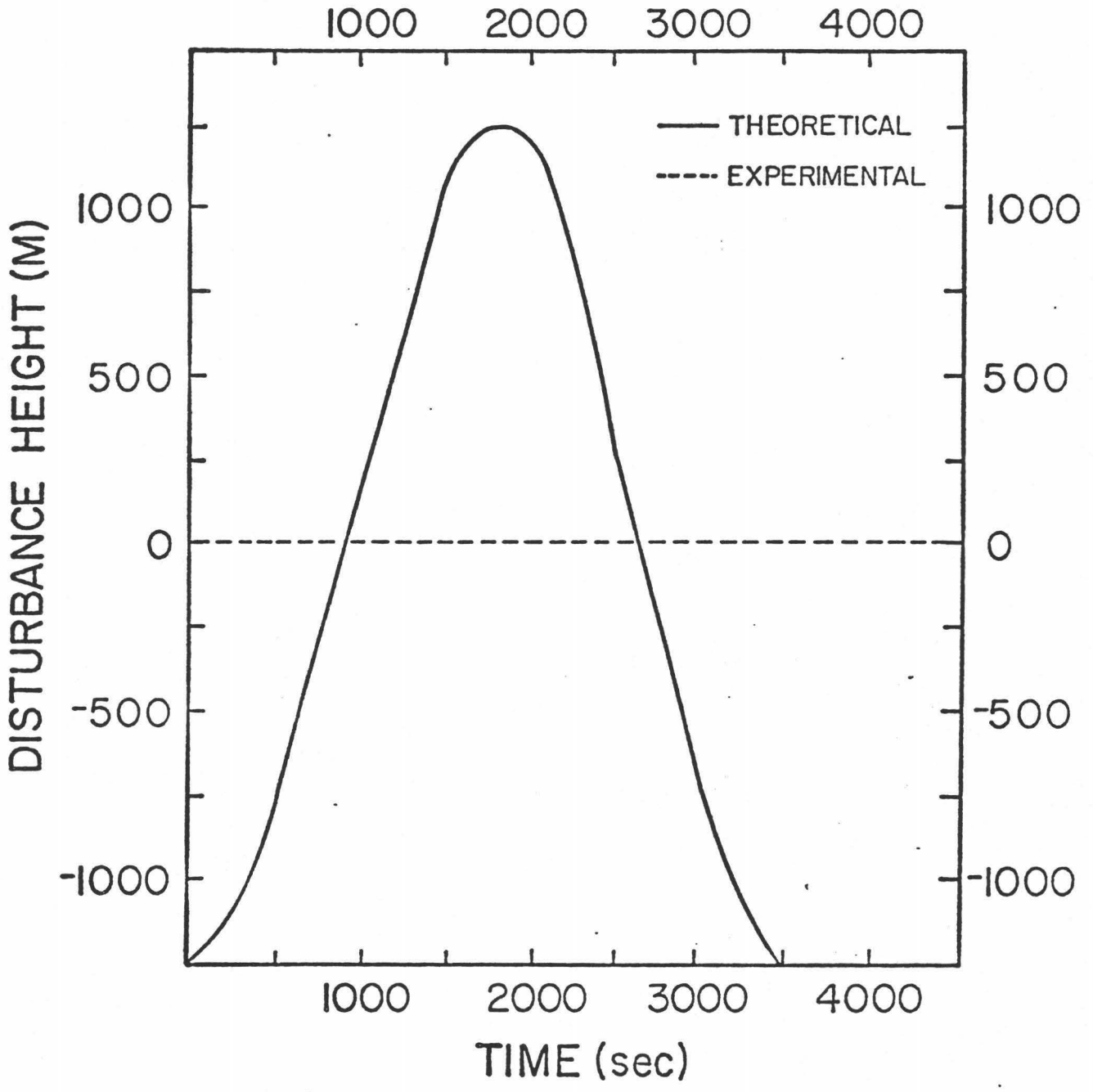

Figure 10. Hydrograph output for planar Ball-Thacker problem at x=1250.

(9.6) $$\eta = \frac{2\pi D_o}{L^2} \cos(wt)(x - \frac{n}{2} \cos(wt))$$

Comparing this expression with that given by Thacker, (9.2), it can be concluded that a typographical error probably was made during the preparation of his manuscript. Taking (9.6) as the correct expression for the disturbance height as a function of position, the theoretical and experimental results for the positions x = 0 and x = 1250 are presented in Figure 11. Although not perfect, the theoretical and experimental values are in reasonable agreement; hence, the model may be considered to have been verified.

In practice, verification by several tests is advisable. Another solution to a nonlinear shallow-water problem is provided by Carrier and Greenspan (1958), and was used as an additional verification for the numerical model developed in Chapter III. They were able to show that certain initially stationary waveforms will climb a sloping beach without breaking (with friction disregarded). Specifically, the wave defined parametrically by:

(9.7) $$\eta^* = \tfrac{1}{2}\varepsilon p^2 e^2 \sigma^4 e^{-\sigma^2 p}$$

and

(9.8) $$x^* = \tfrac{1}{2}\varepsilon e^2 p^2 \sigma^4 e^{-\sigma^2 p} - \sigma^2/16$$

where $1/p = 8(1+\varepsilon)$, $\alpha^* = \eta/\alpha l_o$ is the dimensionless disturbance, α is the beach slope, x^* is a dimensionless length scale given by $x^* = x/l_o$, and l_0 is a characteristic length, is shown to inundate inland without breaking a distance:

(9.9) $$x^*_{max} = 1.451\varepsilon$$

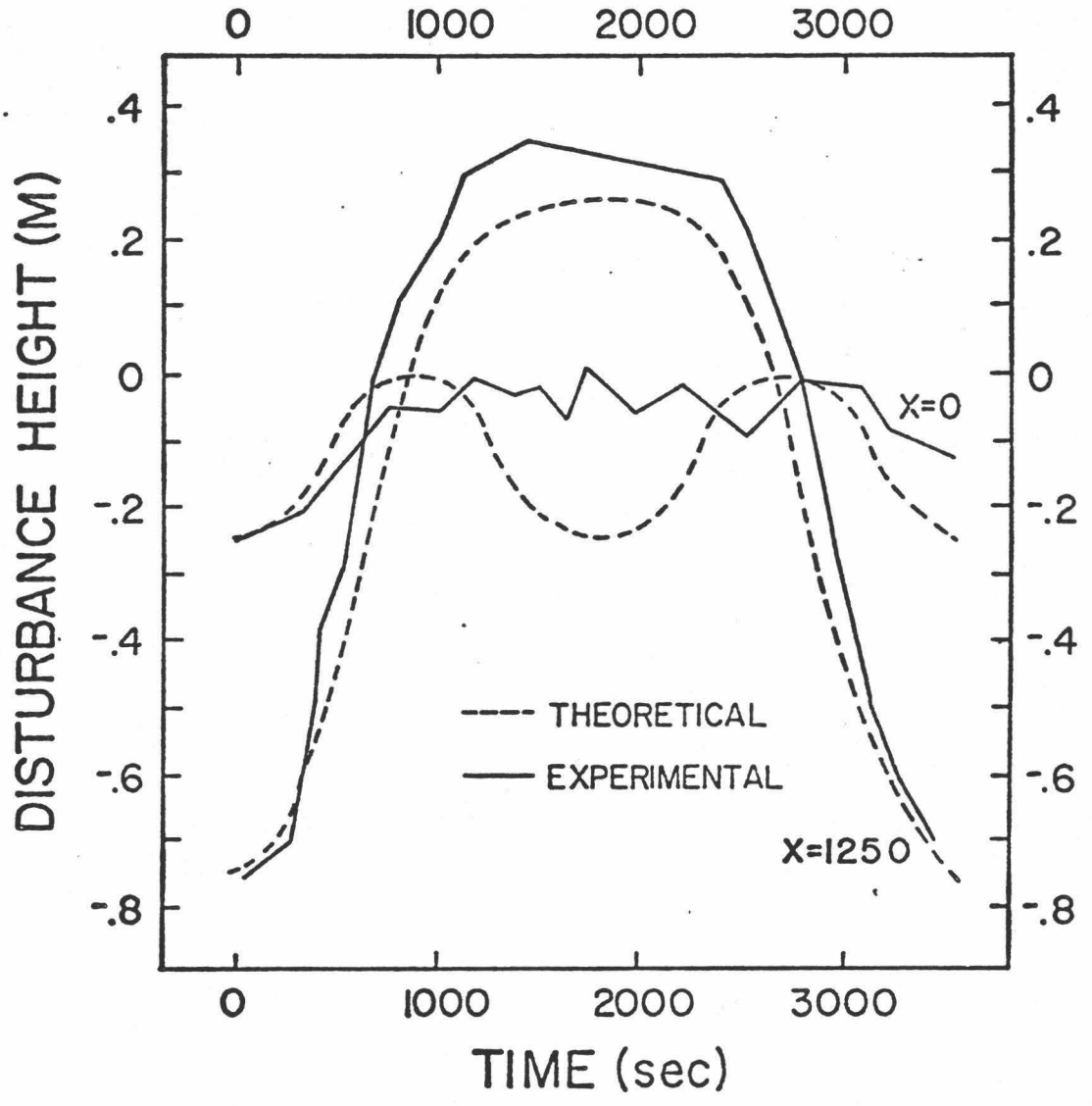

Figure 11. Corrected hydrograph output for planar Ball-Thacker model at x=0 and x=1250.

when the wave family parameter, , is sufficiently small. For this verification test, the following values for parameters were used:

(9.10) $\varepsilon = .1; \quad \alpha = .01; \quad l_o = 100m; \quad \Delta x^* = .05; \quad \Delta t^* = 5 \cdot 10^{-4}; \quad f = 0.0$

where $t^* = t \sqrt{g/l_o}$ is a dimensionless time scale. The initial waveform is given in Table I and is shown in Figure 12a. The subsequent run-up is depicted in Figure 12 b-d. The sloping bottom extends 100 m oceanward to a depth of 1.05 m, and 20 m landward to an elevation of 20 cm. Vertical exaggeration is x 600. The wave is seen to move smoothly up the beach to a position three grid cells inland, or $x^*_{max} = .15$, as theoretically predicted. Thus, the basic numerical model given by equations (3.2), (3.3), and (3.5) is verified.

Table 1
Initial dimensionless waveform used for
Carrier-Greenspan verification test

x^*	η^*	x^*	η^*
0.0000	0.0000	-2.3500	0.0450
-0.0500	0.0015	-2.4000	0.0429
-0.1000	0.0056	-2.4500	0.0409
-0.1500	0.0119	-2.5000	0.0389
-0.2000	0.0198	-2.5500	0.0370
-0.2500	0.0286	-2.6000	0.0352
-0.3000	0.0377	-2.6500	0.0334
-0.3500	0.0467	-2.7000	0.0317
-0.4000	0.0553	-2.7500	0.0301
-0.4500	0.0633	-2.8000	0.0285
-0.5000	0.0704	-2.8500	0.0270
-0.5500	0.0768	-2.9000	0.0256
-0.6000	0.0822	-2.9500	0.0242
-0.6500	0.0868	-3.0000	0.0229
-0.7000	0.0907	-3.0500	0.0216
-0.7500	0.0938	-3.1000	0.0204
-0.8000	0.0962	-3.1500	0.0193
-0.8500	0.0979	-3.2000	0.0182
-0.9000	0.0991	-3.2500	0.0172
-0.9500	0.0998	-3.3000	0.0162
-1.0000	0.1000	-3.3500	0.0152
-1.0500	0.0998	-3.4000	0.0143
-1.1000	0.0992	-3.4500	0.0135
-1.1500	0.0984	-3.5000	0.0127
-1.2000	0.0972	-3.5500	0.0119
-1.2500	0.0957	-3.6000	0.0112
-1.3000	0.0941	-3.6500	0.0105
-1.3500	0.0923	-3.7000	0.0099
-1.4000	0.0903	-3.7500	0.0093
-1.4500	0.0882	-3.8000	0.0087
-1.5000	0.0859	-3.8500	0.0082
-1.5500	0.0836	-3.9000	0.0077
-1.6000	0.0812	-3.9500	0.0072
-1.6500	0.0787	-4.0000	0.0067
-1.7000	0.0763	-4.0500	0.0063
-1.7500	0.0737	-4.1000	0.0059
-1.8000	0.0712	-4.1500	0.0055
-1.8500	0.0687	-4.2000	0.0052
-1.9000	0.0662	-4.2500	0.0048
-1.9500	0.0636	-4.3000	0.0045
-2.0000	0.0612	-4.3500	0.0042
-2.0500	0.0587	-4.4000	0.0039
-2.1000	0.0563	-4.4500	0.0037
-2.1500	0.0539	-4.5000	0.0034
-2.2000	0.0516	-4.5500	0.0032
-2.2500	0.0494	-4.6000	0.0030
-2.3000	0.0472	-4.6500	0.0028

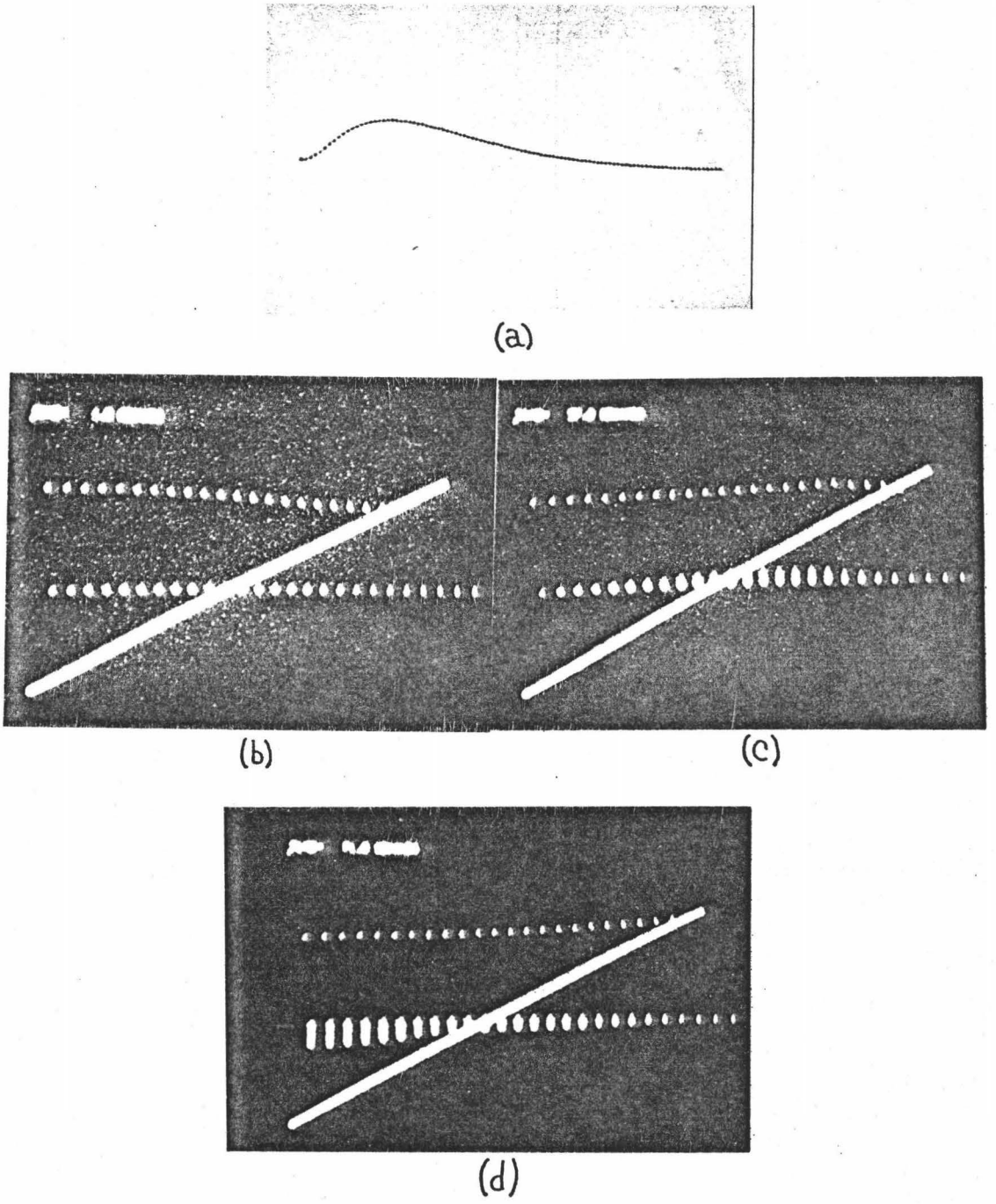

Figure 12. Initial waveform (reversed) and subsequent run-up of Carrier-Greenspan verification test.

CHAPTER X

COMPUTATIONAL RESULTS

Results were obtained upon application of the numerical analogue to the nonlinear shallow-water equations for the various initial conditions, advection term formulations, and moving boundary conditions described previously. In addition, other computational schemes discussed in this chapter were tested. Qualitative information derived from motion pictures of the results proved to be invaluable in the analysis of specific scheme success or failure, and necessary corrective measures often were made obvious by careful film viewing. The quantitative results served mainly to quantify the results observable qualitatively; hence, they are treated lightly in this work. An exception to this is the statistical summary of model performance, which served to concisely characterize model behavior.

This chapter is divided into two sections which treat the two primary categories of results obtained. Section A reports on the appropriateness of various flooding schemes as a function of the roughness of the bathymetry and topography; Section B explores the causes of instabilties encountered during the modelling process, and suggestions for their alleviation; also treated in Section B are asymmetries that arose during the modelling of a symmetrical problem, with guidelines for the avoidance of unknowingly utilizing false, asymmetrical results.

A. Effect of Bathymetric Smoothness on Model Performance

Once the spatial dimension of the computational mesh is chosen, and a boundary is fixed over an arbitrary bathymetry, the discrete representation of the bathymetry is completely determined. The converse is not true; given a finite-difference representation of some bathymetry, that bathymetry is in no way

uniquely determined. The only constraint placed upon it is that the average elevation within a grid cell be equal to the elevation given for that cell. The bathymetry could, in fact, be identical to its stairstep-like representation. At the other extreme, the bathymetry may be considered to be very smooth and continuous, with grid cell elevations representing true values sampled at spatial intervals of one grid cell width. If the mesh structure is fine enough so that no bathymetric features has a wavelength shorter than two grid cells, then the true bathymetry may be reconstructed to any desired accuracy over the entire grid through the use of a Fourier synthesis. For cases intermediate to these two extremes, the true bathymetry can be reasonably approximated by linear interpolation between specified elevations at the center of grid cells. This is the assumption implicitly made by all investigators who approximate the water depth at a cell interface as the average of the depths in the two adjacent cells. As the computed flux across the cell interface is largely dependent upon the interface depth, this assumption is seen to have important implications for the flooding model.

An illustration of this is provided by Figure 13a-h. The flooding method of Sielecki and Wurtele (1970) is used, whereby the total water depth is first extrapolated onto the first dry cell, j+1, from the previous two wet cells, j-1 and j, followed by a one-sided difference of momentum computation involving a similarly extrapolated value of the flux, to obtain as a new value for the total wave depth:

$$\xi_{j+1}^{n+1} = \left[\xi_{j+1}^{n+1}\right]_{\text{extrap}} - \frac{\Delta t}{\Delta x}\left\{\left[\xi_{j+1}^{n}\, u_{j+1}^{n}\right]_{\text{extrap}} - \xi_{j}^{n}\, u_{j}^{n}\right\} \tag{10.1}$$

This value is then included in the normal computational cycle. They reported a high order of accuracy obtained in this faction for their treatment of fluid

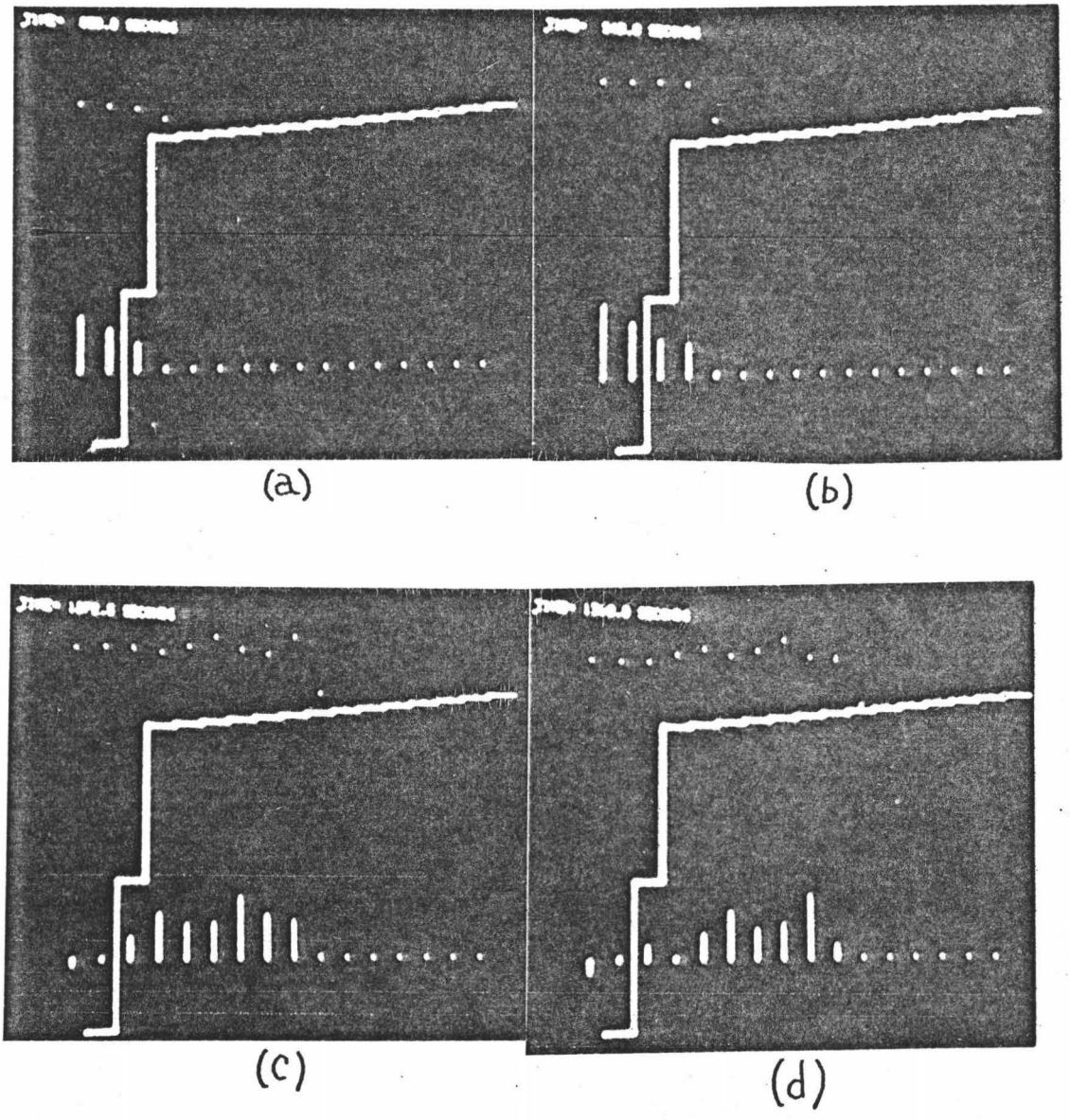

Figure 13. Close-up of tsunami flooding sloping beach as computed using Sielecki-Wurtele extrapolation scheme.

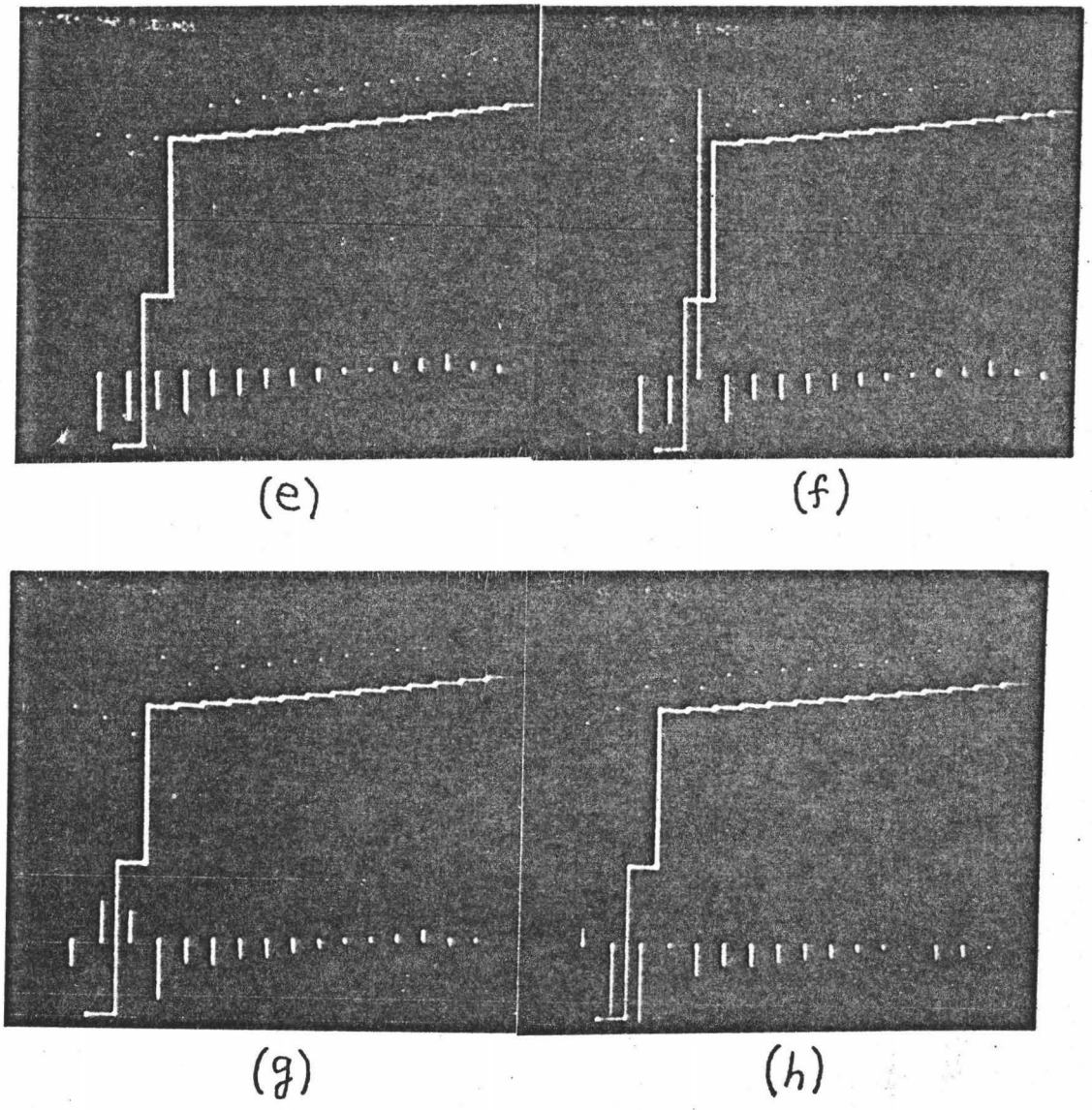

Figure 13 (continued). Close-up of tsunami flooding sloping beach as computed using Sielecki-Wurtele extrapolation scheme.

oscillations in a smooth parabolic basin as described by Ball (1964). For the purpose of this experiment, a bathymetry exhibiting a break-in-slope was used. Beginning at the oceanside boundary and extending shoreward was 7.75 km of 20 m deep water, then a 1.2^0 sloping bottom up to the shoreline, followed by a topography with a grade of 2cm/50m. Only the last two underwater cells are included in Figure 13, of depths 2 m and 1 m respectively, followed by the gently-sloping initially-dry beach zone starting at 2 cm elevation. The vertical exaggeration in the figure is 333. An offset sinusoidal wave of period 1000 s and waveheight 30 cm was input to the grid by forcing the oceanside open boundary cell. In addition, the following model-parameters were used:

(10.2) $\Delta x = 50m$; $\Delta t = 2.5s$; $f = .0025$

The water surface over each grid cell is represented by a dot, and the vertically-oriented vectors in the lower portion of each figure represent volume transport, as before--upwards indicating rightward fluid flux, downward signifying leftward flow.

The flooding is seen to begin smoothly on the first dry cell. As the second dry cell becomes inundated, the leading edge of the wave becomes steepened. The leading edge remains steep and a surface irregularity propagates backward from the wavefront to contaminate interior results for the duration of the flooding phase (Figure 13a-d). During the recessional phase, the body of water over the originally dry land lags behind the primary disturbance offshore. The result is a divergence of fluid at the shoreline, causing the shoreline cell to go dry. At this point the model is seen to "blow up", or behave in a discontinuous manner. Sudden shoreward convergence of volume transport is generated, throwing water up onto the dry shoreline cell and depressing the water level in the

adjoining cells. The fluxes and disturbance heights then oscillated for about 10 time steps with steadily decaying amplitudes, until an apparent "healing" had taken place. The explanation for this behavior is as follows: During the initial stages of flooding, the extrapolation of water depths placed water onto the first land cell. Taking the depth at the ocean-land interface as the average of the depths in the two adjoining cells gave a value comparable to that in the nearby ocean, and permitted a comparable flux to be generated. This, in turn, permitted apparently smooth flooding. After the first land cell had been flooded, the extrapolation to the next dry cell involved a "deep" ocean cell and a very shallow inland cell. The result was an extrapolated depth of less than zero, which was taken as zero. When the depth at the first wet cell/dry cell interface was calculated, the result was almost one order of magnitude smaller than the previous depth; the result is sluggish flooding, which produces a steep wavefront. Once a steep wavefront is produced, it tends to maintain itself due to the steeply dipping extrapolation of depths to zero on the next dry cell, causing a repetition of the cycle just described. During the recessional phase, the disturbance can be expected to propagate more rapidly in the deeper ocean cells than over shallowly inundated land, as can be seen by considering that the primary disturbance propagation velocity is given by $c=\sqrt{gD}$, making the volume transport go as $D^{3/2}$. This draws water out of the first land cell faster than it can be replaced from inland, causing it to eventually go dry. At this point a kink exists in the water surface, and the model attempts to eliminate it by artifically rapid convergence of fluid into the kinked cell.

A further elucidation of the failure of the Sielecki-Wurtele extrapolation method on other than smoothly varying bathymetries can be obtained by considering Figure 14. The situation at time step n, with the first dry cell occuring at location j+1, is shown in Figure 14a. At time step n+1 an extrapolation

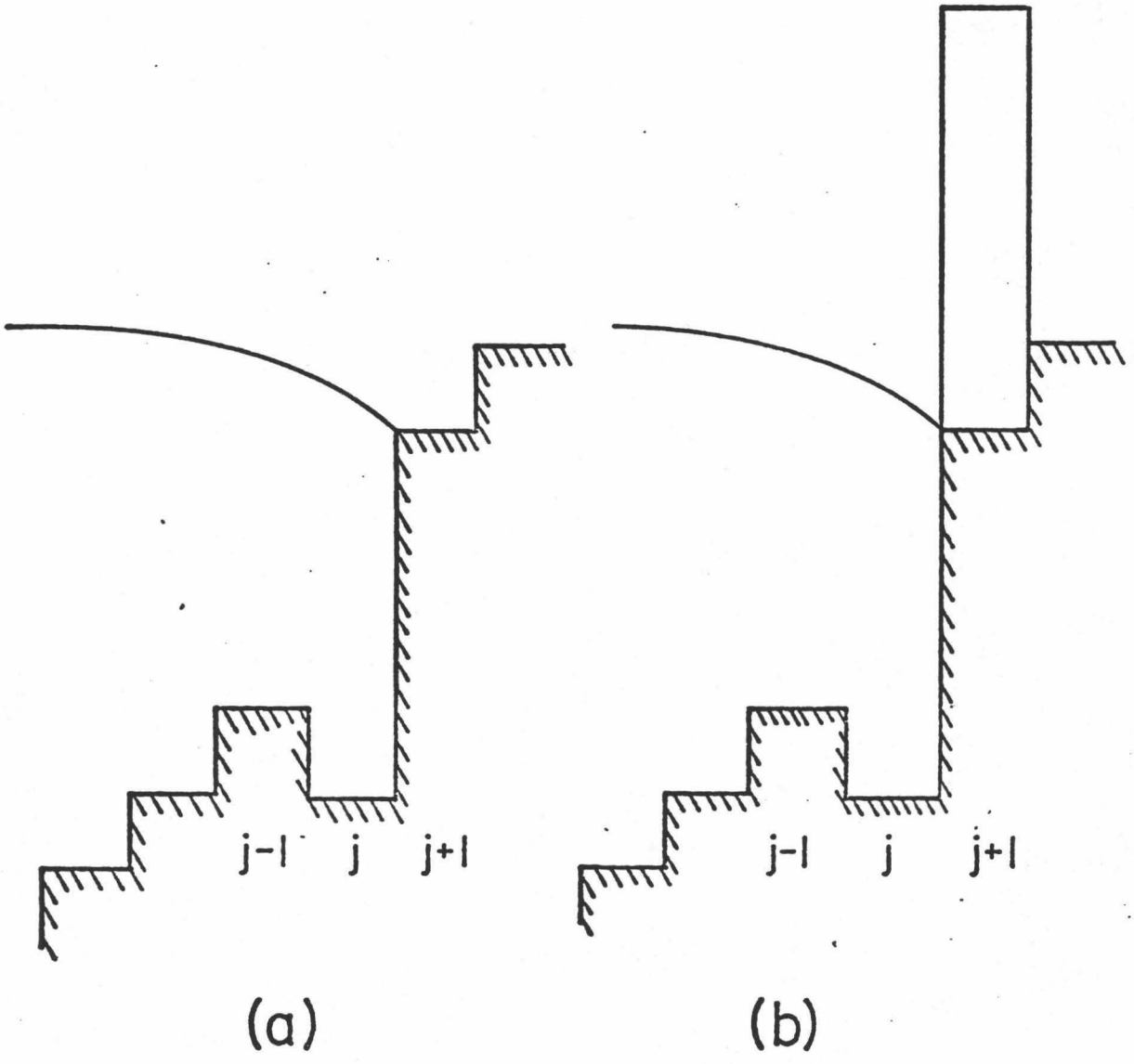

Figure 14. Failure of Sielecki-Wurtele extrapolation scheme for non-smooth bathymetry.

of total wave depth is made from cells j-1 and j onto j+1, and is shown in Figure 14b. Depending on the configuration of volume transport vectors, the resulting artificial column of water may be either raised or lowered upon application of the one-sided difference of momentum equation (10.1). The result is a clearly inappropriate depth calculation for both the first dry cell and at the water-land interface.

The need is apparent for a scheme which will permit realistic flooding over a discontinuous bathymetry. The method of Reid and Bodine (1968) was a first attempt in this direction. They treated three special cases differently than the usual internal calculations: (1) Their boundary condition for the normal component of flow, Q_n, at the juncture of a flooded cell and a dry cell is

$$Q_n = 0 \tag{10.3}$$

when the elevation of water in the wet cell is less than that of the adjacent dry land. (2) If the water elevation is greater than that of the adjacent dry land, then the land is considered to be a barrier that is being overtopped by water, and the volume transport is given by (their equation 9):

$$Q_n = \pm C_o D_b \sqrt{gD_b} \tag{10.4}$$

where D_b is the depth of water over the crest of the barrier, and C_0 is an appropriate nondimensional overflow coefficient, usually less than .5. (3) Where the water level on both sides of an internal barrier exceeds the barrier elevation, the flux is computed as for a submerged weir (their equation 10):

$$Q_n = \pm C_s D_b \sqrt{g|\eta_1 - \eta_2|} \tag{10.5}$$

in which D_b is the average barrier overtopping level, $(\eta_1+\eta_2)/2+H_b$; η_1 and η_2 are the distrubance heights relative to MSL on opposite sides of the barrier; H_b is the depth to the barrier top relative to MSL (positive below and negative above); and C_s is an appropriate nondimensional discharge coefficient for the submerged barrier, generally less than $\sqrt{2}$. The sign in both equation (10.4) and (10.5) is taken to be such that the flow is directed toward the low-head side of the barrier.

This scheme was incorporated into our numerical model for evaluation. Some representative results obtained by utilizing the same bathymetry, topography and input wave as was used previously for the Sielecki-Wurtele flooding method are presented in Figure 15. The same parameter values were used as for the previous case, with the addition that C_0 was taken to be 1.1 and C_s was set equal to 2.0. The resulting flooding is seen to proceed smoothly. Although the same configuration that produced the discontinuity when using the Sielecki-Wurtele extrapolation scheme reoccured, the Reid-Bodine empirically-oriented flooding scheme was able to properly manage the fluxes at the shoreline. This was found to be due in part to the high values assigned to the nondimensional discharge coefficients, C_0 and C_s. This resulted in flooding rapid enough to smooth out kinks quickly. The reduced surface irregularity is apparent during the flooding, as well as the recessional, stages.

A view of the entire computational grid used for the previous two examples is given in Figure 16. The vertical exaggeration of the bathymetry and volume transport is x 162, while that of the surface disturbance is x 1620. As the water level is initially set equal to the land elevation over dry land, the difference in vertical exaggeration produces an apparent separation of the two. Although Figure 16 was produced by the Reid-Bodine version of the numerical flooding model up to the time the blowup occurred, the results for the Sielecki-Wurtele

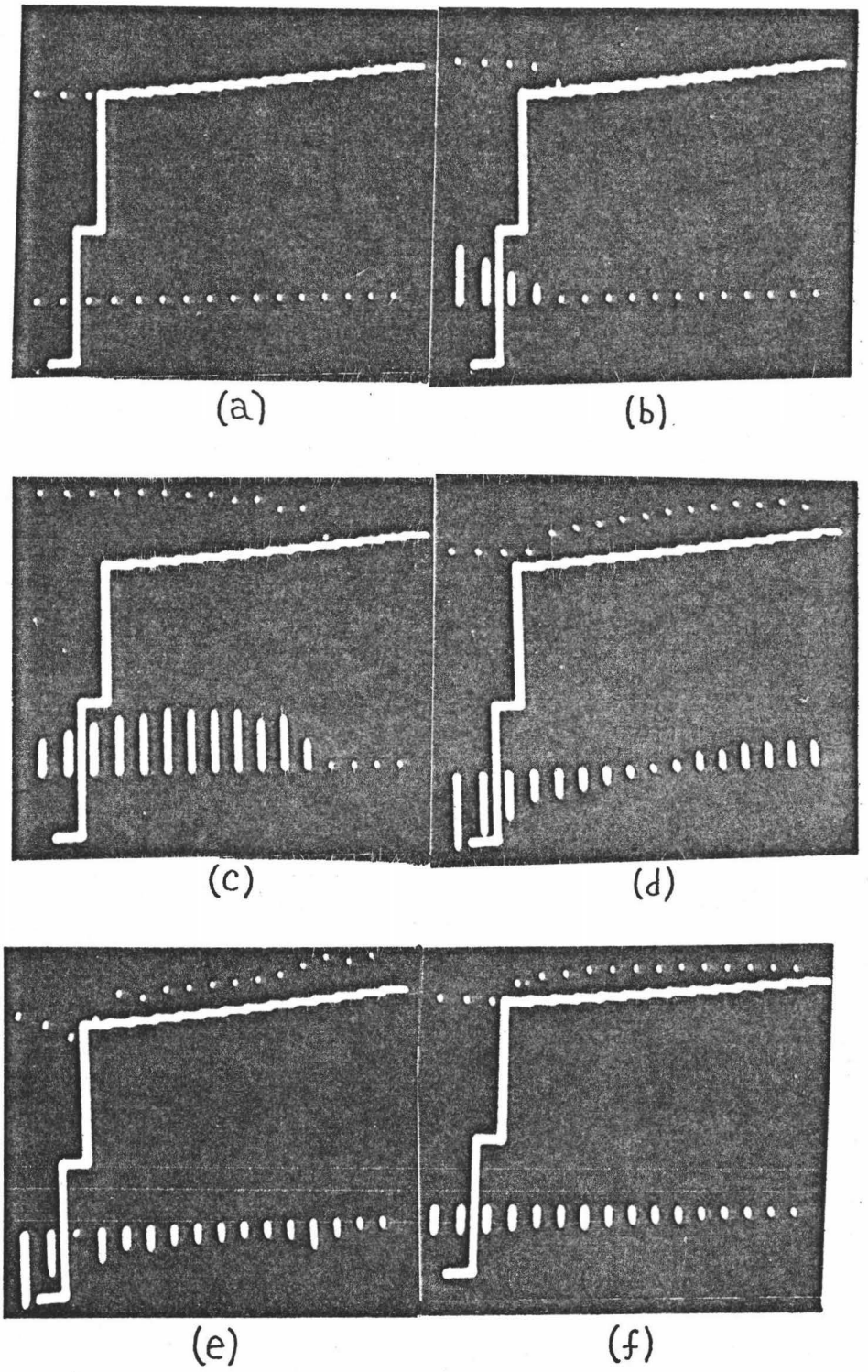

Figure 15. Close-up of tsunami flooding sloping beach as computed using Reid-Bodine flooding scheme.

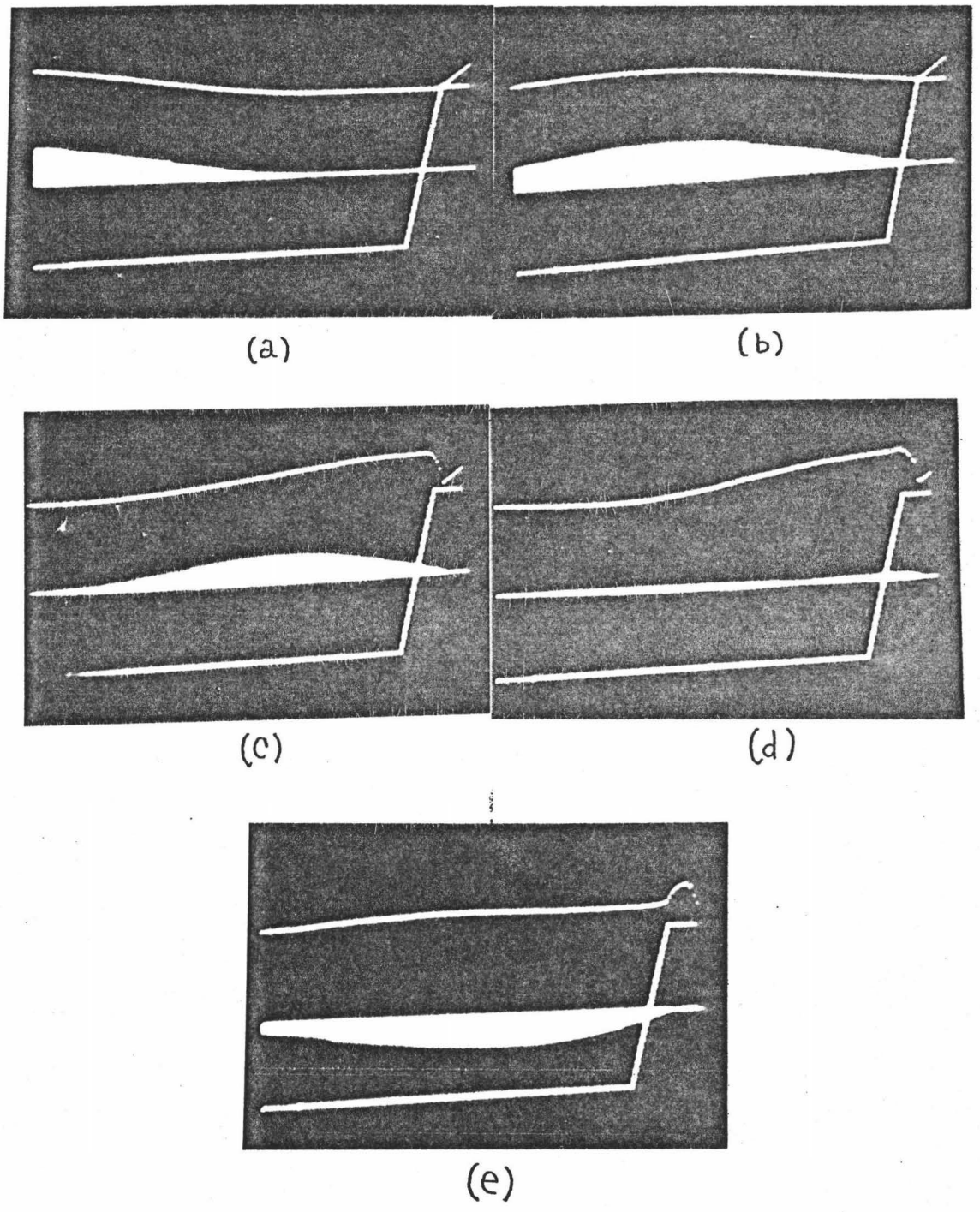

Figure 16. View of entire computational grid showing tsunami-flooding as computed using Reid-Bedine flooding scheme.

case were very similar up to the same point. Figure 16a shows the offset sine wave entering the grid and travelling toward shore; Figures 16b and 16c depict the onset of flooding; Figure 16c shows most of the wave energy stored as potential energy, but with some ongoing inland penetration, and some seagoing reflection from the 1.2^0 slopping bottom. Figure 16e vividly illustrates the situation where most of the primary disturbance has been reflected oceanward, yet inland flooding is still progressing. This run also provided a successful test of the oceanside open-boundary condition formulated in Chapter IV.

Although the results of the Reid and Bodine flooding-scheme are encouraging, there are several aspects of the method that make further modifications desirable. The values used for C_0 and C_s were determined by trying several values and chosing the ones that resulted in the smoothest flooding. This somewhat arbitrary technique is reminiscent of the calibration discussed in the previous chapter. Another shortcoming of the method is the requirement that flow over'barriers' always be directed toward the low-head side. This precludes the possibility of advective run-up occurring over land. For this same reason, fluid surface irregularities that develop over barriers can dramatically reverse the direction of flow. The problem here is that the current configuration entirely determines the instantaneous volume transport, rather than merely a change from the previous time step as with the usual computations. Problems associated with this behavior were avoided in our test by the addition of special program logic which did not permit a reversal of the volume transport sign if that would result in a polarity opposite to that of both neighboring fluxes. Again, this is a somewhat arbitrary procedure which cannot be expected to provide a complete correction in all circumstances. Finally, the requirement that predetermined "barriers" such as dry land always be treated differently as a special case is contrary to the true physics of the flooding phenomenon; for, once dry land is

inundated, the traveling disturbance is incapable of distinguishing between it and original ocean bottom.

After careful consideration of the difficulties associated with the flooding schemes just described, an attempt was made in this work to develop a flooding scheme which would at once flood properly, give no special treatment to any portion of the grid, and remain valid whether the stairstep-like representation of the bathymetry/topography was interpreted as representing a smooth bottom or an actual stairstep structure. This was thought best accomplished by an appropriate assignment of the depth and surface gradient at each cell interface, then performing the usual computations using the finite-difference prognostic equations (3.2), (3.3), and (3.5). Consider the set of possible adjacent grid cell configurations shown in Figure 17. This constitutes an exhaustive set of possible configurations. The heuristic depth assignment at the cell interface, together with the driving surface gradient are indicated for each cell configuration of Figure 17. Normally, the interface depth is taken as the average total depth in adjacent cells; this is the depth the disturbance will travel through during its propagation from one cell to the next. An examination of the heuristic depth assignments in Figure 17 that differ from this normal value will reveal that an intuitively reasonable assignment has been made in each case for the depth the primary disturbance can be expected to travel through. Consider, for example, case 2 of Figure 17. For models that employ a fixed boundary condition at the shoreline, the depth in this case would not be computed; the volume transport would simply be set to zero across this interface (if it were indeed the shoreline). The Sielecki-Wurtele treatment would be to first extrapolate some amount of water onto the dry cell, depending on the depth of the two preceding wet cells, and then take the average total depth as that at the interface. The Reid-Bodine treatment would be to use the barrier overtopping equation if the dry cell had

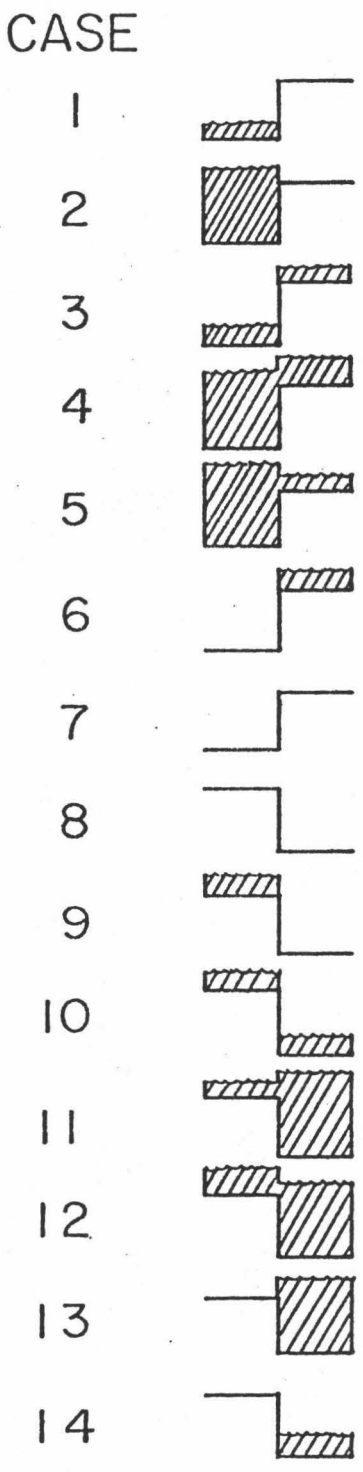

Figure 17. Set of possible adjacent grid-cell configurations.

been previously tagged as a barrier, or half the depth in the wet cell otherwise. The heuristic depth assignment scheme presented here gives as the interface depth the thickness of fluid in the wet cell that overtops the average cell elevation. This is physically reasonable and is applied uniformly throughout the computational domain. Similarly, the surface gradient, $\Delta\eta$, is assigned in each case a value consistent with its role as the driving force for changes in fluid motion. Reference to case 9 of Figure 17 will illustrate this assertion. The normal treatment would assign to $\Delta\eta_{j+\frac{1}{2}}$ the value $\eta_j - \eta_{j+1}$ (the polarity of $\Delta\eta$ is such that a positive value indicates a rightward tendency to flow). Recalling that for dry cells, $\eta = -h$, it is seen that the driving head depends on the difference in cell elevations. This is physically unreasonable, however, as a simple analogy demonstrates: Imagine pouring fluid from a container; obviously the rate of fluid flow to the ground will not depend on the distance to the ground, but rather on the height of the fluid surface above the spout through which it is poured. The same is taken to be true for cases 9, 3, 6, and 10.

The program logic required to implement the heuristic depth-assignment scheme is similar to that for the Reid-Bodine scheme. A test was made using the values for parameters given by (10.2). In addition, a shallow lagoon was inserted into the topography to enable evaluation of model performance for all 14 cell configurations given in Figure 17. The lagoon is 350 m wide and 6 cm deep, followed by a 2 m wall and separated from the ocean by 250 m of dry land with a grade of 2 cm/50 m. The initial results are presented in Figure 18. The lagoon inundation is seen to proceed without difficulty until shortly after the inundating wave is reflected from the wall at the right side of the lagoon. This introduces a high-frequency leftward-traveling disturbance, and about the same time a 'blowup' is seen to occur near the original shoreline. Interestingly, this discontinuity is almost identical to that

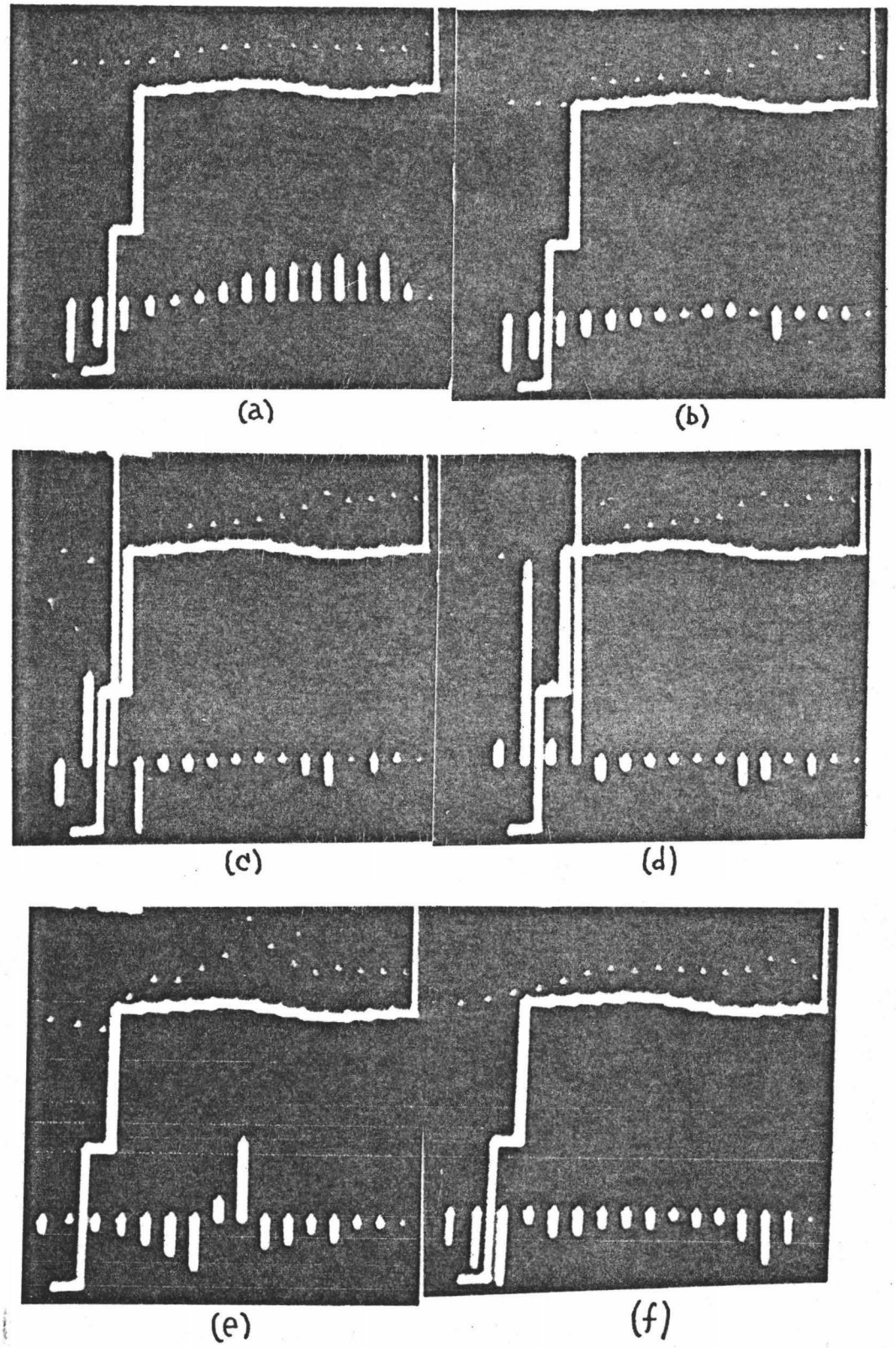

Figure 18. Close-up of tsunami flooding lagoon as computed using heuristic flooding scheme.

occuring in the Seilecki-Wurtele flooding test. A disturbance is then generated which travels inland and collides with the wall reflection in Figure 18e. After some fluid-like sloshing about, the surface assumes a smooth continuation of the expected recessional profile (Figure 18f).

The same run as seen on the entire grid is presented in Figure 19. The parameters are unchanged, but the vertical exaggeration is x 162 for the bathymetry, topography and volume transport vectors, and x 1620 for the surface disturbance. Figures 19a-d depict the smooth inundation of land by the sinusoidal tsunami. The shoreline blowup is seen occurring in Figure 19e. A phenomenon not observable in the closeup view is the large disturbance generated by the discontinuous behavior which travels oceanward, as seen in Figure 19f. Its wavelike characteristics make it conceivable that it could be mistaken for a real effect rather than the computational artifact that it is. This was prevented here by knowledge of the blowup obtained by monitoring all results.

Several measures were taken to improve the model performance depicted in Figures 18 and 19. The logical approach was to first determine the cause of the recurring shoreline discontinuity. It was initially thought that the discontinuous progression of heuristic depth assignments caused by the transition of cell configurations from case 14 to case 3 was responsible for the behavior in question; however, the strong similarity to the blowup that occurred during the Sielecke-Wurtele flooding model test suggested a common cause. Investigations reported in Section B of this chapter indicated that the finite-difference approximation to $\partial Q/\partial x$ that had been used, $DQDX_2$ (equation 5.5), resulted in model instability when used in conjunction with the heuristic flooding scheme. Smoothing was also found desirable to eliminate high-frequency wave components that often led to instabilties.

The results of the modified numerical flooding scheme are found in Figure 20.

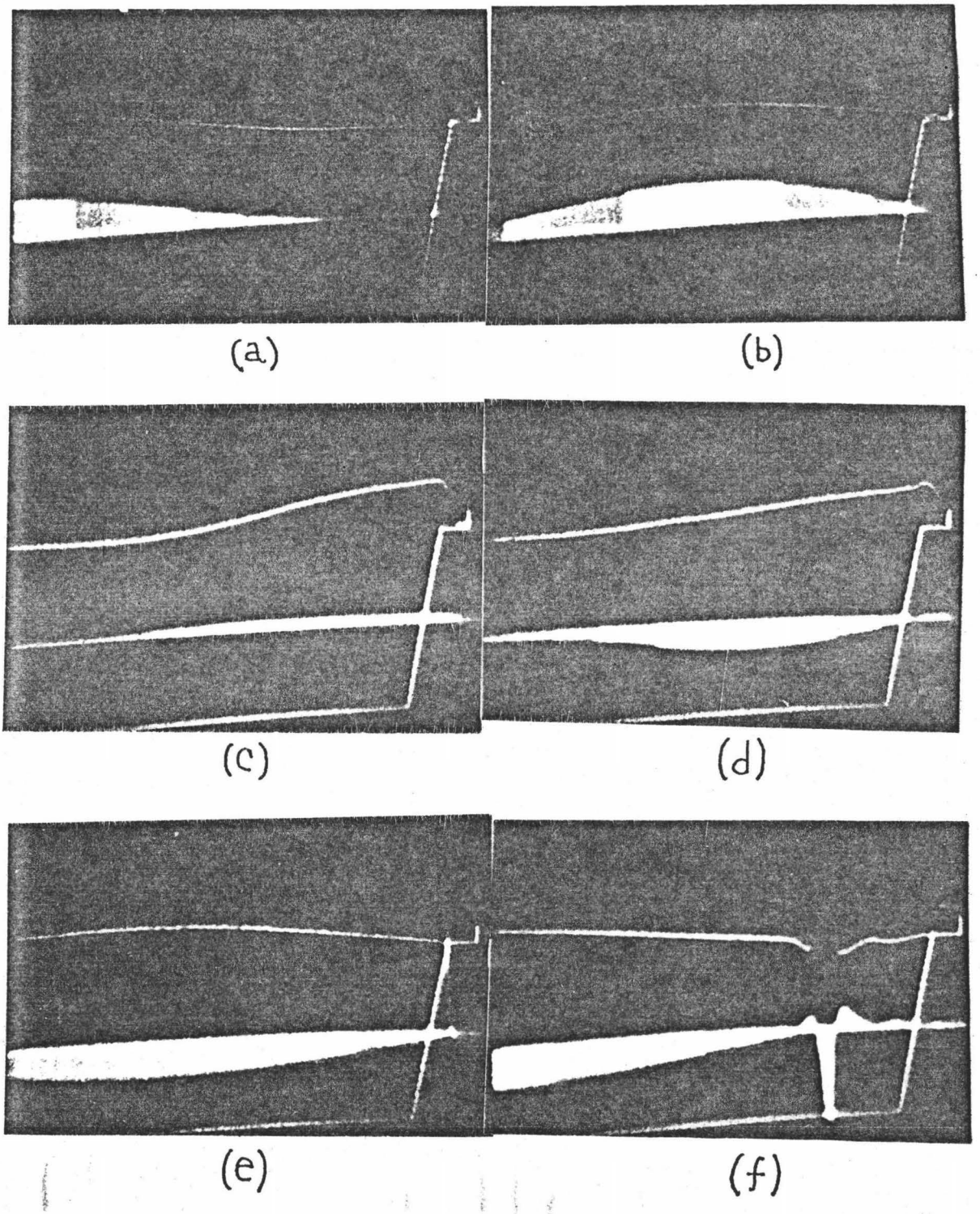

Figure 19. View of entire computational grid showing artifiial wave generated by "blow-up" of heuristic-flooding model.

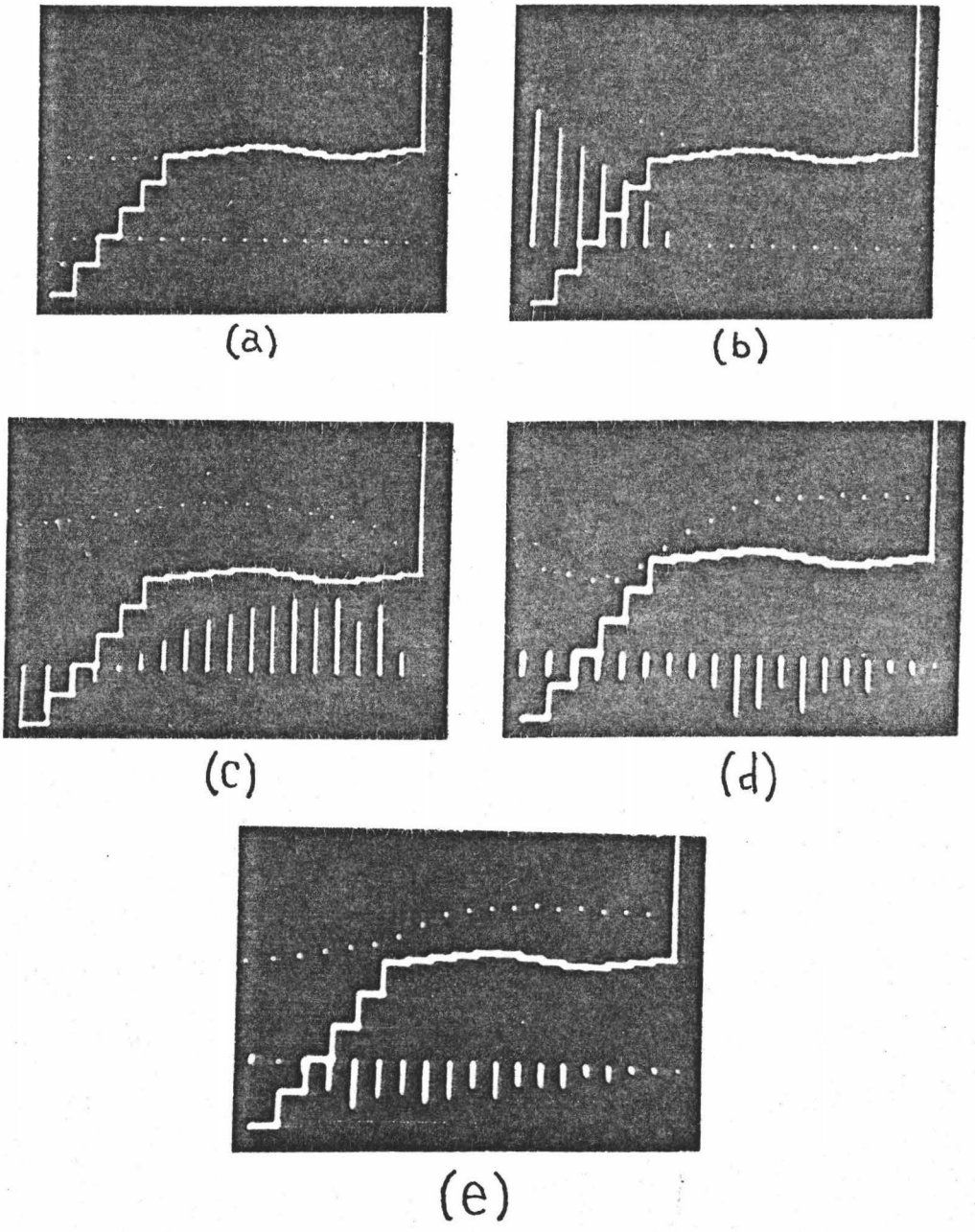

Figure 20. Close-up of tsunami flooding lagoon as computed using heuristic flooding scheme with $DQDX_3$ and smoothing.

The model parameter values given by (10.2), and the right-handed time extrapolation approximation to $\partial Q/\partial x$, $DQDX_3$ (equation 5.6), are used. In addition, 3-, 5-, and 7-point moving averages are taken for the second, third, and fourth nonzero values of disturbance height from each grid boundary, respectively; the first nonzero disturbance height from each grid boundary is left as is; and, all remaining interior surface values are smoothed using a fourth-order smoothing operator developed by Shapiro (1970) especially to damp all wave components of wavelengths $2\Delta x$ (his equation 26): (10.6)

$$\bar{\eta}_i^n = \frac{1}{256}\left\{186\eta_i^n + 56\left(\eta_{i-1}^n + \eta_{i+1}^n\right) - 28\left(\eta_{i-2}^n + \eta_{i+2}^n\right) + 8\left(\eta_{i-3}^n + \eta_{i+3}^n\right) - \left(\eta_{i-4}^n + \eta_{i+4}^n\right)\right\}$$

Finally, the sharp slope-break at the shoreline has been smoothed by the insertion of a 5-cell, 15' sloping-bottom for the last meter up to the shoreline. The result is a smooth, continuous, physically realizable flooding and recession.

Figure 21 contains the case-counts for this run. These are the frequencies of occurrence of each configuration shown in Figure 17 involving at least one dry cell or originally dry cell. For comparison, the case counts obtained for the initial test run depicted in Figure 18, and also for the Reid-Bodine flooding test shown in Figure 15 are included. Except for the absence of cases 8-11 for the Reid-Bodine run, the character of the results is almost identical for each case. The only significant difference is the total absence of case 6 for the modified heuristic flooding case. This is seen to be an improvement over the previous two methods, as case 6 is not expected to realistically occur under the given circumstances. There is also a notable decrease in the frequency with which cases 2 and 3 occur for the modified heuristic flooding scheme; the first indicating a more vigorous flooding than previously, the second indicating a less sluggish recession of water over shallow, originally dry land. Both are seen as an improvement over

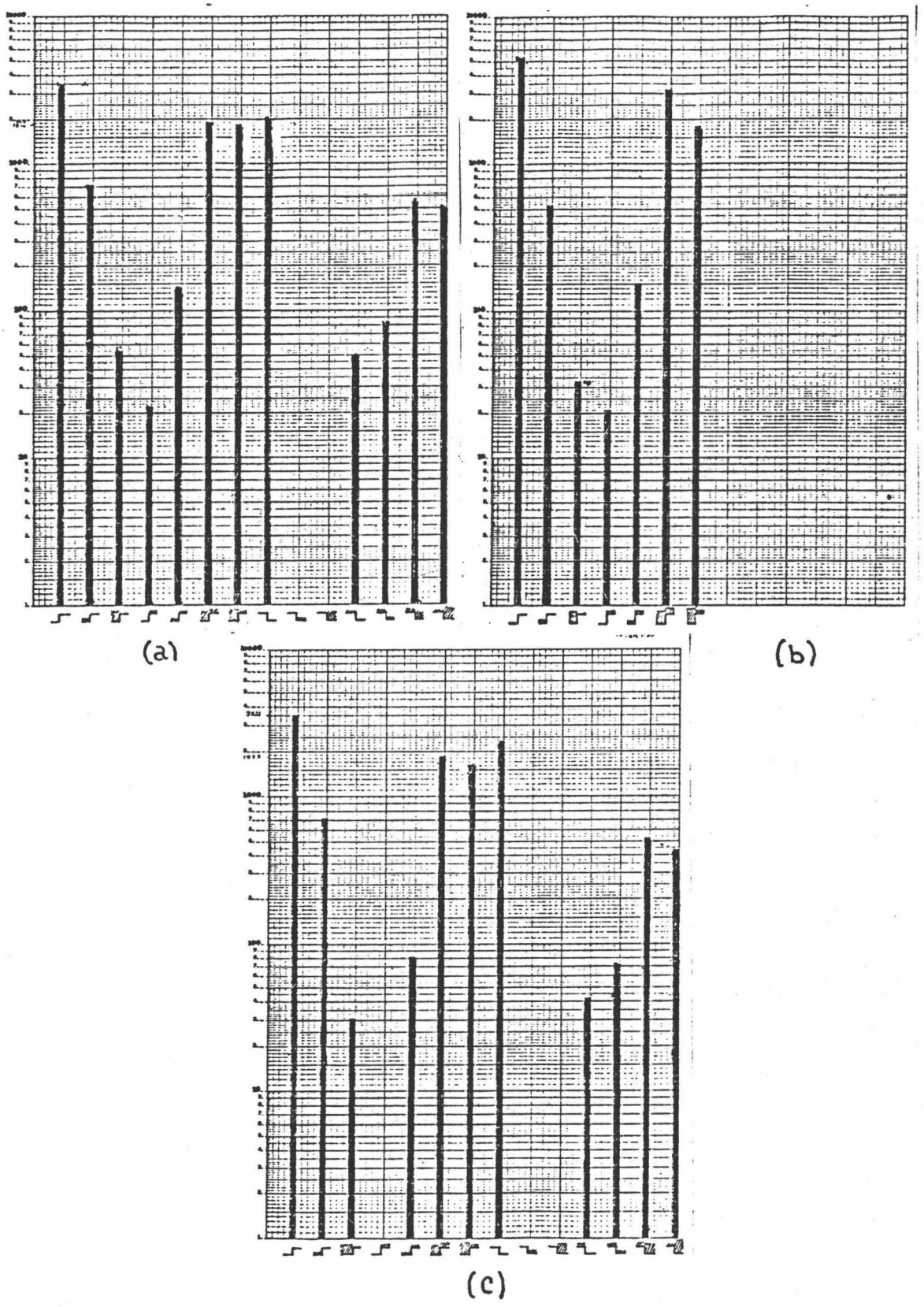

Figure 21. Adjacent cell case-counts for (a) Sielecki-Wurtele flooding test, (b) Reid-Bodine flooding test, and (c) modified heuristic flooding test.

previously tested schemes, yet the overall character of the flooding process, as revealed by the statistics of Figure 21, has not been drastically altered.

B. Instabilities and Asymmetries Encountered During the Modelling Process

Tests were made using the Ball-Thacker problem discussed in Chapter VIII to assess the stability properties of each of the advective term formulations given in Chapter V when used in conjunction with the heuristic depth assignment flooding scheme. $DQDX_1$ was first tested, using a time step of one second and the remaining parameter values of (9.5). This was less than half the critical value as indicated by the Von Neumann stability analysis of Chapter VI. Representative results are presented in Figure 22. The most outstanding feature is a modulated oscillation of wavelength $2\,\Delta x$ seen to develop rapidly at the leading edge of the fluid. This is thought to be the nonlinear or 'aliasing' instability discussed by Phillips (1959). It is caused by nonlinear numerical interactions that tend to direct energy toward ever-shorter wavelengths, eventually beyond the capacity of the computational grid to resolve without aliasing. The instability was not prevented by decreasing the time step, in agreement with Phillips' work, so the $DQDX_1$ formulation was abandoned.

Next, a test was performed using the diagonal extrapolation approximation to $\partial Q/\partial x$ given by (5.5), $DQDX_2$. All parameter values are as in (8.5). The results are shown in Figure 23. The irregular behavior was unexpected, and led to the development of $DQDX_3$.

It was thought best to develop and test $DQDX_3$ using a symmetrical problem for verification, as the anomalies encountered in the previous two tests exhibited a certin asymmetry, or handedness, occurring in each case on the left-hand side of the fluid body. For this purpose another solution to the nonlinear shallow-water equations developed by Thacker (1980), following Ball (1962), was used. Although

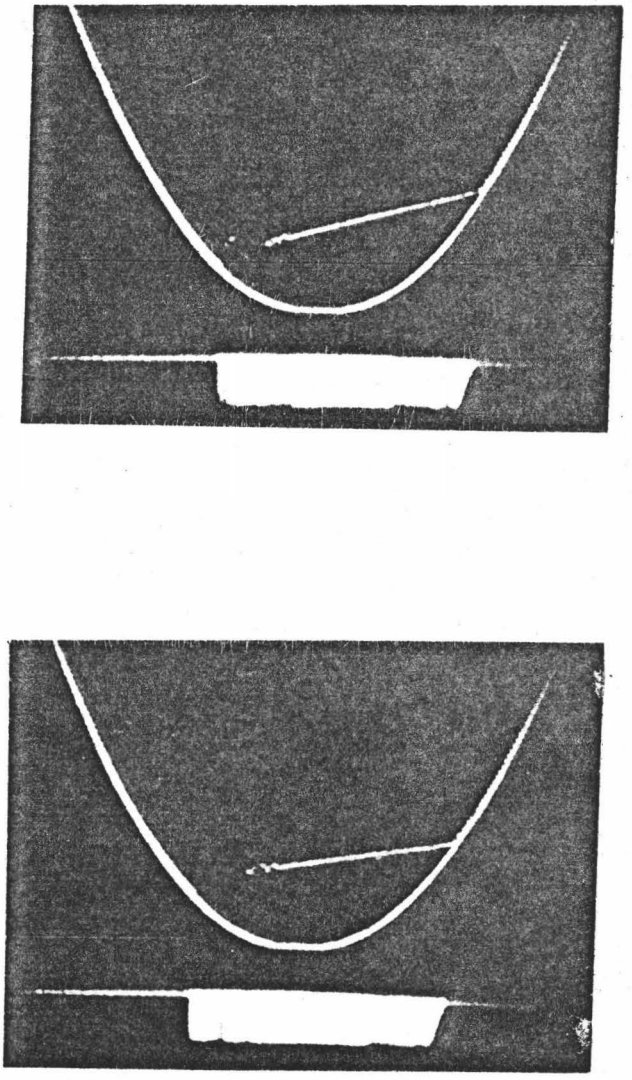

Figure 22. Non-linear instability encountered in planar Ball-Thacker model during test of $DQDX_1$ in conjunction with heuristic flooding scheme.

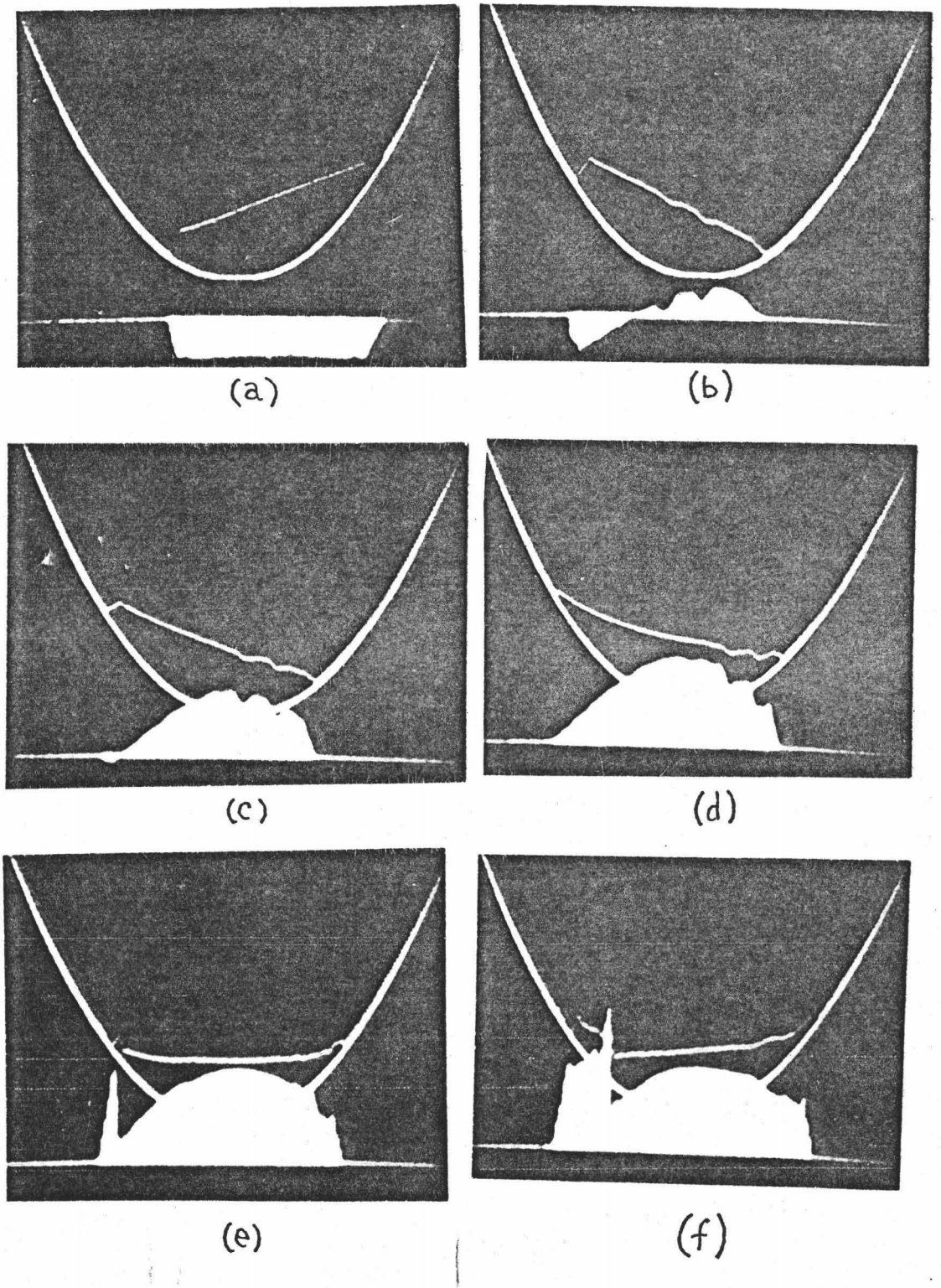

Figure 23. Test of DQDX$_2$ in conjunction with heuristic flooding scheme, using planar Ball-Thacker model.

similar to the solution given in Chapter IX, in this case the initial surface configuration of the water is parabolic. Thacker showed that the surface would remain parabolic, oscillating between the two extremes of opposite concavity. Figure 24 shows the results of an early test of $DQDX_3$ for the resulting problem. The parameter values given in (9.5) are used. The parabolic basin is 199 cells wide, with the initial water configuration onlapping the basin at cells 25 and 175. The equilibrium of water is 1.6 cells. A fourth-order smoothing operator developed by Shapiro (1970) is applied to the disturbance heights and fluxes (see equation (10.6)). The smoothing operator is symmetrical and involves four values on each side of the value to be smoothed. This operator was applied across the entire fluid body uniformly, with the value zero given to disturbance heights off the fluid body when the operator was applied to a value within four cells of the fluid edge. The resulting fluid motion is erratic near the edges, most likely due to the zero boundary condition applied there when smoothing. The effect is similar to the 'ringing' encountered with any sharply-cutoff filter.

In order to alleviate the 'ringing' associated with the zero boundary condition, moving averages were taken near the boundaries. The nine-point Shapiro smoothing-operator could be applied up to the fifth point from the fluid boundary; the nonzero boundary value was left unchanged; the next value was smoothed using a simple 3-point average; the third smoothed value from the boundary was obtained by a 5-point average; and the fourth interior point was smoothed by a 7-point average. As a further precaution against the development of any asymmetries in the solution, special program logic was implemented to alternate the direction of passes across the computational grid at each time iteration, thus alternating the handedness of all calculations.

The results of these efforts are presented in Figure 25. Surprisingly, a strong asymmetry developed in the solution. The left edge of the fluid boundary is seen

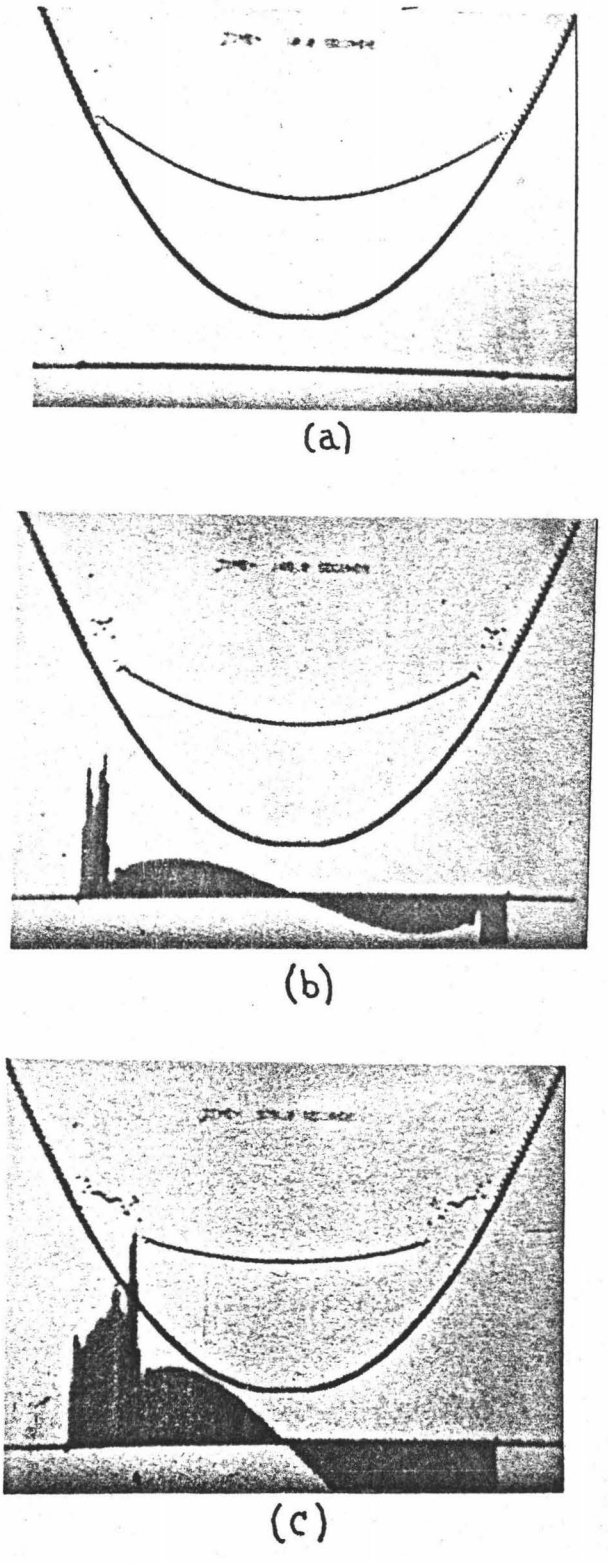

Figure 24. Test of $DQDX_3$ with heuristic flooding using paraboloidal-pulse Ball-Thacker model, illustrating 'ringing' effect resulting from smoothing with zero boundary-conditions.

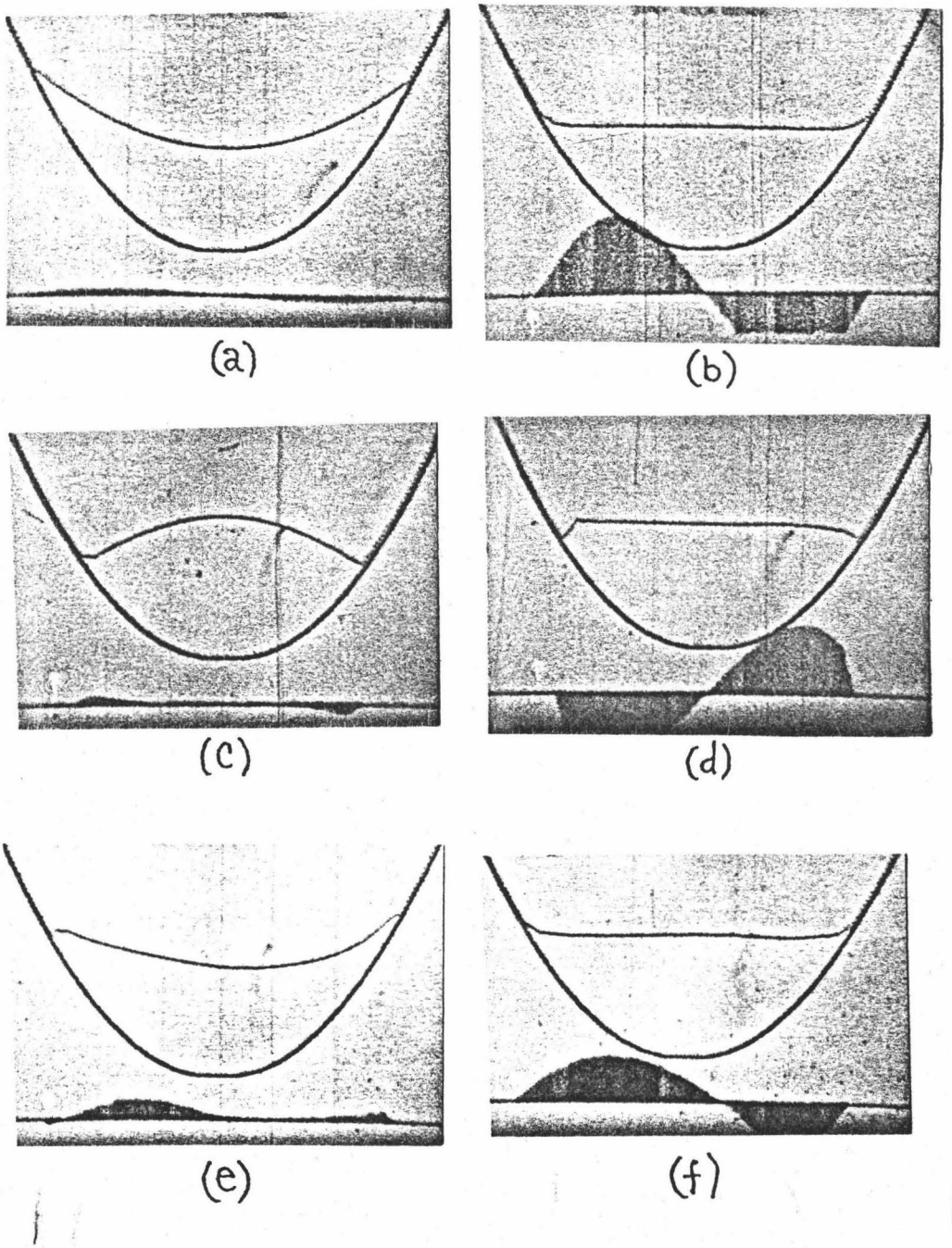

Figure 25. Asymmetrical results in paraboloidal Ball-Thacker model using $DQDX_3$ and heuristic flooding, produced despite alternating computational grid-pass directions.

to be lagging behind the right edge during the recessional stage, shown in Figure 25c. As flooding resumes in Figure 25d, a bore develops on the left leading edge. The visible portion of the volume transport vectors has a generally symmetrical appearance. In Figure 25e the fluid has nearly attained its original configuration after one complete oscillation, and neither the surface nor the fluxes are symmetrical. A quarter cycle later the surface is apparently symmetrical (Figure 25f), but the volume transport vectors have assumed a definite handedness.

The overall performance of the preceding test was encouraging, so $DQDX_3$ was adopted for the advective term evaluation of the heuristic flooding model. The cause of the asymmetry observed during the test was not immediately discerned, though it was later discovered to result from a test that determined the first flux value eligible to be smoothed near either fluid boundary. Passing over the grid from left to right, the first eligible flux value was the first one associated with a wet cell to its left, and the last eligible flux was the last one that was associated with a wet cell to its left. While the direction in which the pass was made was alternated, the basic test was not. This small computational handedness produced the dramatic effects of Figure 25.

CHAPTER XI

SUMMARY AND CONCLUSIONS

The purpose of this work was to develop a numerical method of integrating the nonlinear shallow-water approximation to the Navier-Stokes equations, while permitting the realistic motion of the fluid boundary that is required to successfully model tsunami flooding over dry land. An incompressible, homogeneous, inviscid fluid was assumed, subject only to the forces of gravity and bottom friction. Vertical advection of momentum was permitted. The numerical scheme developed for this purpose was a finite-difference, split-step, midpoint leapfrog system.

Analysis of the numerical scheme's stability in Chapter VI resulted in constraints placed on the permissible relation between the spatial computational grid dimension and the time step used. Boundary conditions and special approximations to the nonlinear advective term, developed in Chapters IV and V, respectively, were not included in the analytical stability analysis, but were tested experimentally. As a result, it was found that the most stable formulation of the nonlinear advective term involved the right-handed time extrapolation of $\partial Q/\partial x$ developed in Chapter V. Also, the expected conformance oceanside open boundary condition developed in Chapter IV was found to permit the unhindered exit from the computational grid of energy reflected from the shore area.

The dependence of moving boundary scheme appropriateness on the interpretation of represented bathymetry was investigated in Chapter X. The duality that exists in the interpretation was discussed. Basically, the question is whether the stairstep finite-difference representation of the bathymetry represents a continuous, smooth bathymetry, or a discreet, discontinuous one. Examples of flooding schemes developed with deference to each of the

possibilities were tested. The method of Sielecki and Wurtele (1970) was identified as having the assumption of a smooth bathymetry at its foundation; that of Reid and Bodine (1968) as making allowance, at least in part, for discontinuous bathymetry. Through the use of these examples, it was concluded that schemes which attempt to extrapolate water depths onto dry grid cells in an effort to include the water/land boundary in a normal computation involving two wet cells are not appropriate when the bathymetry is not smooth. On the other hand, schemes which treat flooding of dry land as a special case through the use of empirical engineering equations with discharge coefficients of unspecified value are concluded to be artificial and arbitrary, with the possibility of abuse through the use of parameter 'calibration' extant. A solution to the dilemma is provided by the introduction of physically reasonable heuristic assignments of interface depth and driving surface gradient for each possible configuration of adjacent grid cells. The prognostic equations are then applied without prejudice uniformily over the entire grid. The results obtained in this fashion are encouraging.

During the course of these investigations, several phenomena were observed which were positively identified as computational artifacts. During the recessional stage of the modelled tsunami inundation, a discontinuous behavior of the flow at the shoreline was seen to generate a wave-like disturbance that propagated oceanward. As the cause of its occurrence was observed, the possibility of it representing a real phenomenon could be discounted. Another artifact was produced by smoothing the fluid surface oscillating in a parabolic basin, with the specification that all fluid heights were zero across the moving boundary. This resulted in a growing disturbance at the fluid edges resembling the 'ringing' of a signal produced by the application of a filter with a sharp cutoff frequency. This effect was eliminated by applying a moving average near the boundary involving only existing values. Finally, cases of asymmetry were

observed where the problem was entirely symmetric. The problem persisted even when all computations were made in a direction across the grid that alternated at each time iteration. At times the fluid surface and transport vectors appeared symmetric about a central axis, at other times one appeared symmetric while the other appeared asymmetric. As all results were expected to be symmetric, there was a tendency to compute and/or display only the basic unit of symmetry in the interests of conservation of computer resources, then deduce the remaining portion. These results emphasize the need to monitor all results at every time iteration. This is best accomplished by producing a motion picture that can be viewed to assess spatial and temporal coherency, and to detect computational anomalies.

Despite its illustrative and informative performance, some improvement could probably be made on the numerical model of tsunami flooding developed in this work. A more satisfactory approximation of the nonlinear advective term might be found that does not exhibit the handedness or suffer the instabilities of those presented here. Also, there are alternative possibilities for the realistic assignment of depths at grid cell interfaces, done here as a heuristic exercise. Finally, the verified model of tsunami flooding should be generalized to the three dimensional case for practical application to the mitigation of the tsunami hazard by enabling accurate inundation predictions to be made at real locations. It is expected that additional work by the author and others will advance this work.

APPENDIX A

Operations Flow Chart

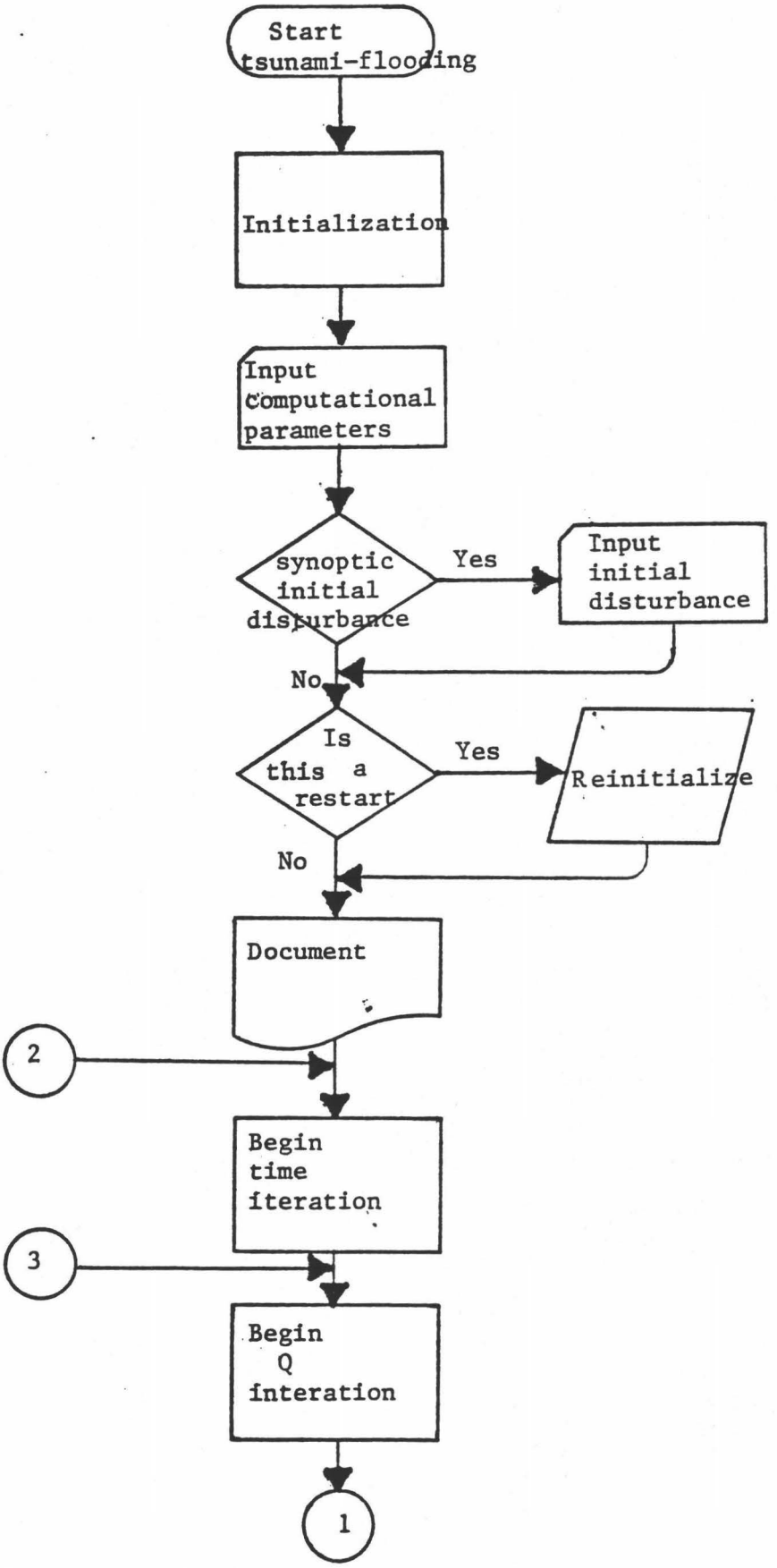
Start
tsunami-flooding
Initialization
Input
computational
parameters
synoptic
initial
disturbance
Yes
Input
initial
disturbance
No
Is
this a
restart
Yes
Reinitialize
No
Document
2
Begin
time
iteration
3
Begin
Q
interation
1

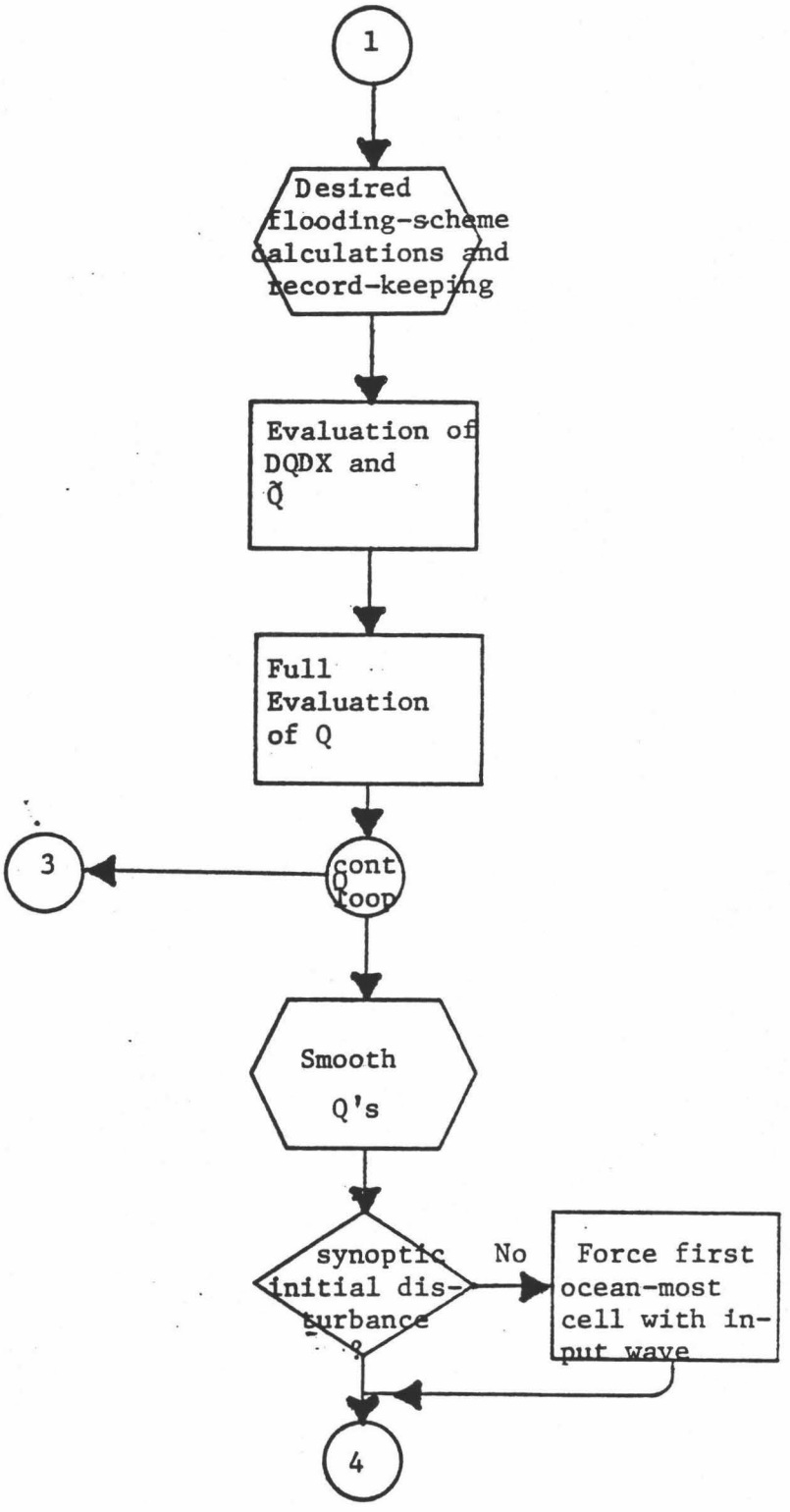
1
Desired flooding-scheme calculations and record-keeping
Evaluation of DQDX and Q̃
Full Evaluation of Q
3
cont Q loop
Smooth Q's
synoptic initial dis-turbance ?
No
Force first ocean-most cell with in-put wave
4

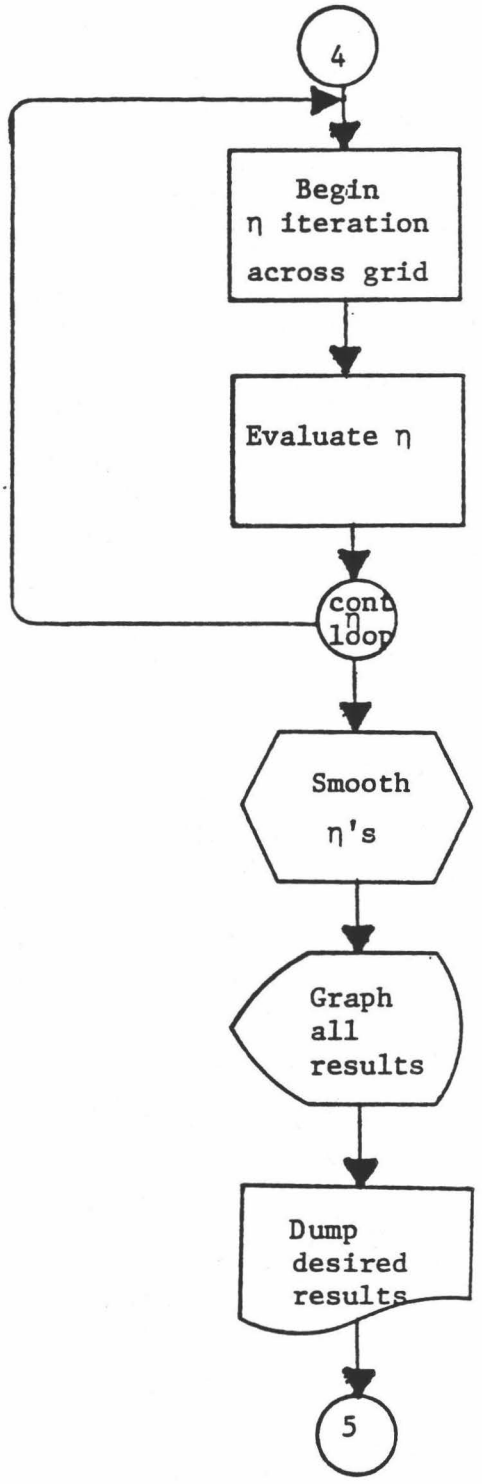
4
Begin
η iteration
across grid
Evaluate η
cont
η
loop
Smooth
η's
Graph
all
results
Dump
desired
results
5

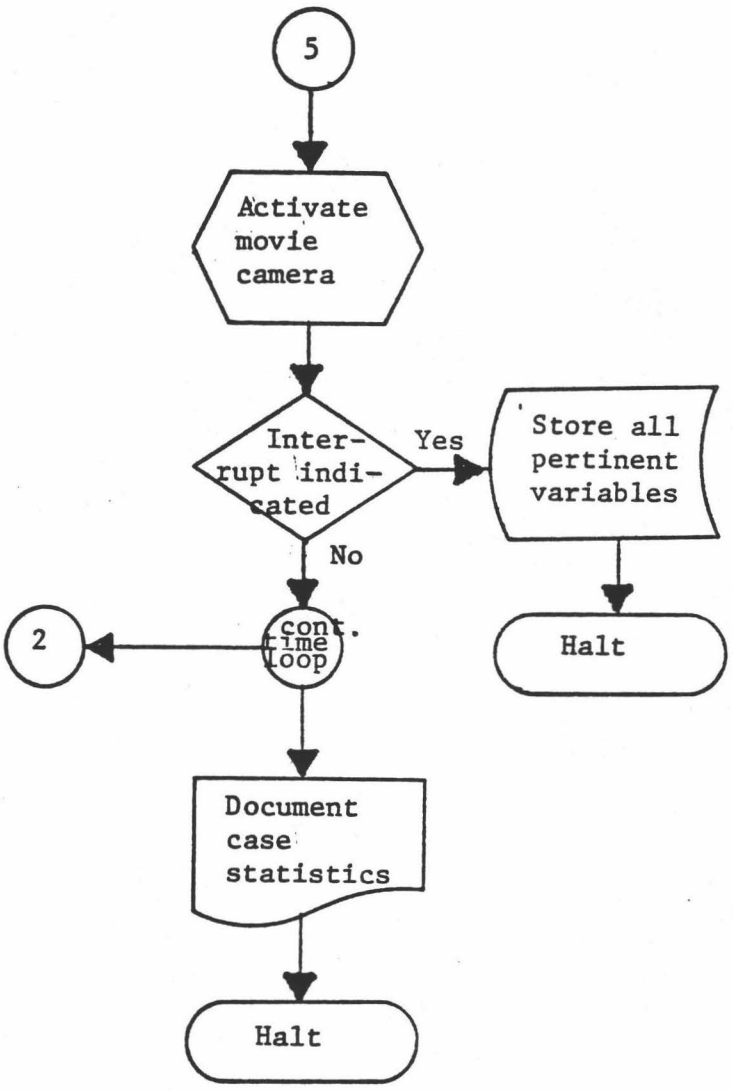
5
Activate movie camera
Inter-rupt indi-cated
Yes
Store all pertinent variables
No
2
cont. time Loop
Halt
Document case statistics
Halt

APPENDIX B

Representative Program

```
C     CG1
C     PROGRAM TO NUMERICALLY INTEGRATE THE LONGWAVE,SHALLOW
C     WATER NAVIER-STOKES EQUATIONS IN 1-DIMENSION USING EXPLICIT,SPACE- AND
      TIME-CENTERED LEAPFROG FINITE DIFFERENCE METHOD
C     WITH SPATIALLY UNIFORM EVALUATIONS OF APPLICABLE EQUATIONS.
C     DIAGNOSTIC AND RESTART CAPABILITIES ARE INCLUDED.
C     A 4TH-ORDER SHAPIRO SMOOTHING OPERATOR IS USED WITH A 1E-6 THRESHOLD.
C     3- 5- AND 7-PT. MOVING AVG.'S ARE TAKEN AT THE BOUNDARIES.
C     ZERO-VALUES ARE UNAFFECTED BY THE SMOOTHING.
C     A CLOSEUP VIEW OF THE SHORELINE AREA IS DISPLAYED.
C     DQ/DX IS APPROXIMATED BY DQDX3.
C     Q IS THE VOLUME TRANSPORT PER UNIT WIDTH.
C     Z IS THE DISTURBANCE HEIGHT RELATIVE TO MSL.
C     MEANING OF OTHER VARIABLES MAY BE DETERMINED BY EXAMINING PROGRAM.
C
C     ------------------------------------------------------------------
C     INITIALIZE
C     ------------------------------------------------------------------
      DOUBLE PRECISION Z(200),Q(200,2),H(200),DDD,HG(200),DELZ
      DOUBLE PRECISION PQIM1N,PQIM1,QTILDE,PZ1N,PZ1,PZ3N,PZ3
      DOUBLE PRECISION ZGRAPH(200),TH(9)
      INTEGER CELL,COUNT(14),FRAMES,CHECKS,CASE(200),WL,WR
      REAL LIN
      COMMON/DFILE/IBUF(4000)
      DATA PI,G,DDD/3.14159,9.8,1D-6,SWITCH/-1,KFIRST/1/,INTRPT/0/
C     ------------------------------------------------------------------
      IDENTIFY RESTART FILES, HYDROGRAPH FILES.  INPUT WAVEFORM FILE:
C     ------------------------------------------------------------------
      CALL ASSIGN(12,'DK1:DATAIN.DAT')
      CALL ASSIGN(14,'DK1:DATOUT.DAT')
      CALL ASSIGN(18,'DK1:HX1T.DAT')
      CALL ASSIGN(20,'DK1:HX2T.DAT')
      CALL ASSIGN(22,'DK1:ETAX.DAT')
C     ------------------------------------------------------------------
```

```
      TURN CAMERA-ACTIVATING RELAY OFF AND INITIALIZE GRAPHIC DISPLAY:
C     ---------------------------------------------------------------
      CALL CLEAR
      CALL INIT(IBUF,4000)
C     ---------------------------------------------------------------
      IDENTIFY CELL TO BE INTENSELY MONITORED.
C     ---------------------------------------------------------------
      CELL=10
      METER=CELL-1
C     ---------------------------------------------------------------
C     MORE INITIALIZATION:
C     ---------------------------------------------------------------
      DO 2 I=1,14
    2 COUNT(I)=0
      PZ1N=0.
      PZ3N=0.
C     ---------------------------------------------------------------
C     INPUT GRID PARAMTERS:
C     ---------------------------------------------------------------
      READ(5,20)N,DX,DT,T,FC,FRAMES,AMP
   20 FORMAT(I3,6X,F7.1,3X,F5.1,5X,F8.1,2X,F7.4,3X,I2,8X,F7.2)
      READ(5,22)DUMPTM,CHECKS
   22 FORMAT(F7.1,2X,I2)
C     ---------------------------------------------------------------
C     MORE INITIALIZATION:
C     ---------------------------------------------------------------
      DO 10 I=1,N
      Q(I,1)=0.
      Q(I,2)=0.
      Z(I)=0.
      CASE(I)=0
   10 CONTINUE
C     ---------------------------------------------------------------
C     READ BATHYMETRY, POSITIVE BELOW MSL, NEGATIVE ABOVE:
```

```
C
      DO 99 IX=1,N
      XI=IX
 99   H(IX)=3.-.05*(XI-1)
C
C     INITIALLY EQUATE WATER LEVEL AND GROUND LEVEL ON DRY LAND:
C
      DO 5555 I=1,N
5555  IF(H(I).LT.0.)Z(I)=-H(I)
C
C     DEFINE INITIAL DISTURBANCE:
C
      DO 23 I=1,60
      READ(22,5559)Z(60-I+1)
 23   CONTINUE
C
C     INSURE TOTAL REFLECTION FROM END OF GRID IN ABSENCE OF WALL:
C
      H(N+1)=H(N)
      Z(N+1)=Z(N)
C
C     FOR GRAPHICS, USE TRUE SIGN OF ELEVATION RELATIVE TO MSL:
C
      DO 5556 I=1,N
5556  HG(I)=-H(I)
C
C     DETERMINE IF THIS IS A RESTART:
C
      READ(5,5557)IRSTRT
5557  FORMAT(I1)
      IF(IRSTRT.NE.1)GO TO 5558
C
C     REINITIALIZE WITH LAST VALUES:
C
```

```
      READ(12,5559)((Q(I,J),I=1,N),J=1,2),(Z(I),I=1,N),PZ1N,PZ3N
 5559 FORMAT(D24.17)
      READ(12,5560)SWITCH
 5560 FORMAT(F3.0)
      READ(12,5561)KFIRST,(COUNT(I),I=1,14)
 5561 FORMAT(I7)
      Z(N+1)=Z(N)
C
C     DOCUMENT:
C
 5558 WRITE(6,80)DX,N*DX,DT,T
 80   FORMAT('1',' CARRIER-GREENSPAN VERIFICATION, ESP=.1',
     *///,' DELTA X (M): ',F7.1,/,'RANGE (M): ',F9.1,/,
     *1' TIME STEP (SEC): ',F5.1,/,' TOTAL MODEL TIME (SEC): ',F8.1)
      WRITE(6,840)FC
 840  FORMAT(' ','BED FRICTION COEFFICIENT: ',F9.5)
      WRITE(6,842)CELL
 842  FORMAT('0','FLUX METER READINGS ARE TAKEN AT SEAWARD'
     *,' BOUNDARY OF CELL ',I3)
      WRITE(6,82)(H(I),I=1,N)
 82   FORMAT('0',' GRID CELL DEPTHS (M): ',/,(/,10(1X,F11.4)))
C
C     DETERMINE CURRENT TIME STEP, PRINT CURRENT Z'S:
C
      KTIME=0
      IF(KFIRST.NE.1)KTIME=KFIRST
      WRITE(6,83)DT*KTIME
 83   FORMAT('0',///,/ T+",F7.1)
      WRITE(6,84)(Z(I),I=1,N)
 84   FORMAT('0',(/.10(1X,E11.4)))
      M=T/DT+1
      IF(KFIRST.NE.1)KFIRST=KFIRST+1
C
      TIME LOOP:
```

```
C
      DO 100 K=KFIRST,M
C
C     DETERMINE WHICH COLUMN OF 0 IS TO CONTAIN NEW VALUES OF FLUX:
C
      IF(SWITCH)86,88,90
 88   WRITE(6,888)
 888  FORMAT('0','SWITCH ERROR')
      STOP
 86   J2=2
      GO TO 92
 90   J2=1
 92   J1=3-J2
      ZK=K-1
      PQIM1N=Q(1,J2)
C
C     Q LOOP:
C
      DO 200 I=1,N-1
C
C     DETERMINE DEPTH AT BOUNDARY BETWEEN CELLS WHERE Q IS TO BE CALCULATED
C     AND WHERE FLUX METER READINGS ARE TO BE TAKEN:
C
      D=(Z(I)+H(I)+Z(I+1)+H(I+1))/2.
      DELZ=Z(I)-Z(I+1)
      DL=(H(METER)+Z(METER)+H(CELL)+Z(CELL))/2.
      ZN=Z(CELL)
      ZNM1=A(METER)
C
C     UNIFORM FLOODING SCHEME, RECORD-KEEPING, HEURISTIC INTERFACE-

C     DEPTH ASSIGNMENT
C
 175  IF(DABS(H(I)+Z(I)).LT.DDD)GO TO 172
```

```
      IF(DABS(H(I+1)+Z(I+1)).LT.DDD)GO TO 174
      IF(H(I).LT.H(I+1))GO TO 176
      IF(Z(I)+H(I+1).GT.DDD)GO TO 178
      D=Z(!+1)+H(I+1)
      DELZ=-D
      COUNT(3)=COUNT(3)+1
      CASE(I)=3
      GO TO 198
178   IF(Z(I).GT.Z(I+1))GO TO 180
      IF(H(I).LT.0..OR.H(I+1).LT.0.)COUNT(4)=COUNT(4)+1
      CASE(I)=4
      GO TO 198
180   IF(H(I).LT.0..OR.H(I+1).LT.0.)COUNT(5)=COUNT(5)+1
      CASE(I)=5
      GO TO 198
176   IF(H(I)+Z(I+1).GT.DDD)GO TO 182
      D+Z(I)+H(I)
      DELZ=D
      COUNT(10)=COUNT(10)+1
      CASE(I)=10
      GO TO 198
182   IF(Z(I).GT.Z(I+1))GO TO 184
      IF(H(I).LT.0..OR.H(I+1).LT.0.)COUNT(11)=COUNT(11)+1
      CASE(I)=11
      GO TO 198
184   IF(H(I).LT.0..OR.H(I+1).LT.0.)COUNT(12)+1
      CASE(I)=12
      GO TO 198
174   IF(H(I).LT.H(I+1)))GO TO 186
      IF(Z(I)+H(I+1).GT.DDD)GO TO 188
      COUNT(1)=COUNT(1)+1
      CASE(I)=1
      Q(I,J2)=0
      GO TO 200
```

```
      GO TO 196
182   DELZ+Z(I)+H(I+1)
      COUNT(2)=COUNT(2)+1
      CASE(I)=2
      GO TO 198
186   D=Z(I)+H(I)
      DELZ=D
      COUNT(9)=COUNT(9)+1
      CASE(I)=9
      GO TO 198
172   IF(DABS(H(I+1)+Z(I+1)).LT.DDD)GO TO 202
      IF(H(I+1).LT.H(I))GO TO 204
      IF(Z(I+1).GT.DDD)GO TO 206
      COUNT(14)=COUNT(14)+1
      CASE(I)=14
      Q(I,J2)=0.
      GO TO 200
      GO TO 198
206   DELZ=-(Z(I+1)+H(I))
      COUNT(13)=COUNT(13)+1
      CASE(I)=13
      GO TO 198
204   D=Z(I+1)+H(I+1)
      DELZ=-D
      COUNT(6)=COUNT(6)+1
      CASE(I)=6
      GO TO 198
202   IF(H(I+1).LT.H(I))GO TO 208
      COUNT(8)=COUNT(8)+1
      CASE(I)=8
      Q(I,J2)=0.
      GO TO 200
203   COUNT(7)=COUNT(7)+1
      CASE(I)=7
```

```
      Q(I,J2)=0.
      GO TO 200
C     ------------------------------------------------------------------
C     INITIALLY CALCULATE Q USING ONLY LINEAR TERM: AFTERWARD USE FRICTIONAL
AND
C     ADVECTIVE TERMS:
C     ------------------------------------------------------------------
 198  IF(I.GT.1)GO TO 160
      Q(I,J2)=Q(I,J1)+DT*G*D/DX
     **DELZ
      IF(DABS(Q(I,J2)).LT.DDD)Q(I,J2)=0.
      GO TO 200
C     ------------------------------------------------------------------
C     EXTRAPOLATE NEXT SPATIAL VALUE OF Q TO CALCULATE DQ/DX
C     (NECESSARY FOR PERFECT CENTERING OF ADVECTIVE TERM):
C     ------------------------------------------------------------------
 160  PQIM1=PQIM1N
      PQIM1N=Q(I,J2)
      IF(I.EQ.METER-1)QPROX+Q(I,J1)-PQIM1/2.+Q(I+1,J1)-Q(I+1,J2)/2.
      DQDX=(3.*Q(I+1,J1)-Q(I-1,J1)-Q(I+1,J2)-Q(I-1,J2))/(4.*DX)
C     ------------------------------------------------------------------
C     CALCULATE Q NEGLECTING FRICTION
C     ------------------------------------------------------------------
      QTILDE=(Q(I,J1)+DT*(G*D*DELZ/DX-Q(I,J1)*DQDX/(2.*D)))
     &/(1+DT*DQDX/(2,*D))
      IF(DABS(QTILDE+Q(I,J1)).GE.2E-35)GO TO 162
      Q(I,J2)=QTILDE
      GO TO 167
C     ------------------------------------------------------------------
C     SEE IF INCLUSION OF FREICTIONAL TERM WILL CAUSE COMPUTER BLOW UP
C     ------------------------------------------------------------------
```

```
162  QTEST=DT*FC*(QTILDE+Q(I,J1))*DABS(QTILDE+Q(I,J1))
    &/(4.*D**2*(1+DT*DQDX/(2.*D)))
     IF(.NOT.((QTEST-DDD.LT.QTILDE).AND.(QTILDE.LT.QTEST+DDD)))
    *GO TO 165
     Q(I,J2)=0
     GO TO 167
C    ------------------------------------------------------------------
C    SPACE- AND TIME-CENTERED EVALUATION OF Q
C    WITH LINEAR, FRICTIONAL AND ADVECTIVE COMPONENTS:
C    ------------------------------------------------------------------
165  Q(I,J2)=QTILDE-QTEST
     IF(DABS(Q(I,J2)).LT.DDD)Q(I,J2)=0.
167  IF(I.EQ.METER)QSAVE=QTILDE
200  CONTINUE
     Q(N,J2)=0.
C    ------------------------------------------------------------------
C    END OF Q CALCULATION LOOP;
C    NOW SMOOTH Q'S:
C    ------------------------------------------------------------------
     WL=1
     I=1
220  ZGRAPH(I)=Q(I,J2)
     IF(DABS(Z(I)+H(I)).GT.DDD) GOT TO 225
     WL=WL+1
     I=I+1
     GO TO 220
225  ZGRAPH(WL+1)=(Q(WL,J2)+Q(WL+1,J2)+Q(WL+2,J2))/3.
     ZGRAPH(WL+2)=(Q(WL,J2)+Q(WL+1.J2)+Q(WL+2,J2)+Q(WL+3,J2)
    &+Q(WL+4,J2))/5.
     ZGRAPH(WL+3)=(Q(WL,J2)+Q(WL+1,J2)+Q(WL+2,J2)+Q(WL+3,J2)
    &+Q(WL+4,J2)+Q(WL+5,J2)+Q(WL+6.J2))/7.
     WR=N
     I=N
230  ZGRAPH(I)+Q(I,J2)
```

```
      IF(DABS(Z(I)+H(I)).GT.DDD)GO TO 235
      WR=WR-1
      I=I-1
      GO TO 230
  235 ZGRAPH(WR-1)=(Q(WR,J2)+Q(WR-1,J2)+Q(WR-2,J2))/3.
     &+Q(WR-4,J2))/5.
      ZGRAPH(WR-3)=(Q(WR,J2)+Q(WR-1,J2)+Q(WR-2,J2)+Q(WR-3,J2)
     &+Q(WR-4,J2)+Q(WR-5,J2)+Q(WR-6,J2))/7.
      DO 201 I=WL+4,WR-4
      DO 2010 J=1,9
      TH(J)=0.
      IF(I+J-5.LT.1.OR.I+J-5.GT.N)GO TO 2010
      TH(J)=Q(I+J-5,J2)
 2010 CONTINUE
      ZGRAPH(I)=(186.*TH(5)+56.*.(TH(4)+TH(6))-28.*(TH(3)
     &+TH(7))+8.*(TH(2)+TH(8))-(TH(1)+TH(9)))/256.
      IF(DABS(ZGRAPH(I)).LT.DDD)ZGRAPH(I)=0.
      IF(Q(I,J2).EQ.0.)ZGRAPH(I)=0.
  201 CONTINUE
      DO 205 I=1,N
      Q(I,J2)=ZGRAPH(I)
  205 CONTINUE
C
C     CALCULATE NEW DISTURBANCE HEIGHTS:
C
      Z(1)=Z(1)-DT/DX*Q(I,J2)
  170 DO 300 I=2,N
      Z(I)=(I)+(DT/DX)*(Q(I-1,J2)-Q(I,J2))
C
C     PREVENT DISTURBANCE FROM GOING BELOW BOTTOM OR UNDERGROUND:
C
  299 IF(Z(I).GE.-H(I)+DDD)GO TO 300
      Z(I)=-H(I)
  300 CONTINUE
```

```
C
CC    ARRANGE FOR TOTAL REFLECTION AT END OF GRID:
C
      Z(N+1)=Z(N)
C
CC    SMOOTH Z'S:
C
      WL=1
      I=1
250   ZGRAPH(I)=Z(I)
      IF(DABS(Z(I)+H(I)).GT.DDD)GO TO 255
      WL=WL+1
      I=I+1
      GO TO 250
255   ZGRAPH(WL+1)=(Z(WL)+Z(WL+1)+Z(WL+2))/3.
      ZGRAPH(WL+2)=(Z(WL)+2(WL+1)+Z(WL+2)+Z(WL+3)+Z(WL+4)/5.
      ZGRAPH(WL+3)=(Z(WL)+Z(WL+1)+Z(WL+2)+Z(WL+3)+Z(WL+4)
     &+Z(WL+5)+Z(WL+6))/7.
      WR=N
      I=N
260   ZGRAPH(I)=Z(I)
      IF(DABS(Z(I)+H(I)).GT.DDD)GO TO 265
      WR=WR-1
      I=I-1
      GO TO 260
265   ZGRAPH(WR-1)=(Z(WR)+Z(WR-1)+Z(WR-2))/3.
      ZGRAPH(WR-2)=(Z(WR)+z(WR-1_+Z(WR-2)+Z(WR-3)
     &+Z(WR-4))/5.
      ZGRAPH(WR-3)=(Z(WR)+Z(WR-1)+Z(WR-2)+Z(WR-3)+Z(WR-4)
     &+Z(WR-5)+Z(WR-6))/7.
      DO 301 I=WL+4,WR-4
      DO 3010 J=1,9
      TH(J)=0.
IF(I+J-5.LT.1.OR.I+J-5.GT.N)GO TO 3010
```

```
      IF(DABS(Z(I_J-5)+H(I+J-5)).LT.DDD)GO TO 3010
      TH(J)=Z(I+J-5)
3010  CONTINUE
305   ZGRAPH(I)=(186.*TH(5)+56.*(TH(4)+TH(6))-28.*(TH(3)+TH(7))
     &8.*(TH(2)+TH(8))-(TH(1)+TH(9))/256.
      IF(DABS(ZGRAPH(I)).LT.DDD)ZGRAPH(I)=0.
 301  CONTINUE
      DO 304 I=1,N
      IF(ZGRAPH(I).LT.-H(I)+DDD)ZGRAPH(I)=-H(I)
      IF(Z(I).EQ.-H(I))ZGRAPH(I)=-H(I)
 304  Z(I)=ZGRAPH(I)
 306  Z(N+1)=Z(N)
C
C     GRAPHIC OUTPUT:
C
      DO 315 I=1,N
      ZGRAPH(I)=AMP*Z(I)
 315  CONTINUE
      IF(K.EQ.1)GO TO 3301
      CALL INIT
3301  CALL SCAL(39.,-1.1,FLOAT(N+1),2.)
      CALL APNT(10.,.5)
      CALL TEXT('TIME=')
      CALL NMBR(10.,DT*K,'F7.1')
      CALL TEXT(' SECONDS')
      X1=39.5
      IM1=40
      IM2=IM1-1
      ISTART=IM1+1
C
C     DISPLAY BATHMETRY:
C
      CALL APNT(X1,HG(IM1))
      DO 330 I=ISTRAT,N
```

```
      IF(DABS(Z(I_J-5)+H(I+J-5)).LT.DDD)GO TO 3010
      TH(J)=Z(I+J-5)
3010  CONTINUE
305   ZGRAPH(I)=(186.*TH(5)+56.*(TH(4)+TH(6))-28.*(TH(#)+TH(7))
     &8.*(TH(2)+TH(8))-(TH(1)+TH(9)))/256.
      IF(DABS(ZGRAPH(I)).LT.DDD)ZGRAPH(I)=0.
 301  CONTINUE
      DO 304 I=1,N
      IF(ZGRAPH(I).LT.-H(I)+DDD)ZGRAPH(I)=-H(I)
      IF(Z(I).EQ.-H(I))ZGRAPH(I)=-H(I)
 304  Z(I)=ZGRAPH(I)
 306  Z(N+1)=Z(N)
C     ------------------------------------------------------------
C     GRAPHIC OUTPUT:
C     ------------------------------------------------------------
      DO 315 I=1,N
      ZGRAPH(I)=AMP*Z(I)
 315  CONTINUE
      IF(K.EQ.1)GO TO 3301
      CALL INIT
3301  CALL SCAL(39.,-1.1,FLOAT(N+1),2.)
      CALL APNT(10.,.5)
      CALL TEXT('TIME=')
      CALL NMBR(10.,DT*K,'F7.1')
      CALL TEXT(' SECONDS')
      X1=39.5
      IM1=40
      IM2=IM1-1
      ISTART=IM1+1
C     ------------------------------------------------------------
C     DISPLAY BATHMETRY:
C     ------------------------------------------------------------
      CALL APNT(X1,HG(IM1))
      DO 330 I=ISTRAT,N
```

```
      CALL VECT(1.,HG(I)-HG(I-1))
  330 CONTINUE
C
C     DISPLAY FREE SURFACE AND VERTICALLY OREINTED FLUX VECTORS:
C
      DO 331 I=IM1,N
      XG=I
      IF(DABS(H(I)+Z(I)).LT.DDD)GO TO 370
      CALL APNT(XG,ZGRAPH(I))
  370 CALL APNT(XG+.4,-.5)
      CALL VECT(0.,Q(I,J2))
  331 CONTINUE
C
C     CALCULATE VARIOUS FLOW COMPONENTS AT MONITORED CELL SEAWARD BOUNDARY
C
      LIN=DT/DX*G*DL*(ZNM1-ZN)
      QNF=Q(METER,J2)+Q(METER,J1)
      IF(ABS(QNF).GE.1E-35)GO TO 335
      ADVEC=0.
      FRIC=0.
      GO TO 3370
  335 FRIC=DT*FC/(4.*DL**2)*QNF*ABS(QNF)
  337 ADVEC=-DT*QNF*(Q(CELL,J2)-Q(METER-1,J2)+Q(CELL,J1)-Q(METER-1,J1))
     */(8.*DL*DX)
C
C     REVERSE SWITCH POLARITY.
C
 3370 SWITCH=-1.*SWITCH
C     DUMP Z'S, Q'S, AND CASES IF DESIRED:
C
      IF(K*DT.LT.DUMPTM.OR.K*DT.GE.DUMPTM+CHECKS*DT)GO TO 3132
      WRITE(6,3133)K*DT
 3133 FORMAT('0',//,' T=,F7.1)
      WRITE(6,84)Z(I),I+1,N)
```

```
      WRITE(6),3134)(Q(I,J2),I=1,N)
3134  FORMAT('0',(/,6X,10(1X,E11.4)))
      WRITE(6,3135)(CASE(I),I=1,N)
3135  FORMAT('0",(/,1X,10(10X,I2)))
      WRITE(6,348)LIN,FRIC,ADVEC
 248  FORMAT('0',47X,'FLUX METER:',6X,'LINEAR',4X,'BED FRICTION'
     *,2X,'VERTICAL ADVECTION',/,31X,'CHANGE SINCE LAST TIME STEP:'
     *,3X,E11.4,2X,E11.4,6X11.4)
      WRITE(6,1000)QPROX,QSAVE
1000  FORMAT(' ",39X,'APPROXIMATION OF Q:'.3X,E11.4./,51X,'QTILDE:'
     *.3X,E11.4)
C     ------------------------------------------------------------------
C     FREEZE FIRST IMAGE UNTIL READY TO PROCEED:
C     ------------------------------------------------------------------
3132  IF(K.NE.KFIRST)GO TO 105
      PAUSE
C     ------------------------------------------------------------------
C     ACTIVATE MOVIE CAMERA:
C     ------------------------------------------------------------------
 105  DO 3136 IFR=1,FRAMES
      CALL PHOTO
3126  CONTINUE
C     ------------------------------------------------------------------
C     SAVE HYDROGRAPH READINGS FOR THIS TIME STEP:
C     ------------------------------------------------------------------
      WRITE(18,3137)Z(40)
      WRITE(20,3137)Z(60)
3137  FORMAT(D24.17)
C     ------------------------------------------------------------------
C     IF FRONT PANEL SWITCH 15 IS UP, SAVE VARIABLES AND HALT:
C     ------------------------------------------------------------------
      CALL CHECK(INTRPT)
      IF(INTRPT.NE.1)GO TO 100
      write914,5559)((Q(I,J),I=1,N),J=1,2),(Z(I),I=1,N),PZ1N,PZ3N
```

```
      WRITE(14,5560)SWITCH
      WRITE(14,5561)K,(COUNT(I),I=1,14)
      END FILE 14
      STOP
  100 CONTINUE
C
C     END OF TIME LOOP.
C     OUTPUT STATISTICAL COMPILATION OF ADJACENT CELL WATER LEVEL CONFIGURATIONS
C     INVOLVING AT LEAST ONE DRY CELL:
C
      WRITE(6,102)
  102 FORMAT('0',CASE    COUNT')
      DO 102 I=1,14
      WRITE(6,104)I,COUNT(I)
  104 FORMAT(' ',2X,I2,4X,17)
  103 CONTINUE
      STOP
      END
```

APPENDIX C

Interrupt Check Subroutine

```
CHECK  MACRO V03.02B11-JAN-80 12:39:36 PAGE 1

 1                              .TITLE CHECK
 2                                                      ; TO USE:  CALL CHECK(IFLAG)
 3                                                      ; IF HIGH BIT SWITCH ON FRONT PANELON,
 4                                                      ; IFLAG SET EQUAL TO 1, OTHERWISE UNCHANGED.
 5 000000  012500               CHECK::MOV (R5)+,R0     ; MAKE RS POINT TO FLAG.
 6 000002  005737 177570              TST @#177570      ; CHECK FRONT PANEL.
 7 000006  100002                    BPL CNTNU         ; INTERRUPT SWITCH NOT SET.
 8 000010  012735  000001            MOV #000001,@(R5)+ ; INTERRUPT SWITCH ON, SET FLAG.
 9 000014  000207               CNTNU: RTS PC           : RETURN TO MAIN PROGRAM.
10        000000'               .END CHECK
```

APPENDIX D

Photo Subroutine

```
        .TITLE PHOTO
PHOTO:  MOV  #177740,@#170406   ; PUT TIME (CLICKS) INTO BUFFER?PRESET REGISTER
        MOV #000013,@#170404    ; START CLOCK COUNTING AT 100 HZ
STAL:   TSTB @#170404           ; CLOCK OVERFLOW FLAG SET ( TIME )?
        BPL STALL               : NO, CHECK AGAIN
        MOV #177740,@#170406    ; YES, RESET DESIRED TIME ( CLICKS )
        MOV #000401,@#170410    ; CLOSE RELAYS (ACTIVATE CAMERA)
        MOV #000013,@#170404    ; START CLOCK COUNTING AT 100 HZ
SHOOT:  TSTB @#170404           ; CLOCK DONE COUNTING (OVERFLOW FLAG SET)?
        BPL SHOOT               : NO, CHECK AGAIN
        CLR @#170410            ; YES, OPEN RELAY 1
        RTS PC                  : RETURN CONTROL TO MAIN PROGRAM
        END PHOTO
```

REFERENCES

Adams, W. M. Expected tsunami inundation for the Hawaiian Islands. Mar. Techn. Soc. J., 1973, 7(8), 29-34.

Aleksandrov, A. D., Kolmogorov, A. N., Lavrent'ev, M. A., (Eds.), Translated by S. H. Gould, Mathematics: Its content, methods and meaning. The MIT Press, Massachusetts Institute of Technology, Vol. II, 1962, 52-53.

Bascom, W. Waves and Beaches. New York: Anchor Books, Doubleday and Company, Inc. 1964.

Ball, F. K. An exact theory of simple finite shallow water oscillations of a rotating earth. Procceedings of the First Australian Conference of Hydraulics and Fluid Mechanics, Pergamon, 1964.

Bretschneider, C. L., & Wybro, P. G. Tsunami inundation prediction. Chapter 60 in Proceedings, Fifteenth Coastal Engineering Conference, Honolulu, American Society of Civil Engineering, 1976, 1, 1006-1024.

Carrier, G. E., & Greenspan, H. P. Water waves of finite amplitude on a sloping beach. Journal of Fluid Mechanics, 1958, 4, 97-109.

Charney, J. G., Fjortoft, R., & Von Neumann, J. Numerical integration of the barotropic vorticity equation. Tellys, 1950, 2(4), 237-254.

Cox, D. C. Local tsunamis in Hawaii: Implications for hazard zoning (Report HIG-79-5) Honolulu: Hawaii Institute of Geophysics, Hawaii, 1979.

Fischer, G. A survey of finite-difference approximations to the primitive equations. Monthly Weather Review, 1965, 93(1), 1-10.

Forsythe, G. E., Wasow, W. R. Finite difference methods for partial differential equations. New York: Wiley & Sons, Co., 1960.

Fromm, J. E. Lectures on large scale finite difference computation of fluid flows. In E. F. Abraham and W. A. Tiller (Eds.), An introduction to computer simulation in

applied science. Palo Alto, Cal: IBM Data Processing Div., 1970.

Gourlay, A. R., & J. L. Morris. A multistep formulation of the optimized Lax-Wendroff method for non-linear hyperbolic systems in two space variables. Mathematical Computations, 1968, 22, 715-719.

Gray, W. G., & D. R. Lynch. Time-stepping schemes for finite element tidal model computations. Advances in Water Resources, 1977, 1(2), 83-95.

Hammack, J. L., & Segur, H. Modelling criteria for long water waves. Journal of Fluid Mechanics, 1978, 84(2), 359-373.

Harlow, F. H. Stability of difference equations selected topics. LAMS-2452 Physics and Mathematics (TID-4500, 15th Ed.) Los Alamos Scientific Laboratory of the University of California, Los Alamos, New Mexico, 1960.

Harlow, F. H., & Amsden, A. A. Fluid dynamics. Los Alamos Scientific Laboratory (Report LA-4700). Los Alamos Scientific Laboratory of the University of California, Los Alamos, New Mexico, 1960.

Harlow, F. H., & Amsden, A. A. A numerical fluid dynamics method for all flow speeds. J. Computational Physics, 1971, 8, 197-213.

Ho, D. V., Meyer, R. E., & Shen, M. C. Long surf (Technical Report 4). Providence, RI: Division of Applied Mathematics, Brown University, 1963.

Houston, J. R., Carver, R. D., & Marble, D. G. Tsunami-wave elevation frequency of occurrence for the Hawaiian Islands (Report H-77-16), Vicksberg: U. S. Army Engineer Waterways Experiment Station, Hydraulic Laboratory, Mississippi, 1977.

Houston, J. R., & Butler, H. L. A numerical model for tsunami inundation (Technical Report HL-79-2), Vicksberg: U.S. Army Engineers, Waterways Experimental Station Hydraulic Laboratory, Mississippi, 1979.

Jelesnianski, C. P. A numerical calculation of storm tides induced by a tropical storm impinging on a continental shelf. Monthly Weather Review, 1965, 93, 343-358.

Kasahara, A. On certain finite-difference methods for fluid dynamics. Monthly

Weather Review, 1965, 93, 27-31.

Knox, J. B. Numerical errors in the time integration of advective processes. Journal of Geophysical Research, 1961, 66(12), 4177-4186.

Kreiss, H. O., & Oliger, J. Methods for the approximate solution of time dependent problems. GARP Publishing Service, No. 10, World Metero. Org. 1973.

Lamb, H. Hydrodynamics, 6th Ed., New York: Dover Publications, 1945.

Lax, P. D. Hyperbolic difference equations: A review of the Courant-Freidrichs-Lewy paper in the light of recent developments. IBM J. 1967, March, 235-238.

Leendertse, J. J. Aspects of a computational model for long-period water-wave progagation (Rand Memorandum RM-5294-PR), Santa Monica, California, 1967.

Lilly, D. K. On the computational stabilty of numerical solutions to time-dependent non-linear geophysical fluid dynamics problems, Monthly Weather Review, 1965, 93(1), 11-25.

Lynch, D. R., & Gray, W. G. Analytic solutions for computer flow model testing. Journal of the Hydraulics Division, ASCE, 1978, 104, 1409-1428.

Lynch, D. R., & Gray, W. G. Finite element stimulation of shallow water problems with moving boundaries. In C. A. Brebbia, W. G. Gray and G. F. Pinder (Eds.), Finite Elements in Water Resources - II, London: Pentech Press, 1978.

Meyer, R. E., & Taylor, A. D. On the equations of surf (Technical Report 5), Providence, RI: Division of Applied Mathematics, Brown University, 1963.

Miyakoda, K. Contribution to the numerical weather prediction: Computation with finite difference. Japanese Journal of Geophysics, 1962, 3, 75-190.

Orszag, S. A., & Israeli, M. Numerical simulation of viscous incompressible flows, Annual Review of Fluid Mechanics, 1974, 281-317.

Phillips, N. A. An example of non-linear computational instability. In B. Bolin (Ed.), The atmosphere and the sea in motion. New York: Rockefeller Institute Press in association with the Oxford University Press, 1959.

Platzman, G. W. The computational stability of the meteorological prediction equations (Report). Chicago: Department of Meteorology, The University of Chicago, 1958.

Platzman, G. W. A numerical computation of the surge of 26 June 1954 on Lake Michigan. Geophysica, 1958, 6, 407-438.

Platzman, G. The lattice structure of the finite difference primitive and vorticity equations. Monthly Weather Review, 1958, 87(8), 285-292.

Reid, R. O., & Bodine, B. R. Numerical model for storm surges in Galveston Bay. Proc. American Society of Civil Engineering Journal Waterways Harbor Div, 1968, 94(33),

Richtmyer, R. D., & Morton, K. W. Difference methods for initial-value problems, 2nd Ed., New York: Interscience Publishers, Inc., 1967.

Roache, R. J. Computational Fluid Dynamics. Albuquerque: Hermosa Publishers, 1972.

Runchal, A. K. Numerical model for storm surge and run-up studies. In Symposium on modeling techniques, 2nd Annual symposium of the Waterways, Harbors, and Coastal Engineering Division of the American Society of Civil Engineers, San Francisco, CA. 1975.

Shapiro, R. Smoothing, filtering and boundary effects. Review of Geophysics and Space Physics, 1970, 8(2), 359-387.

Shepard, E. F., Macdonald, G. A., & Cox, D. C. The tsunami of April 1, 1946. Bull. Scripps Inst. Oceanog, 1950, 5(6), 391-528.

Sklarz, M. A., & Spielvogel, L. Q. Delaying open boundary reflection interference by averaging solutions for the 1975 Hawaii tsunami simulation. Computers and Fluids, 1979, 7, 305-313.

Sielecki, A., & Wurtele, M. G. The numerical integration of the nonlinear shallow-water equations with sloping boundaries. Journal of Computational Physics, 1970, 6, 219-236.

Stoker, J. J. Water waves. New York: Interscience Publishers, Inc., 1957.

Strang, G. On the construction and comparison of difference schemes. J. SIAM Numer. Anal., 1968, 5, 506-517.

Thacker, W. C. Some exact solutions to the nonlinear shallow-water wave equations. Journal of Fluid Mechanics, 1981, 107, 499-508.

Thacker, W. C. A spliced numerical grid having applications to storm surge (NOAA Technical Memorandum ERL AOML-26), NOAA, ERL, AOML, Miami, 1976.

Ursell, F. The long-wave paradox in the theory of gravity waves. Proc. Camb. Phil. Soc., 1953, 49, 685-694.

Wanstrath, J. J. An open-coast mathematical storm surge model with coastal flooding for Louisiana (Miscellaneous Paper H-78-5), U. S. Army Engineer Waterways Experiment Station Hydraulic Laboratory, Vicksbury, Miss., 1978.

Wanstrath, J. J., Whitaker, R. O., Reid, R. O., & Vastano, A. C. Storm surge simulation in transformed coordinates (Tech. Report 76-3) U. S. Army Corps of Engineers Coastal Engineering Research Center, 1976.

Welander, P. Numerical prediction of storm surges. Advan. Geophys., 1961, 8, 316-379.

Wurtele, M. G., Paegle, J., & Sielecki, A. The use of open boundary conditions with the storm-surge equations. Monthly Weather Review, 1971, 99, 537-544.

Xanthopoulos, T., & Koutitas, C. Numerical simulation of a two dimensional flood wave propagation due to dam failure. Journal of Hydraulic Research, 1976, 14(4), 321-331.

Yeh, G. E., & Chou, F. K. Moving boundary numerical surge model. Journal of the Waterway, Port, Coastal and Ocean Division. Proceedings of the American Society of Civil Engineers, 1979, 105(WW3), 247-263.